EUROPEAN ORGANIZATION FOR NUCLEAR RESEARCH (CERN)

CERN-EP-2021-054
2021/04/27

CMS-HIG-19-009

Constraints on anomalous Higgs boson couplings to vector bosons and fermions in its production and decay using the four-lepton final state

The CMS Collaboration*

Abstract

Studies of *CP* violation and anomalous couplings of the Higgs boson to vector bosons and fermions are presented. The data were acquired by the CMS experiment at the LHC and correspond to an integrated luminosity of 137 fb^{-1} at a proton-proton collision energy of 13 TeV. The kinematic effects in the Higgs boson's four-lepton decay $\text{H} \to 4\ell$ and its production in association with two jets, a vector boson, or top quarks are analyzed, using a full detector simulation and matrix element techniques to identify the production mechanisms and to increase sensitivity to the Higgs boson tensor structure of the interactions. A simultaneous measurement is performed of up to five Higgs boson couplings to electroweak vector bosons (HVV), two couplings to gluons (Hgg), and two couplings to top quarks (Htt). The *CP* measurement in the Htt interaction is combined with the recent measurement in the $\text{H} \to \gamma\gamma$ channel. The results are presented in the framework of anomalous couplings and are also interpreted in the framework of effective field theory, including the first study of *CP* properties of the Htt and effective Hgg couplings from a simultaneous analysis of the gluon fusion and top-associated processes. The results are consistent with the standard model of particle physics.

Submitted to Physical Review D

*See Appendix A for the list of collaboration members

Contents

1 Introduction

The discovery by the ATLAS and CMS Collaborations of a Higgs boson (H) with a mass of $\approx$125 GeV [1–3] has confirmed the predictions of the standard model (SM) of particle physics [4–10]. The CMS [11–18] and ATLAS [19–25] experiments have set constraints on the spin-parity properties of the H boson and anomalous HVV couplings, where V stands for W, Z, and γ electroweak (EW) gauge bosons, finding its quantum numbers to be consistent with $J^{PC} = 0^{++}$, but leaving room for small anomalous HVV couplings. In theories beyond the SM (BSM), H boson interactions may generate several of them, which lead to new tensor structures of interactions, both CP-even and CP-odd. The new anomalous tensor structures of the H boson interactions may also appear through loop corrections in SM processes, but the size of their contributions is beyond the current experimental sensitivity. The CP-odd anomalous couplings between the H boson and either the top quark or new BSM particles, fermions or bosons, contributing to the gluon fusion loop may generate CP violation in Hgg interactions. Possible CP violation effects in couplings to fermions, Hff, had not been experimentally probed until recently, when the first

constraints were reported by CMS [26] and ATLAS [27] in $\mathrm{t\bar{t}H}$ production using the $\mathrm{H} \to \gamma\gamma$ channel.

In this paper, we study the tensor structure of the HVV, Hgg (where g stands for gluon), and Htt (where t stands for top quark) interactions, and we search for several anomalous effects, including *CP* violation, using the four-lepton final state $\mathrm{H} \to \mathrm{VV} \to 4\ell$, where $\ell = \mu$ or e. The H boson production processes considered in this paper include gluon fusion (ggH), vector boson fusion (VBF), associated production with a weak vector boson (VH, either ZH or WH), with a top quark pair ($\mathrm{t\bar{t}H}$), with a single top quark (tH), and with a bottom quark pair ($\mathrm{b\bar{b}H}$). The Feynman diagrams for these processes are shown in Figs. 1–5 and discussed in detail in Section 2. Kinematic effects in the H boson's decay and its production in association with two jets generated in either the VBF or ggH processes, with a vector boson, or with top quarks are analyzed. Production and decay processes of the H boson are sensitive to certain anomalous contributions, or equivalently higher-dimensional operators in the effective field theory (EFT) [28], which modify the kinematic distributions of the H boson's decay products and of the particles produced in association with the H boson. Prior measurements of EW processes limit the allowed values of certain EFT operators, and the preferred EFT basis used in this paper is chosen to minimize the number of independent operators and their correlations. This allows us to reduce the number of operators to be measured. The results are also translated and reported in different, frequently used EFT bases. The effects of EFT modifications in backgrounds are found to be negligible because of the high purity of the signal peak in the four-lepton invariant mass distribution and further constraints on the backgrounds from sidebands.

Each production process of the H boson is identified using its kinematic features, and events are assigned to corresponding categories. Two categorization schemes are employed in this analysis, one targeting Htt and Hgg and the other targeting HVV anomalous couplings. Within each category, the matrix element likelihood approach (MELA) [29–33] is employed to construct observables that are optimal for the measurement of the chosen anomalous couplings, or EFT operators, including *CP*-sensitive observables to search for *CP*-violating operators. In our approach, fully simulated Monte Carlo (MC) signal samples that include anomalous couplings allow the incorporation of detector effects into the likelihood analysis, and observables explore all kinematic features of the events, including those sensitive to *CP* violation and to simultaneous anomalous effects in the production and decay of the H boson. These features distinguish our analysis from the recent measurements by the ATLAS Collaboration in the same $\mathrm{H} \to 4\ell$ decay channel [34, 35], in which case the measurements are derived from the differential distributions based on either the simplified template cross sections (STXS) [28] or unfolded fiducial measurements.

We follow the formalism used in the study of anomalous couplings in the earlier analyses of CMS data in Refs. [11–18, 26]. We focus on the measurements where the H boson is produced on-shell; the extension to the off-shell region is considered in Ref. [17], where joint constraints on the H boson width Γ_{H} and its anomalous couplings are obtained using a partial data set. Some of the theoretical foundations relevant to the present analysis can be found in Refs. [28–33, 36–66]. The results are presented in a model-independent way, which allows interpretation in the scattering amplitude or effective Lagrangian approach, for example in the frameworks of the standard model effective field theory (SMEFT) [67–70] or pseudo observables (PO) [28].

Compared to our previous results on anomalous HVV couplings [16, 17], which used a subset of the data presented here, several substantial improvements have been introduced. First, as a result of the increased number of $\mathrm{H} \to 4\ell$ events, the expected 95% confidence level (CL)

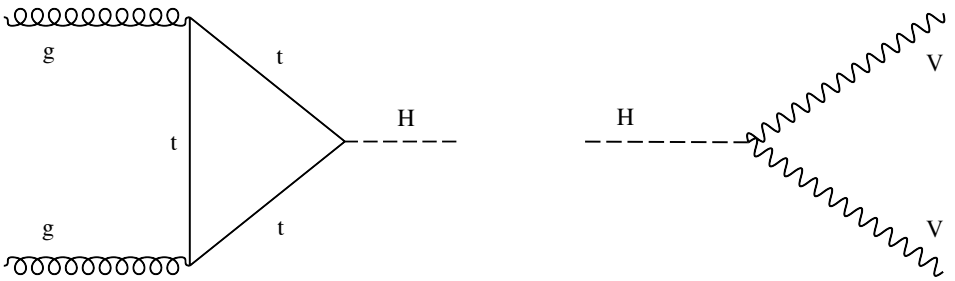

Figure 1: Leading-order Feynman diagrams for the gluon fusion production mode (left) and $H \to VV$ decay (right).

constraints on HVV couplings are now dominated by the tight limits from the analysis of kinematic distributions of particles produced in association with the H boson in the VBF and VH processes. Second, an improved fit implementation allows for the simultaneous measurement of up to five independent HVV, two Hgg, and two Htt couplings using the single decay channel $H \to 4\ell$. The couplings are parameterized with the signal strength and the fractional cross section contributions of the anomalous couplings. A direct constraint on *CP* violation in the Hgg coupling is obtained for the first time by employing *CP*-sensitive observables. The *CP* violation measurement in the Htt coupling closely follows our recent measurement in the $H \to \gamma\gamma$ channel [26], and the results are combined. We also perform the first study of *CP* properties in the Htt and effective Hgg couplings from a simultaneous analysis of the gluon fusion and top-associated processes. For all anomalous couplings, we interpret our results via the SMEFT framework in terms of HVV, Hgg, and Htt operators.

The rest of this paper is organized as follows. The phenomenology of anomalous HVV, Hgg, and Hff couplings and considerations in the EFT framework are discussed in Section 2. The data and MC simulation, event reconstruction and selection are discussed in Section 3. The kinematic variables associated with the H boson's production and decay and its MELA analysis are introduced in Section 4. The implementation of the maximum likelihood fit is shown in Section 5. The results are presented and discussed in Section 6. We conclude in Section 7.

2 Parameterization of H boson production and decay processes

The goal of this study is to search for *CP* violation and, more generally, anomalous couplings of the H boson, in its interactions with fermions and vector bosons in the production and decay processes. These potential sources of *CP* violation and anomalous tensor structures of interactions may arise from BSM effects, including those considered in the EFT formulation. The dominant processes sensitive to such interactions are shown in Figs. 1–5 [28].

The main decay process considered in this paper is $H \to VV \to 4\ell$, with the HVV vertex shown in Fig. 1, right. The dominant H boson production mechanism is gluon fusion ggH, shown in Fig. 1, left. The dominant contribution to the gluon fusion loop comes from the top quark, with smaller contributions from the bottom quark and lighter quarks. However, contribution of new BSM states to the loop and variation of *CP* properties of the H boson couplings to SM quarks are also possible and are considered in this paper. The HVV vertex also appears in the vector boson fusion VBF and associated production with a weak vector boson ZH or WH, shown in Fig. 2, which are the next dominant production mechanisms of the H boson.

The production of an H boson in association with a top quark pair $t\bar{t}H$ is shown in Fig. 3, left. This is the main channel that allows to study the *CP* property in the H boson coupling

to fermions. We also combine our results with the recent $t\bar{t}H$ measurements in the $H \to \gamma\gamma$ channel [26]. The production of an H boson in association with a single top quark tH is shown in Fig. 4. This production receives contributions from both HVV and Htt couplings, but its expected cross section is smaller than that of $t\bar{t}H$. Both HVV and Htt couplings also contribute to the $gg \to ZH$ production mode, shown in Fig. 5. However, this gluon fusion production mode of ZH is expected to contribute only about 5% of the VH process cross section shown in Fig. 2, the dependence on anomalous HVV couplings is suppressed in this process [33], and for these reasons this production mode is neglected in this analysis. Finally, we also consider the $b\bar{b}H$ production mode shown in Fig. 3, right. However, this process does not provide kinematic features that could distinguish the *CP* structure of interactions [32] or the experimental signatures that would allow its isolation from the other more dominant production mechanisms.

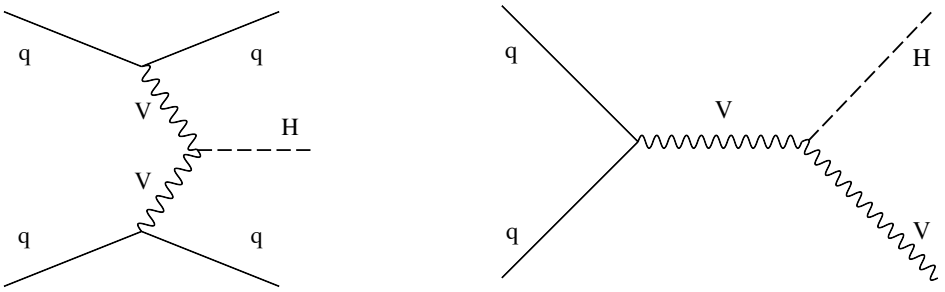

Figure 2: Leading-order Feynman diagrams for the VBF (left) and VH (right) production modes.

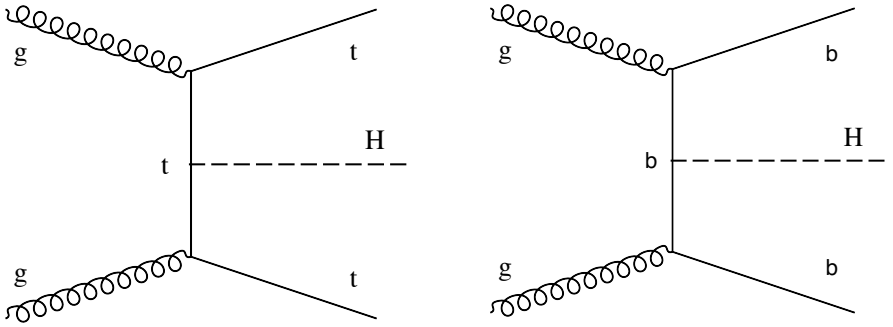

Figure 3: Examples of leading-order Feynman diagrams for the $t\bar{t}H$ (left) and $b\bar{b}H$ (right) production modes.

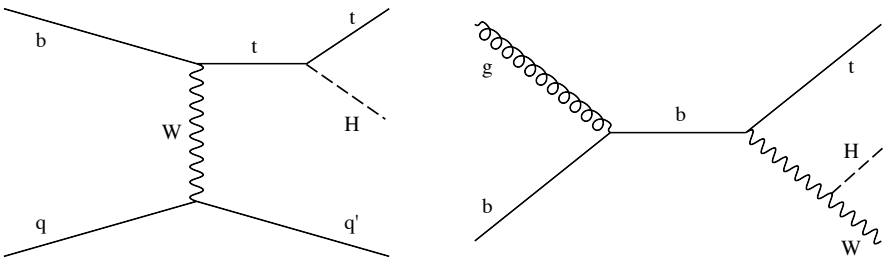

Figure 4: Examples of leading-order Feynman diagrams for the tH production mode.

2.1 Parameterization of production and decay amplitudes

Anomalous effects in the H boson couplings to fermions, such as in the $t\bar{t}H$ and $b\bar{b}H$ production and partially in the tH and $gg \to ZH$ production, can be parameterized with the

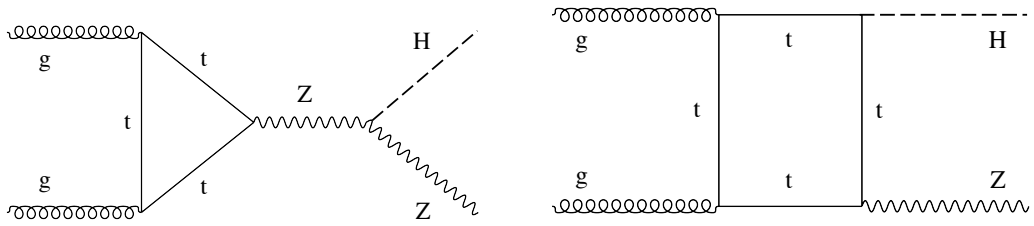

Figure 5: Leading-order Feynman diagrams for the gg $\to$ ZH production mode.

amplitude

$$A(\mathrm{Hff}) = -\frac{m_\mathrm{f}}{v}\overline{\psi}_\mathrm{f}\left(\kappa_\mathrm{f} + \mathrm{i}\tilde{\kappa}_\mathrm{f}\gamma_5\right)\psi_\mathrm{f}, \tag{1}$$

defined for each fermion type f, where $\overline{\psi}_\mathrm{f}$ and ψ_f are the fermions' Dirac spinors, κ_f and $\tilde{\kappa}_\mathrm{f}$ are the corresponding coupling strengths, m_f is the fermion mass, and v is the SM Higgs field vacuum expectation value. In the SM, the coupling strengths are $\kappa_\mathrm{f} = 1$ and $\tilde{\kappa}_\mathrm{f} = 0$. The presence of both CP-even κ_f and CP-odd $\tilde{\kappa}_\mathrm{f}$ couplings will lead to CP violation. In an experimental analysis of the $\mathrm{b\bar{b}H}$ process it is not possible to resolve the κ_b and $\tilde{\kappa}_\mathrm{b}$ couplings [32], but it is possible to resolve the κ_t and $\tilde{\kappa}_\mathrm{t}$ couplings in the $\mathrm{t\bar{t}H}$ and tH processes, which we explore in this paper.

Anomalous effects in EW H boson production (VBF, ZH, and WH), ggH production, H $\to$ VV decay, and partially in the tH and gg $\to$ ZH production, are described by the $\mathrm{HV_1V_2}$ couplings. The scattering amplitude describing the interaction between a spin-zero H boson and two spin-one gauge bosons $\mathrm{V_1V_2}$, such as ZZ, Zγ, $\gamma\gamma$, WW, or gg, is written as

$$A(\mathrm{HV_1V_2}) = \frac{1}{v}\left[a_1^{\mathrm{VV}} + \frac{\kappa_1^{\mathrm{VV}}q_{\mathrm{V1}}^2 + \kappa_2^{\mathrm{VV}}q_{\mathrm{V2}}^2}{\left(\Lambda_1^{\mathrm{VV}}\right)^2} + \frac{\kappa_3^{\mathrm{VV}}(q_{\mathrm{V1}}+q_{\mathrm{V2}})^2}{\left(\Lambda_\mathrm{Q}^{\mathrm{VV}}\right)^2}\right] m_{\mathrm{V1}}^2\epsilon_{\mathrm{V1}}^*\epsilon_{\mathrm{V2}}^* + \frac{1}{v}a_2^{\mathrm{VV}}f_{\mu\nu}^{*(1)}f^{*(2),\mu\nu} + \frac{1}{v}a_3^{\mathrm{VV}}f_{\mu\nu}^{*(1)}\tilde{f}^{*(2),\mu\nu}, \tag{2}$$

where $f^{(i)\mu\nu} = \epsilon_{\mathrm{V}i}^\mu q_{\mathrm{V}i}^\nu - \epsilon_{\mathrm{V}i}^\nu q_{\mathrm{V}i}^\mu$, $\tilde{f}_{\mu\nu}^{(i)} = \frac{1}{2}\epsilon_{\mu\nu\rho\sigma}f^{(i),\rho\sigma}$, and $\epsilon_{\mathrm{V}i}$, $q_{\mathrm{V}i}$, and $m_{\mathrm{V}i}$ are the polarization vector, four-momentum, and pole mass of a gauge boson $i = 1$ or 2. The constants Λ_1 and Λ_Q are the scales of BSM physics necessary to keep the κ_i^{VV} couplings unitless, and a_1^{VV}, a_2^{VV}, a_3^{VV}, κ_1^{VV}, κ_2^{VV}, and κ_3^{VV} are real numbers that modify the corresponding amplitude terms. Equation (2) describes couplings to both EW bosons and gluons, so $\mathrm{HV_1V_2}$ can stand for HVV or Hgg.

In Eq. (2), the only nonzero tree-level contributions in the SM are $a_1^{\mathrm{ZZ}} \neq 0$ and $a_1^{\mathrm{WW}} \neq 0$. In the SM, $a_1^{\mathrm{ZZ}} = a_1^{\mathrm{WW}} = 2$. The rest of the ZZ and WW couplings are considered to be anomalous contributions, which are either small contributions arising in the SM because of loop effects or new BSM contributions. Among the anomalous contributions, considerations of symmetry and gauge invariance require $\kappa_1^{\mathrm{ZZ}} = \kappa_2^{\mathrm{ZZ}}$, $\kappa_1^{\mathrm{WW}} = \kappa_2^{\mathrm{WW}}$, and $a_1^{\mathrm{Z}\gamma} = a_1^{\gamma\gamma} = a_1^{\mathrm{gg}} = \kappa_1^{\gamma\gamma} = \kappa_2^{\gamma\gamma} = \kappa_1^{\mathrm{gg}} = \kappa_2^{\mathrm{gg}} = \kappa_1^{\mathrm{Z}\gamma} = \kappa_3^{\mathrm{VV}} = 0$ [33]. Therefore, there are a total of 13 independent parameters describing couplings of the H boson to EW gauge bosons and two parameters describing couplings to gluons. The presence of any of the CP-odd couplings a_3^{VV} together with any of the other couplings, which are all CP-even, will lead to CP violation in a given process.

Since in our analysis it is not possible to disentangle the top quark, bottom quark, and any other heavy BSM particle contributions to the gluon fusion loop from kinematic features of the event, we parameterize the Hgg coupling with only two parameters: CP-even a_2^{gg} and CP-odd a_3^{gg}, which absorb all SM and BSM loop contributions. However, when the gluon fusion process is analyzed jointly with the $t\bar{t}H$ and tH processes, it may be possible to disentangle the top quark contributions in the loop from the relative rates of the processes, and we allow these contributions to be separated.

2.2 Symmetry considerations and SMEFT formulation

The formulation in Eqs. (1) and (2) is presented in the approach of anomalous amplitude decomposition. However, it is fully equivalent to the Lagrangian parameterization with dimension-4 operators, such as the a_1^{VV} term in Eq. (2), and dimension-6 operators, such as the other terms in Eq. (2), using the mass eigenstate basis [28]. The dimension-8 and higher-dimension contributions are neglected. We apply additional symmetry considerations discussed below, which reduce the number of independent parameters to be measured. The chosen basis coincides with the Higgs basis [28] under SU(2)×U(1) symmetry. The choice of the EFT operator basis is motivated by the natural parameterization in terms of observable states and, as a consequence, allows more transparent construction of the data analysis and presentation of the results. However, we also present results in the Warsaw basis [28], using tools in Refs. [33, 71] to perform the translation. Our approach with SU(2)×U(1) symmetry is equivalent to the SMEFT formulation [28].

The parameterization in Eq. (2) is the most general one, and we apply SU(2)×U(1) symmetry in the relationships of anomalous couplings as follows [28, 33]:

$$a_1^{WW} = a_1^{ZZ} + \frac{\Delta m_W}{m_W}, \tag{3}$$

$$a_2^{WW} = c_w^2 a_2^{ZZ} + s_w^2 a_2^{\gamma\gamma} + 2 s_w c_w a_2^{Z\gamma}, \tag{4}$$

$$a_3^{WW} = c_w^2 a_3^{ZZ} + s_w^2 a_3^{\gamma\gamma} + 2 s_w c_w a_3^{Z\gamma}, \tag{5}$$

$$\frac{\kappa_1^{WW}}{(\Lambda_1^{WW})^2}(c_w^2 - s_w^2) = \frac{\kappa_1^{ZZ}}{(\Lambda_1^{ZZ})^2} + 2 s_w^2 \frac{a_2^{\gamma\gamma} - a_2^{ZZ}}{m_Z^2} + 2\frac{s_w}{c_w}(c_w^2 - s_w^2)\frac{a_2^{Z\gamma}}{m_Z^2}, \tag{6}$$

$$\frac{\kappa_2^{Z\gamma}}{(\Lambda_1^{Z\gamma})^2}(c_w^2 - s_w^2) = 2 s_w c_w \left(\frac{\kappa_1^{ZZ}}{(\Lambda_1^{ZZ})^2} + \frac{a_2^{\gamma\gamma} - a_2^{ZZ}}{m_Z^2} \right) + 2(c_w^2 - s_w^2)\frac{a_2^{Z\gamma}}{m_Z^2}, \tag{7}$$

where $c_w = \cos\theta_W$, $s_w = \sin\theta_W$, m_W and m_Z are the W and Z boson masses, and Δm_W is a shift in the W mass. Since m_W is measured to high precision [72], we set $\Delta m_W = 0$, leading to $a_1^{ZZ} = a_1^{WW}$. The latter relationship also appears under custodial symmetry [73]. Therefore, the set of $13 + 2$ independent parameters describing the HVV + Hgg couplings can be reduced to $8 + 2$ with the above symmetry relationships.

In our measurements, we further reduce the number of independent parameters in the following way. We assume that the four loop-induced couplings $a_{2,3}^{\gamma\gamma}$ and $a_{2,3}^{Z\gamma}$ are constrained to yield the SM rates of the direct decays $H \to \gamma\gamma$ and $Z\gamma$. Therefore, in our analysis of EW production and $H \to 4\ell$ decay, we set these four couplings to zero because their allowed values are expected to have negligible effect in our coupling measurements. These four anomalous couplings have been tested in our earlier analysis of the $H \to VV \to 4\ell$ process with Run 1 data [13] and the obtained constraints were significantly looser than those from the direct decays with on-shell photons.

We adopt two approaches to set the relationship between the HZZ and HWW couplings. The HWW couplings do not contribute to the $H \to 4\ell$ decay, but they do contribute to the EW production. In this paper, the relationship between the HZZ and HWW couplings is mostly relevant for VBF production with ZZ and WW fusion. There are no kinematic differences between these two processes and it is impossible to disentangle the HZZ and HWW couplings from these data. We used Approach 1 in our previous publications [16–18], where we set $a_i^{WW} = a_i^{ZZ}$. Approach 2 corresponds to the SMEFT formulation with SU(2)×U(1) symmetry.

In Approach 1, we set the ZZ and WW couplings to be equal, $a_i^{WW} = a_i^{ZZ}$. Formally, this could be considered as the relationship in Eqs. (3–6) in the limiting case $c_w = 1$. As a result, we are left with four anomalous couplings to be measured, in addition to the SM-like couplings a_1: a_2, a_3, $\kappa_1/(\Lambda_1)^2$, and $\kappa_2^{Z\gamma}/(\Lambda_1^{Z\gamma})^2$, where we drop the ZZ superscript from the couplings. We adopt this approach both for its simplicity and to be able to relate the four anomalous couplings constrained with the $H \to 4\ell$ decay to the equivalent four couplings in the PO approach. This requires an independent measurement of the $\kappa_2^{Z\gamma}$ term, which would otherwise be eliminated by the relationship in Eq. (7). Therefore, this approach is slightly less restrictive than the SMEFT formulation adopted in Approach 2 discussed below.

In Approach 2, we adopt the full set of SU(2)×U(1) symmetry relationships in Eqs. (3–7) with $s_w^2 = 0.23119$ [72]. The number of independent HVV parameters is further reduced from five to four: a_1, a_2, a_3, and $\kappa_1/(\Lambda_1)^2$. There is a linear one-to-one relationship between the amplitude couplings in Eq. (2) and the EFT couplings in the Higgs basis in the notation of Refs. [28, 33]:

$$\delta c_z = \frac{1}{2}a_1 - 1, \tag{8}$$

$$c_{z\Box} = \frac{m_Z^2 s_w^2}{4\pi\alpha}\frac{\kappa_1}{(\Lambda_1)^2}, \tag{9}$$

$$c_{zz} = -\frac{s_w^2 c_w^2}{2\pi\alpha}a_2, \tag{10}$$

$$\tilde{c}_{zz} = -\frac{s_w^2 c_w^2}{2\pi\alpha}a_3. \tag{11}$$

Ignoring small loop-induced corrections, the above four parameters are expected to be zero in the SM. Since we set $a_{2,3}^{\gamma\gamma}$ and $a_{2,3}^{Z\gamma}$ to zero, the four corresponding parameters in the EFT Higgs basis $c_{\gamma\gamma}$, $c_{z\gamma}$, $\tilde{c}_{\gamma\gamma}$, and $\tilde{c}_{z\gamma}$ are also zero.

In the case of Hgg couplings, the two EFT parameters are defined following the notation of Refs. [28, 33] as:

$$c_{gg} = -\frac{1}{2\pi\alpha_S}a_2^{gg}, \tag{12}$$

$$\tilde{c}_{gg} = -\frac{1}{2\pi\alpha_S}a_3^{gg}, \tag{13}$$

where in the SM, $c_{gg} = 0$ and $\tilde{c}_{gg} = 0$, and the SM process is generated by the quark loop not accounted for in the a_2^{gg} coupling. Finally, in the case of the Hff couplings, the κ_f and $\tilde{\kappa}_f$ parameters in Eq. (1) can be treated as EFT parameters [28], where in the SM, $\kappa_f = 1$ and $\tilde{\kappa}_f = 0$.

2.3 Parameterization of cross sections

We use the narrow-width approximation and parameterize differential cross section of the on-shell H boson production process j and decay to a final state f following Refs. [28, 33] as:

$$\sigma(j \to \mathrm{H} \to f) \propto \frac{\left(\sum_{il} \alpha_{il}^{(j)} a_i a_l\right)\left(\sum_{mn} \alpha_{mn}^{(f)} a_m a_n\right)}{\Gamma_{\mathrm{H}}}, \tag{14}$$

where a_i are the real couplings describing the Hff, Hgg, or HVV interactions and include generically the κ_i in Eqs. (1) and (2). The coefficients $\alpha_{il}^{(k)}$ are in general functions of kinematic observables for the differential cross section distributions and are modeled with simulation. The total width Γ_{H} depends on the couplings a_i and potentially on the partial decay width to unobserved or invisible final states, a dependence that must be taken into account when interpreting cross section measurements in terms of couplings.

When we perform the amplitude analysis of the data, in the likelihood based on Eq. (14), we keep all cross-terms in the expansion of powers of Λ^{-N} with $N = 0, 2, 4, 6, 8$, where formally each dimension-6 operator, or anomalous a_i coupling, receives the Λ^{-2} contribution in Eq. (2), even if not explicitly shown, while the SM tree-level coupling carries no such contribution. While this may create inconsistency in the EFT approach with the Λ^{-N} terms kept or neglected from the higher-dimension contributions, this allows us to keep the likelihood positive definite, which is an important consideration in the experimental analysis of the data discussed in Section 5. Because interference contributions may become negative, dropping certain terms in the expansion may lead to negative probability. The importance of $N = 4, 6, 8$ contributions may be considered as testing whether the current precision is sufficient to treat our results within the EFT approach, and we leave this test to the interpretation of the results. However, regardless of EFT validity, our results are presented in a fully self-consistent formulation of amplitude decomposition, which can either be translated to the EFT interpretation or treated as a test of consistency of the data with the SM, including the search for new sources of CP violation.

2.4 Parameterization of the signal strength and cross section fractions

We present the primary results in terms of cross sections, or equivalently, signal strengths $\mu_j = \sigma_j/\sigma_j^{\mathrm{SM}}$, and the fractional contributions f_{ai} of the couplings a_i to cross sections $(\sum_{mn} \alpha_{mn} a_m a_n)$ of a given decay process. The ratios of couplings entering Eq. (14) can be expressed through f_{ai}, and the common factors, such as the total width Γ_{H} and the SM-like coupling squared, are absorbed into the signal strength. This formulation with μ_j and f_{ai} allows presentation of experimental results in the most direct way, with a minimal and complete set of parameters describing the given processes. This approach has several convenient features. The cross sections and their ratios are invariant with respect to the coupling convention, such as the scaling in Eqs. (8–13). The cross section fractions f_{ai} reflect kinematic features in either production or decay in a direct way. They are conveniently bound between -1 and $+1$, and most systematic uncertainties cancel in the ratio.

The cross section fraction for Hff couplings is defined as

$$f_{\mathrm{CP}}^{\mathrm{Hff}} = \frac{|\tilde{\kappa}_{\mathrm{f}}|^2}{|\kappa_{\mathrm{f}}|^2 + |\tilde{\kappa}_{\mathrm{f}}|^2}\ \mathrm{sign}\left(\frac{\tilde{\kappa}_{\mathrm{f}}}{\kappa_{\mathrm{f}}}\right). \tag{15}$$

Similarly, the cross section fraction for Hgg couplings is defined as

$$f_{a3}^{\mathrm{ggH}} = \frac{|a_3^{\mathrm{gg}}|^2}{|a_2^{\mathrm{gg}}|^2 + |a_3^{\mathrm{gg}}|^2}\ \mathrm{sign}\left(\frac{a_3^{\mathrm{gg}}}{a_2^{\mathrm{gg}}}\right). \tag{16}$$

Both definitions incorporate the relative sign of the possible BSM CP-odd and SM-like CP-even couplings. They are based on the observation that the cross sections of the $\mathrm{H} \to \mathrm{gg}$ process are equal for $a_2^{\mathrm{gg}} = 1$ and $a_3^{\mathrm{gg}} = 1$, as are the cross sections of the $\mathrm{H} \to \mathrm{f\bar{f}}$ process for $\kappa_\mathrm{f} = 1$ and $\tilde{\kappa}_\mathrm{f} = 1$ in the limit of $m_\mathrm{f} \ll m_\mathrm{H}$. We note that f_{a3}^{ggH} is defined following the convention that a_2^{gg} and a_3^{gg} absorb both point-like interactions and quark contributions to the loop. Following Ref. [33], the f_{a3}^{ggH} measurement can also be interpreted in terms of $f_{\mathrm{CP}}^{\mathrm{Hff}}$ under the assumption that only the top and bottom quarks contribute to gluon fusion with $\kappa_\mathrm{t} = \kappa_\mathrm{b}$ and $\tilde{\kappa}_\mathrm{t} = \tilde{\kappa}_\mathrm{b}$:

$$|f_{\mathrm{CP}}^{\mathrm{Hff}}| = \left(1 + 2.38 \left[\frac{1}{|f_{a3}^{\mathrm{ggH}}|} - 1\right]\right)^{-1} = \sin^2 \alpha^{\mathrm{Hff}}, \tag{17}$$

where the signs of $f_{\mathrm{CP}}^{\mathrm{Hff}}$ and f_{a3}^{ggH} are equal, and α^{Hff} is an effective parameter sometimes used to describe the CP-odd contribution to the H boson Yukawa couplings. A more detailed analysis of the gluon fusion loop could be performed without the assumption that only the top and bottom quarks contribute.

The cross section fractions in the HVV couplings of the H boson to EW gauge bosons require more parameters. Since in both of our approaches the HWW couplings are expressed through other a_i^{VV} couplings following Eqs. (3–6), and because we prefer that our definitions not depend on parton distribution functions (PDFs) and other effects that involve measurement uncertainties, we use the $\mathrm{H} \to \mathrm{ZZ}$ / $\mathrm{Z}\gamma^*$ / $\gamma^*\gamma^* \to 2\mathrm{e}2\mu$ decay process to define the cross section fractions as

$$f_{ai}^{\mathrm{VV}} = \frac{|a_i^{\mathrm{VV}}|^2 \alpha_{ii}^{(2\mathrm{e}2\mu)}}{\sum_j |a_j^{\mathrm{VV}}|^2 \alpha_{jj}^{(2\mathrm{e}2\mu)}} \operatorname{sign}\left(\frac{a_i^{\mathrm{VV}}}{a_1}\right), \tag{18}$$

where the $\alpha_{ii}^{(2\mathrm{e}2\mu)}$ coefficients are introduced in Eq. (14). The numerical values of these coefficients are given in Table 1, where they are normalized with respect to the $\alpha_{11}^{(2\mathrm{e}2\mu)}$ coefficient, corresponding to the cross section calculated for $a_1 = 1$. The $\alpha_{ii}^{(2\mathrm{e}2\mu)}$ are the cross sections for $a_i^{\mathrm{VV}} = 1$, which are different in the two approaches of the coupling relationship as a result of Eq. (7) adopted in Approach 2. The cross section fractions in Eq. (18) can be converted to coupling ratios as

$$\frac{a_i^{\mathrm{VV}}}{a_j^{\mathrm{VV}}} = \sqrt{\frac{|f_{ai}^{\mathrm{VV}}| \alpha_{jj}^{(2\mathrm{e}2\mu)}}{|f_{aj}^{\mathrm{VV}}| \alpha_{ii}^{(2\mathrm{e}2\mu)}}} \operatorname{sign}\left(f_{ai}^{\mathrm{VV}} f_{aj}^{\mathrm{VV}}\right). \tag{19}$$

The measured values of μ_j and f_{ai} should be sufficient to adopt them in the fits for EFT parameters jointly with the data from other H boson, top quark, and EW measurements. They allow constraints on the κ_i and a_i couplings in Eqs. (1) and (2). However, it is required to perform a simultaneous measurement of all production and decay channels of the H boson, including unobserved and invisible channels, as they contribute to the total width in Eq. (14). In this paper, we present only a limited interpretation of our data in terms of couplings by making certain assumptions about their relationship. We leave more extensive interpretation to a future combination with other channels.

Table 1: List of anomalous HVV couplings a_i^{VV} considered, the corresponding measured cross section fractions f_{ai}^{VV} defined in Eq. (18), and the translation coefficients α_{ii}/α_{11} in this definition with the relationship $a_i^{ZZ} = a_i^{WW}$ (Approach 1), and with the SMEFT relationship according to Eqs. (3–7) (Approach 2). In the case of the κ_1 and $\kappa_2^{Z\gamma}$ couplings, the numerical values $\Lambda_1 = \Lambda_1^{Z\gamma} = 100\,\text{GeV}$ are adopted in this calculation to make the coefficients have the same order of magnitude.

Coupling a_i^{VV}	Fraction f_{ai}^{VV}	Approach 1 α_{ii}/α_{11}	Approach 2 α_{ii}/α_{11}
a_3	f_{a3}	0.153	0.153
a_2	f_{a2}	0.361	6.376
κ_1	$f_{\Lambda 1}$	0.682	5.241
$\kappa_2^{Z\gamma}$	$f_{\Lambda 1}^{Z\gamma}$	1.746	—

3 The CMS detector, data sets, and event reconstruction

The $H \to 4\ell$ decay candidates are produced in proton-proton (pp) collisions at the LHC and are collected and reconstructed in the CMS detector [74]. The data sample used in this analysis corresponds to integrated luminosities of 35.9 fb^{-1} collected in 2016, 41.5 fb^{-1} collected in 2017, and 59.7 fb^{-1} collected in 2018, for a total of 137 fb^{-1} collected during Run 2 at a pp center-of-mass energy of 13 TeV.

The CMS detector comprises a silicon pixel and strip tracker, a lead tungstate crystal electromagnetic calorimeter (ECAL), and a brass/scintillator hadron calorimeter, each composed of a barrel and two endcap sections, all within a superconducting solenoid of 6 m internal diameter, providing a magnetic field of 3.8 T. Extensive forward calorimetry complements the coverage provided by the barrel and endcap detectors. Outside the solenoid are the gas-ionization detectors for muon measurements, which are embedded in the steel flux-return yoke. A detailed description of the CMS detector can be found in Ref. [74].

Events of interest are selected using a two-tiered trigger system. The first level, composed of custom hardware processors, uses information from the calorimeters and muon detectors to select events at a rate of around 100 KHz within a fixed latency of about 4 μs [75]. The second level, known as the high-level trigger, consists of a farm of processors running a version of the full event reconstruction software optimized for fast processing, and reduces the event rate to around 1 KHz before data storage [76].

3.1 Event reconstruction and selection

The selection of 4ℓ events and associated particles closely follows the methods used in the analyses of the Run 1 [12, 13] and Run 2 [16, 17, 77, 78] data sets. The main triggers for the Run 2 analysis select either a pair of electrons or muons, or an electron and a muon, passing loose identification and isolation requirements. The transverse momentum (p_T) for the leading electron or muon is required to be larger than 23 or 17 GeV, while that of the subleading lepton is required to be larger than 12 or 8 GeV, respectively. To maximize the signal acceptance, triggers requiring three leptons with lower p_T thresholds and no isolation requirement are also used, as well as isolated single-electron and single-muon triggers with thresholds of 27 and 22 GeV in 2016, or 35 and 27 GeV in 2017 and 2018, respectively. The overall trigger efficiency for simulated signal events that pass the full selection chain of this analysis is larger than 99%.

Event reconstruction is based on the particle-flow algorithm [79], which exploits information from all the CMS subdetectors to identify and reconstruct individual particles in the event. The particle-flow candidates are classified as charged or neutral hadrons, photons, electrons, or muons, and they are then used to build higher-level objects, such as jets, and to calculate the lepton isolation quantities. Electrons or muons are reconstructed within the geometrical acceptance defined by a requirement on the pseudorapidity $|\eta| < 2.5$ or 2.4 and $p_{\mathrm{T}} > 7$ or 5 GeV, with an algorithm that combines information from the tracker and the ECAL or muon system, respectively. Muons are selected from a list of reconstructed muon track candidates by applying minimal requirements on the track in both the muon system and inner tracker system, and taking into account compatibility with small energy deposits in the calorimeters.

To discriminate between leptons from prompt particle decays and those arising from hadron decays within jets, an isolation variable is calculated for electrons and muons [78]. An isolation requirement is imposed on the muons. Electrons are identified using a multivariate discriminant which includes observables sensitive to the presence of bremsstrahlung along the electron trajectory, the geometrical and momentum-energy matching between the electron trajectory and the associated cluster in the ECAL, the shape of the electromagnetic shower in the ECAL, and variables that discriminate against electrons originating from photon conversions. This discriminant also includes the isolation to suppress electrons originating from EW decays of hadrons within jets [78]. A dedicated algorithm is used to collect the final-state radiation of leptons [77].

The jets are clustered using the anti-k_{T} jet finding algorithm [80, 81] with a distance parameter of 0.4. The jet momentum is determined as the vector sum of all particle momenta in the jet. Jets must satisfy $p_{\mathrm{T}} > 30$ GeV and $|\eta| < 4.7$ and must be separated from all selected lepton candidates and any selected final-state radiation photons with a requirement on the distance parameter $\Delta R(\ell/\gamma, \mathrm{jet}) > 0.4$, where $(\Delta R)^2 = (\Delta\eta)^2 + (\Delta\phi)^2$. Jets are b-tagged using the DeepCSV algorithm [82], which combines information about impact parameter significance, the secondary vertex, and jet kinematics.

The reconstructed vertex with the largest value of summed physics-object p_{T}^2 is taken to be the primary pp interaction vertex. The physics objects are the jets, clustered using the jet finding algorithm [80, 81] with the tracks assigned to candidate vertices as inputs, and the associated missing transverse momentum, taken as the negative vector p_{T} sum of those jets. In order to suppress muons from in-flight decays of hadrons and electrons from photon conversions, leptons are rejected if the ratio of their impact parameter in three dimensions, computed with respect to the primary vertex position, to their uncertainty is greater than four.

We consider three mutually exclusive lepton flavor channels: $\mathrm{H} \to \mathrm{VV} \to 4\mathrm{e}$, 4μ, and $2\mathrm{e}2\mu$. At least two leptons are required to have $p_{\mathrm{T}} > 10$ GeV, and at least one is required to have $p_{\mathrm{T}} > 20$ GeV. All four pairs of oppositely charged leptons that can be built with the four leptons are required to satisfy $m_{\ell^+\ell^-} > 4$ GeV, regardless of lepton flavor, to further suppress events with leptons originating from hadron decays in jet fragmentation or from the decay of low-mass resonances. The V candidates are formed with pairs of leptons of the same flavor and opposite charge that pass the requirement $12 < m_{\ell^+\ell^-} < 120$ GeV, where m_1 is the invariant mass of the V candidate that is closest to the nominal Z boson mass and m_2 is the mass of the other one. A value of $m_1 > 40$ GeV is required. The reconstructed four-lepton invariant mass, $m_{4\ell}$, distribution in the region between 70 and 170 GeV is shown in Fig. 6. The $m_{4\ell}$ region between 105 and 140 GeV is considered in this analysis, which is wide enough to use sidebands for constraining the background normalization in the later fitting procedure [78].

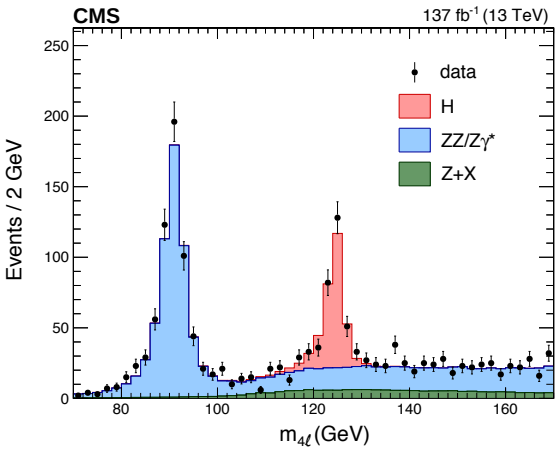

Figure 6: Four-lepton invariant mass distribution of observed events (data points) and expectation from MC simulation or background estimates (histograms) in the region between 70 and 170 GeV [78]. The peaks from the Z and H $\rightarrow 4\ell$ decays are visible near 91 and 125 GeV, respectively.

3.2 Event categorization

In order to perform a dedicated study of a particular kinematic topology, events are further split into several mutually exclusive categories based on the presence of other particles produced in association with the H boson candidate [78]. Two independent categorization, Schemes 1 and 2, discussed below, are followed in this study. Scheme 1 targets Htt and Hgg anomalous couplings, while Scheme 2 targets HVV anomalous couplings.

We use the values of kinematic discriminants and other selection requirements to perform the categorization. The definition of these discriminants can be found in Refs. [16, 17, 77, 78] and is further discussed in Section 4. They are calculated using the MELA approach while employing the matrix elements at leading order (LO) in quantum chromodynamics (QCD). These discriminants use full kinematic information from the H boson and from associated jet production and are labeled to indicate a specific topology (1jet, 2jet) and production mechanism (VBF, WH, ZH), which is discriminated against the dominant gluon fusion process: $\mathcal{D}^{\text{VBF}}_{\text{1jet}}$, $\mathcal{D}^{\text{VBF}}_{\text{2jet}}$, $\mathcal{D}^{\text{ZH}}_{\text{2jet}}$, and $\mathcal{D}^{\text{WH}}_{\text{2jet}}$. The $\mathcal{D}_{\text{2jet}}$ discriminants are calculated using both SM and anomalous coupling hypotheses, leading to a set $\mathcal{D}^{i}_{\text{2jet}}$, all of which are tested in order to maintain high efficiency of VBF and VH categorization in the presence of anomalous couplings. The discriminants defined for the two-jet topology are illustrated in Fig. 7, where the expected distributions are based on the MC signal simulation discussed in Section 3.3 and the background estimate in Section 3.4. To enhance the signal to background ratio in this illustration in Fig. 7, a selection of $\mathcal{D}_{\text{bkg}} > 0.7$ is applied. This observable uses information from the lepton kinematic distributions and does not use information from associated jets, as also discussed in Section 4.

In categorization Scheme 1, the Htt and Hgg anomalous couplings are targeted. The categories and selection criteria are identical to the first step of the categorization scheme in Ref. [78] and are optimized to measure the rates of H boson production modes. Because anomalous Htt and Hgg couplings have only a small effect on the fractions of $\text{t}\bar{\text{t}}\text{H}$ and ggH events in each category, the optimization based on SM kinematic distributions used for the study in Ref. [78] remains optimal here. The sequential selection criteria in Scheme 1 are as follows:

– The VBF-2jet category requires exactly four leptons. In addition, there must be either two or three jets of which at most one is b-tagged, or at least four jets and no b-tagged

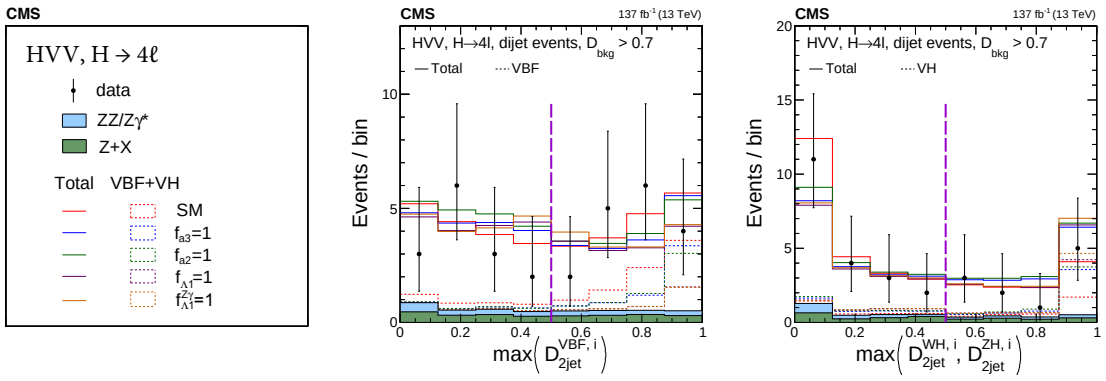

Figure 7: The distributions of observed events (data points) and expectation (histograms) for $\max\left(\mathcal{D}_{\text{2jet}}^{\text{VBF},i}\right)$ (middle) and $\max\left(\mathcal{D}_{\text{2jet}}^{\text{WH},i}, \mathcal{D}_{\text{2jet}}^{\text{ZH},i}\right)$ (right), where maximum is evaluated over the the SM and the four anomalous coupling hypotheses i, described in the legend (left). Only events with at least two reconstructed jets are shown, and the requirement $\mathcal{D}_{\text{bkg}} > 0.7$ is applied in order to enhance the signal contribution over the background, where $\mathcal{D}_{\text{bkg}}$ is calculated using decay information only. The expectation is shown for the total distribution, including background and all production mechanisms of the H boson, and for the VBF (middle) and VH (right) signals, which are enhanced in the region above 0.5, indicated with the vertical dashed line.

jets. Finally, $\mathcal{D}_{\text{2jet}}^{\text{VBF}} > 0.5$ is required.

- The VH-hadronic category requires exactly four leptons. In addition, there must be either two or three jets, or at least four jets and no b-tagged jets. Finally, $\mathcal{D}_{\text{2jet}}^{\text{VH}} = \max\left(\mathcal{D}_{\text{2jet}}^{\text{WH}}, \mathcal{D}_{\text{2jet}}^{\text{ZH}}\right) > 0.5$ is required.
- The VH-leptonic category requires no more than three jets and no b-tagged jets in the event, and exactly one additional lepton or one additional pair of opposite-sign same-flavor leptons. This category also includes events with no jets and at least one additional lepton.
- The $\mathrm{t\bar{t}H}$-hadronic category requires at least four jets, if one is a b-tagged jet, and no additional leptons.
- The $\mathrm{t\bar{t}H}$-leptonic category requires at least one additional lepton in the event.
- The VBF-1jet category requires exactly four leptons, exactly one jet and $\mathcal{D}_{\text{1jet}}^{\text{VBF}} > 0.7$.
- The Untagged category consists of the remaining events.

The number of events expected from signal simulation and background estimation are shown along with the observed number of events for each Scheme 1 category in Table 2.

In categorization Scheme 2, which targets anomalous HVV couplings, the categorization sequence is modified in three ways in order to be more sensitive to the HVV couplings. First, the $\mathcal{D}_{\text{2jet}}$ discriminants calculated using the SM hypothesis for VBF or VH are less sensitive to anomalous VBF or VH production, so the selection for the VBF-2jet and VH-hadronic categories is modified to be more efficient for BSM hypotheses. Second, the $\mathrm{t\bar{t}H}$ categories are dropped and these events are merged into the Untagged category; $\mathrm{t\bar{t}H}$ forms a small background to VBF and VH. Third, a Boosted category is added. This category, adapted from the second (and finer) categorization scheme in Ref. [78], is designed for events where not all associated particles are fully reconstructed, so that the full kinematic information cannot be used to measure anomalous couplings. After these modifications, Scheme 2 contains six categories,

Table 2: The numbers of events expected in the SM for different H signal (sig) and background (bkg) contributions and the observed number of events in each category defined in Scheme 1 targeting Hff and Hgg anomalous couplings. The $t\bar{t}H$ signal expectation is quoted for the SM and anomalous coupling ($\kappa_t = 0$, $\tilde{\kappa}_t = 1.6$) scenario, both generated with the same cross section.

	Untagged	VBF-1jet	VBF-2jet	VH-leptonic	VH-hadronic	$t\bar{t}H$-leptonic	$t\bar{t}H$-hadronic
ggH sig	182.98	15.50	6.70	0.35	4.68	0.02	0.18
VBF sig	7.23	3.28	7.23	0.05	0.28	0.01	0.05
WH sig	2.68	0.22	0.22	1.07	1.17	0.03	0.03
ZH sig	2.20	0.14	0.15	0.26	0.78	0.02	0.05
$b\bar{b}H$ sig	1.90	0.13	0.08	0.03	0.07	0.00	0.01
$t\bar{t}H$ sig	0.43	0.00	0.08	0.14	0.15	0.68	0.86
($\tilde{\kappa}_t = 1.6$)	(0.45)	(0.00)	(0.12)	(0.15)	(0.15)	(0.87)	(1.18)
tH sig	0.14	0.01	0.10	0.04	0.03	0.04	0.03
Signal	197.89	19.31	14.57	2.00	7.40	0.80	1.23
$q\bar{q} \to 4\ell$ bkg	210.50	6.93	1.92	2.23	1.87	0.08	0.04
$gg \to 4\ell$ bkg	19.79	1.53	0.56	0.38	0.24	0.01	0.01
EW bkg	3.43	0.18	1.37	0.26	0.57	0.24	1.07
Z + X bkg	77.94	2.46	4.88	1.20	3.29	0.21	1.07
Total	509.55	30.41	23.30	6.05	13.38	1.33	3.41
Observed	539	27	20	10	12	0	2

with sequential selection criteria as follows:

- The VBF-2jet category requires exactly four leptons. In addition, there must be either two or three jets of which at most one is b-tagged, or at least four jets and no b-tagged jets. Finally, $\max\left(\mathcal{D}_{2jet}^{VBF,i}\right) > 0.5$ using either the SM or any of the four BSM signal hypotheses (i) for the VBF production is required. See Fig. 7 (middle) for illustration.
- The VH-hadronic category requires exactly four leptons. In addition, there must be either two or three jets, or at least four jets and no b-tagged jets.
  Finally, $\max\left(\mathcal{D}_{2jet}^{WH,i}, \mathcal{D}_{2jet}^{ZH,i}\right) > 0.5$ using either the SM or any of the four BSM signal hypotheses (i) for the VH production is required. See Fig. 7 (right) for illustration.
- The VH-leptonic category requires no more than three jets and no b-tagged jets in the event, and exactly one additional lepton or one additional pair of opposite-sign same-flavor leptons. This category also includes events with no jets and at least one additional lepton.
- The VBF-1jet category requires exactly four leptons, exactly one jet and $\mathcal{D}_{1jet}^{VBF} > 0.7$.
- The Boosted category requires exactly four leptons, three or fewer jets, or at least four jets and no b-tagged jets, and the transverse momentum of the four-lepton system $p_T^{4\ell} > 120\,\text{GeV}$.
- The Untagged category consists of the remaining events.

The number of events expected from signal simulation and background estimation are shown along with the observed number of events for each Scheme 2 category in Table 3.

Table 3: The numbers of events expected in the SM for different H signal (sig) and background (bkg) contributions and the observed number of events in each category defined in Scheme 2 targeting HVV anomalous couplings. The EW (VBF, WH, and ZH) signal expectation is quoted for the SM and four anomalous coupling ($a_3/a_2/\kappa_1/\kappa_2^{Z\gamma}$) scenarios $f_{ai} = 1$, all generated with the same total EW production cross section.

	Untagged	Boosted	VBF-1jet	VBF-2jet	VH-leptonic	VH-hadronic
ggH sig	171.46	6.48	15.15	10.44	0.35	5.99
VBF sig ($a_3/a_2/\kappa_1/\kappa_2^{Z\gamma}$)	5.06 (0.29/0.29/0.05/0.09)	1.18 (0.69/0.54/0.52/0.48)	2.64 (0.12/0.09/0.03/0.05)	8.60 (6.10/4.95/1.91/1.83)	0.06 (0.03/0.02/0.01/0.01)	0.54 (0.28/0.21/0.07/0.07)
WH sig ($a_3/a_2/\kappa_1/\kappa_2^{Z\gamma}$)	2.18 (1.93/3.15/0.72/0.00)	0.43 (3.81/3.20/6.28/0.00)	0.29 (0.83/0.92/0.22/0.00)	0.22 (1.20/1.05/2.04/0.00)	1.11 (2.75/2.86/3.47/0.00)	1.20 (3.43/3.33/2.93/0.00)
ZH sig ($a_3/a_2/\kappa_1/\kappa_2^{Z\gamma}$)	1.87 (0.99/1.89/0.68/1.17)	0.34 (1.87/1.66/4.14/12.34)	0.16 (0.30/0.35/0.12/0.27)	0.16 (0.56/0.51/1.30/3.88)	0.26 (0.42/0.48/0.65/1.82)	0.79 (1.42/1.53/1.84/4.69)
$b\bar{b}H$ sig	1.84	0.04	0.13	0.09	0.03	0.09
$t\bar{t}H$ sig	1.65	0.04	0.00	0.32	0.13	0.19
tH sig	0.13	0.02	0.01	0.12	0.04	0.05
Signal ($a_3/a_2/\kappa_1/\kappa_2^{Z\gamma}$)	184.1 (178.2/180.3/176.4/176.2)	8.5 (12.9/12.0/17.5/19.4)	18.4 (16.5/16.7/15.7/15.6)	19.8 (18.7/17.4/16.1/16.6)	1.9 (3.7/3.9/4.6/2.3)	8.8 (11.4/11.4/11.1/11.0)
$q\bar{q} \to 4\ell$ bkg	206.05	1.89	6.78	2.78	2.21	2.30
$gg \to 4\ell$ bkg	19.05	0.38	1.52	0.76	0.37	0.31
EW bkg	3.50	0.66	0.20	1.98	0.23	0.85
Z + X bkg	69.87	3.73	2.46	9.70	1.20	4.10
Total ($a_3/a_2/\kappa_1/\kappa_2^{Z\gamma}$)	481.3 (475.4/477.5/473.6/473.4)	15.1 (19.5/18.6/24.1/26.0)	29.3 (27.4/27.6/26.6/26.5)	34.9 (33.8/32.4/31.1/31.6)	5.9 (7.7/7.9/8.6/6.3)	16.24 (18.83/18.78/18.54/18.47)
Observed	512	18	27	30	10	13

The events in each category in either Scheme 1 or 2 are further characterized with several observables using the kinematic features of the H boson decay and associated particles, as discussed in Section 4.

3.3 Monte Carlo simulation

Monte Carlo simulation is used to model signal processes, which involve the H boson, and background processes in pp interactions at the LHC and their reconstruction in the CMS detector. All MC samples are interfaced with PYTHIA 8 [83] to simulate parton showering and multi-parton interactions, using version 8.230 for all years with the CUETP8M1 tune [84] for the simulation of the 2016 data-taking period, and the CP5 tune [85] for the simulation of the 2017 and 2018 data taking periods. The NNPDF 3.0 parton distribution functions are used [86]. Simulated events include the contribution from additional pp interactions within the same or adjacent bunch crossings (pileup) and are weighted to reproduce the observed pileup distribution in data. The MC samples are further processed through a dedicated simulation of the CMS detector based on GEANT4 [87].

The JHUGEN 7.3.0 [29–33] MC program is used to simulate all anomalous couplings in the

H boson production and $H \to ZZ$ / $Z\gamma^*$ / $\gamma^*\gamma^* \to 4\ell$ decay as discussed in Section 2. The MELA [29–33] package contains a library of matrix elements from JHUGEN for the signal and MCFM 7.0.1 [88] for the background; these matrix elements are used to apply weights to events in any MC sample to model any other set of anomalous or SM couplings.

The SM production of the H boson through VBF, in association with a W or Z boson, or with a $t\bar{t}$ pair is simulated using both JHUGEN at LO in QCD and POWHEG 2 [89–93] at next-to-leading order (NLO) in QCD. Production in association with a $b\bar{b}$ pair or single top quark is simulated at LO in QCD via JHUGEN. In the VBF, VH, and $t\bar{t}H$ production modes, the JHUGEN and POWHEG simulations are explicitly compared after parton showering in the SM case, and no significant differences are found in kinematic observables. Therefore, the JHUGEN simulation is adopted to describe kinematic distributions in the VBF, VH, $t\bar{t}H$, tH, and $b\bar{b}H$ production modes with anomalous couplings, with the expected yields scaled to match the SM theoretical predictions [28] for inclusive cross sections and POWHEG simulation for categorization of events based on associated particles in the SM. There are no observable anomalous effects in kinematic distributions of the $b\bar{b}H$ process [32], but we keep this process in modeling its event contribution. The considered VH process does not include $gg \to ZH$ production, which is expected to contribute about 5% of the VH cross section and is therefore neglected in this analysis. This process has been studied with JHUGEN, including anomalous HVV and Hff couplings, and it was found that the dependence on anomalous HVV couplings is suppressed [33].

Gluon fusion production is simulated with the POWHEG 2 event generator at NLO in QCD. The kinematic features of events produced in gluon fusion with two associated jets are also modified by anomalous Hgg couplings. These effects are studied using MADGRAPH5_aMC@NLO 2.6.0 [63, 94] and JHUGEN. Simulation with the MINLO [95] program at NLO in QCD is used for evaluation of systematic uncertainties related to the modeling of two associated jets.

In all of the above cases, the subsequent decay $H \to ZZ$ / $Z\gamma^*$ / $\gamma^*\gamma^* \to 4\ell$ is modeled with JHUGEN. All signal processes have been generated under the assumption that the H boson mass is $m_H = 125\,\text{GeV}$. This value has been used in calculations in Sections 2 and 3. However, in the analysis of the data discussed in Sections 4 and 6, the $m_H = 125.38\,\text{GeV}$ value from Ref. [96] is used. The $m_{4\ell}$ parameterization, the cross sections and the branching fractions of all processes [28] are adjusted according to $m_H = 125.38\,\text{GeV}$, but the effect on other kinematic distributions of the H boson decay products and associated particles is neglected owing to the small difference between the two m_H values.

3.4 Background modeling

The main background in this analysis, $q\bar{q} \to ZZ/Z\gamma^*/\gamma^*\gamma^* \to 4\ell$, is estimated from NLO simulation with POWHEG. A fully differential cross section has been computed at next-to-next-to-leading order (NNLO) in QCD [97] and the NNLO/NLO QCD correction is applied as a function of $m_{4\ell}$. The $gg \to ZZ/Z\gamma^*/\gamma^*\gamma^* \to 4\ell$ background process is simulated with MCFM 7.0.1 [88, 98–100] at LO in QCD. The cross section of this background process is corrected with an NNLO K factor as a function of $m_{4\ell}$ [101–103], assuming that the signal and background processes have the same correction for higher orders in QCD. The EW background includes the vector boson scattering and VZZ processes, generated within the JHUGEN framework by adopting the MCFM matrix elements for the background processes. The EW background also incorporates other VVV, $t\bar{t}VV$, and $t\bar{t}V$ processes, which are generated with MADGRAPH5_aMC@NLO.

Other background contributions are estimated using control samples in reconstructed data without relying on simulation. Different sources of leptons such as leptons originating from

decays of heavy flavor quarks or light mesons may produce additional background to the H boson signal. We denote this background collectively as the Z + X background and employ a data-driven method for its estimation. The same method has been used in the analyses of Run 1 [12, 13] and Run 2 [16, 17, 77, 78] data sets. The lepton misidentification rates are first derived using Z + 1ℓ control regions with relaxed selection requirements on the third lepton, and the extracted rates are then applied in Z + 2ℓ control regions, where the two additional leptons with relaxed selection requirements have the same lepton flavor of equal or opposite charge [78].

4 Kinematic effects in production and decay of the H boson

Kinematic distributions of particles produced in the H boson decay or in association with the H boson production are sensitive to the quantum numbers and anomalous couplings of the H boson. Four main production topologies are studied: ggH, VBF, ZH or WH, and $t\bar{t}H$ or tH, as illustrated in Fig. 8.

In the $H \to VV \to 4\ell$ decay, shown in Fig. 8, lower right, eight observables fully characterize the kinematic distributions of the decay products and the orientation of the decay frame with respect to the production axis $\mathbf{\Omega}^{\text{dec}} = \{\theta_1, \theta_2, \Phi, \theta^*, \Phi_1, m_1, m_2, m_{4\ell}\}$ [29]. Sets of observables $\mathbf{\Omega}^{\text{prod}}$ for the ggH, VBF, VH, and $t\bar{t}H$ production processes are defined in a similar way [31, 32], as shown in Fig. 8. As a result, 13 or more kinematic observables can be defined for the associated production process, with subsequent H boson decay to a four-fermion final state. The MELA approach is designed to reduce the number of observables to a minimum, while retaining all essential information.

4.1 Kinematic discriminants

Full kinematic information from each event, using either the $H \to VV \to 4\ell$ decay or associated particles in its production, is extracted using discriminants from matrix element calculations using the MELA package. The discriminants use a complete set of mass and angular input observables $\mathbf{\Omega}$ [29, 31, 32] to describe kinematic distributions at LO in QCD. Full reconstruction of the four-lepton decay chain and associated particles is employed in the matrix element calculation, following the selection chain discussed in Section 3. Events with partial reconstruction of associated particles are retained in the analysis by using other kinematic observables, such as the transverse momentum of the reconstructed H boson. In the case of the $t\bar{t}H$ topology, where full reconstruction of the full decay chain of the top quarks is a challenging task, an approximation to the matrix element approach is achieved with machine learning [33].

Two types of discriminants are defined for either the production process, the decay process, or the full production + decay process. These discriminants are

$$\mathcal{D}_{\text{alt}}(\mathbf{\Omega}) = \frac{\mathcal{P}_{\text{sig}}(\mathbf{\Omega})}{\mathcal{P}_{\text{sig}}(\mathbf{\Omega}) + \mathcal{P}_{\text{alt}}(\mathbf{\Omega})}, \tag{20}$$

$$\mathcal{D}_{\text{int}}(\mathbf{\Omega}) = \frac{\mathcal{P}_{\text{int}}(\mathbf{\Omega})}{2\sqrt{\mathcal{P}_{\text{sig}}(\mathbf{\Omega})\ \mathcal{P}_{\text{alt}}(\mathbf{\Omega})}}, \tag{21}$$

where the probability density $\mathcal{P}$ of a certain process is calculated using the full kinematic description characterized by $\mathbf{\Omega}$ for the processes denoted as "sig" for a signal model and "alt" for an alternative model, which could be an alternative H boson production mechanism (used to categorize events), background (to isolate signal), or an alternative H boson coupling model

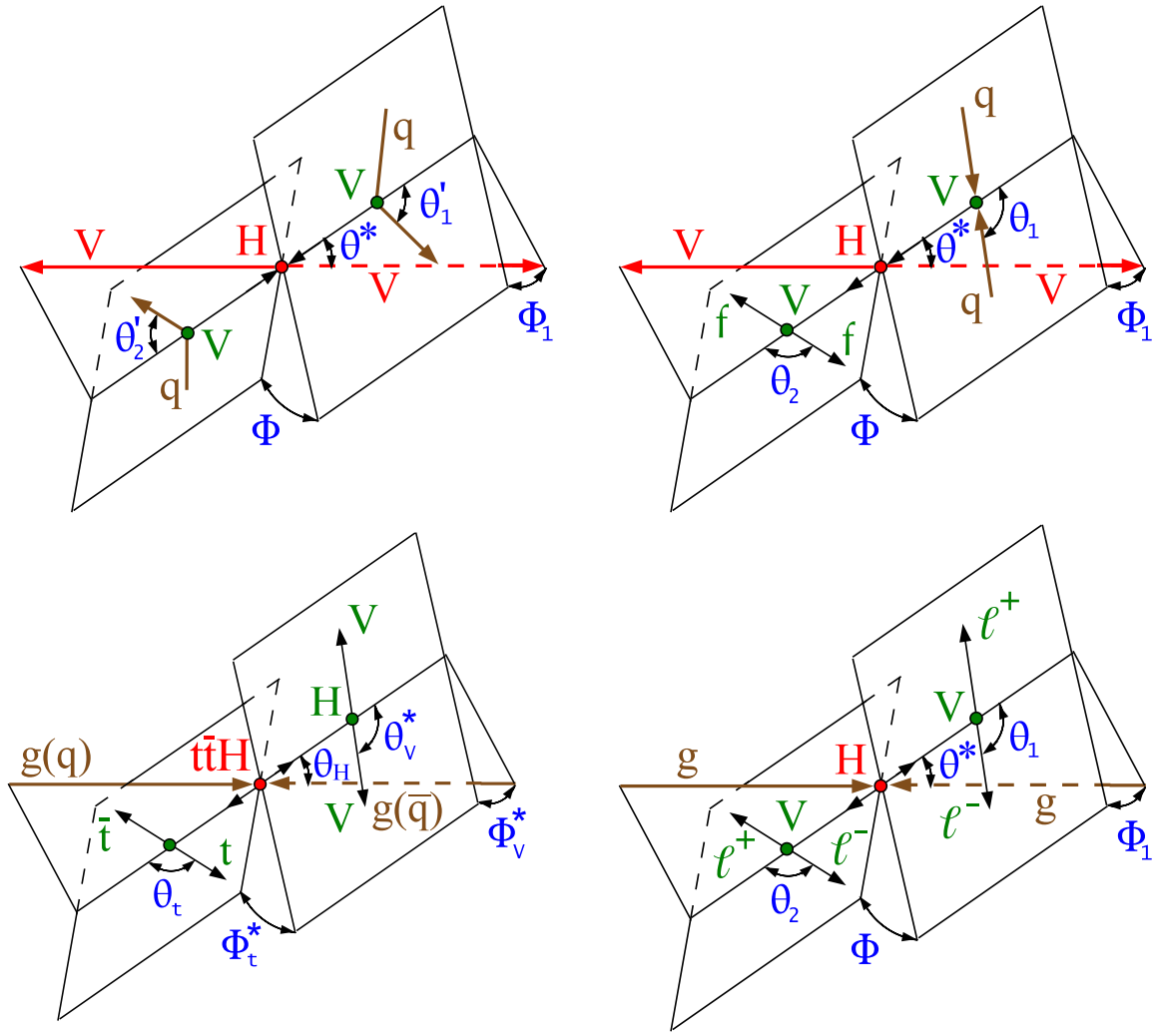

Figure 8: Four topologies of the H boson production and decay: gluon or EW vector boson fusion $qq \to V_1V_2(qq) \to H(qq) \to (VV)(qq)$ (upper left); associated production $qq \to V \to VH \to (ff)\,(VV)$ (upper right); H boson production in association with the top quarks $t\bar{t}H$ or tH (lower left); and four-lepton decay $H \to VV \to 4\ell$ where the incoming gluons gg indicate the collision axis (lower right), and which proceeds either with or without associated particles. The incoming partons are shown in brown and the intermediate or final-state particles are shown in red and green. The angles characterizing kinematic distributions are shown in blue and are defined in the respective rest frames [29, 31, 32]. The subsequent top quark decay is not shown. See Ref. [32] for details.

Table 4: The list of kinematic observables used for category selection and fitting in categorization Schemes 1 and 2. Only the main features involving the kinematic discriminants in the category selection are listed, while complete details are given in Section 3. The Untagged category includes the events not selected in the other categories.

Category	Selection	Observables $\vec{x}$ for fitting
Scheme 1		
VBF-1jet	$\mathcal{D}_{1\text{jet}}^{\text{VBF}} > 0.7$	$\mathcal{D}_{\text{bkg}}$
VBF-2jet	$\mathcal{D}_{2\text{jet}}^{\text{VBF}} > 0.5$	$\mathcal{D}_{\text{bkg}}, \mathcal{D}_{2\text{jet}}^{\text{VBF}}, \mathcal{D}_{0-}^{\text{ggH}}, \mathcal{D}_{\text{CP}}^{\text{ggH}}$
VH-hadronic	$\mathcal{D}_{2\text{jet}}^{\text{VH}} > 0.5$	$\mathcal{D}_{\text{bkg}}$
VH-leptonic	see Section 3	$\mathcal{D}_{\text{bkg}}$
$\text{t}\bar{\text{t}}\text{H}$-hadronic	see Section 3	$\mathcal{D}_{\text{bkg}}, \mathcal{D}_{0-}^{\text{t}\bar{\text{t}}\text{H}}$
$\text{t}\bar{\text{t}}\text{H}$-leptonic	see Section 3	$\mathcal{D}_{\text{bkg}}, \mathcal{D}_{0-}^{\text{t}\bar{\text{t}}\text{H}}$
Untagged	none of the above	$\mathcal{D}_{\text{bkg}}$
Scheme 2		
Boosted	$p_{\text{T}}^{4\ell} > 120\,\text{GeV}$	$\mathcal{D}_{\text{bkg}}, p_{\text{T}}^{4\ell}$
VBF-1jet	$\mathcal{D}_{1\text{jet}}^{\text{VBF}} > 0.7$	$\mathcal{D}_{\text{bkg}}, p_{\text{T}}^{4\ell}$
VBF-2jet	$\mathcal{D}_{2\text{jet}}^{\text{VBF}} > 0.5$	$\mathcal{D}_{\text{bkg}}^{\text{EW}}, \mathcal{D}_{0\text{h}+}^{\text{VBF+dec}}, \mathcal{D}_{0-}^{\text{VBF+dec}}, \mathcal{D}_{\Lambda 1}^{\text{VBF+dec}}, \mathcal{D}_{\Lambda 1}^{\text{Z}\gamma,\text{VBF+dec}}, \mathcal{D}_{\text{int}}^{\text{VBF}}, \mathcal{D}_{\text{CP}}^{\text{VBF}}$
VH-hadronic	$\mathcal{D}_{2\text{jet}}^{\text{VH}} > 0.5$	$\mathcal{D}_{\text{bkg}}^{\text{EW}}, \mathcal{D}_{0\text{h}+}^{\text{VH+dec}}, \mathcal{D}_{0-}^{\text{VH+dec}}, \mathcal{D}_{\Lambda 1}^{\text{VH+dec}}, \mathcal{D}_{\Lambda 1}^{\text{Z}\gamma,\text{VH+dec}}, \mathcal{D}_{\text{int}}^{\text{VH}}, \mathcal{D}_{\text{CP}}^{\text{VH}}$
VH-leptonic	see Section 3	$\mathcal{D}_{\text{bkg}}, p_{\text{T}}^{4\ell}$
Untagged	none of the above	$\mathcal{D}_{\text{bkg}}, \mathcal{D}_{0\text{h}+}^{\text{dec}}, \mathcal{D}_{0-}^{\text{dec}}, \mathcal{D}_{\Lambda 1}^{\text{dec}}, \mathcal{D}_{\Lambda 1}^{\text{Z}\gamma,\text{dec}}, \mathcal{D}_{\text{int}}^{\text{dec}}, \mathcal{D}_{\text{CP}}^{\text{dec}}$

(to measure coupling parameters). The "int" label refers to the interference between the two model contributions. The probability densities $\mathcal{P}$ are calculated from the matrix elements provided by the MELA package and are normalized to give the same integrated cross section for both processes in the relevant phase space. This normalization leads to a balanced distribution of events in the range between 0 and 1 for the $\mathcal{D}_{\text{alt}}$ discriminants, or between -1 and 1 for $\mathcal{D}_{\text{int}}$. In the special case where the $\mathcal{D}_{\text{int}}$ is calculated between CP-even and CP-odd models, it is denoted as $\mathcal{D}_{\text{CP}}$. The $\mathcal{D}_{\text{CP}}$ observable is CP-odd, and a forward-backward asymmetry in its distribution would indicate CP violation. This motivates the index "CP".

When events are split into the VBF-1/2jet and VH-hadronic categories, a set of discriminants $\mathcal{D}_{1/2\text{jet}}$ is constructed, following Eq. (20), where $\mathcal{P}_{\text{sig}}$ corresponds to the signal probability density for the VBF (WH or ZH) production hypothesis in the VBF-tagged (VH-tagged) category, and $\mathcal{P}_{\text{alt}}$ corresponds to that of H boson production in association with two jets via gluon fusion. When more than two jets pass the selection criteria, the two jets with the highest p_{T} are chosen for the matrix element calculations. Thereby, the $\mathcal{D}_{1/2\text{jet}}$ discriminants separate the target production mode of each category from gluon fusion production, in all cases using only the kinematic properties of the H boson and two associated jets. The application of the $\mathcal{D}_{1/2\text{jet}}$ discriminants is described in Section 3, where we introduce four types of discriminants $\mathcal{D}_{1\text{jet}}^{\text{VBF}}$, $\mathcal{D}_{2\text{jet}}^{\text{VBF},i}$, $\mathcal{D}_{2\text{jet}}^{\text{ZH},i}$, and $\mathcal{D}_{2\text{jet}}^{\text{WH},i}$, with the SM and the four anomalous coupling hypotheses i considered in the signal model.

Several arrays of observables $\vec{x}$ are defined in each category of events, uniquely targeting kinematic features of each category, and are listed in Table 4. One observable, $\mathcal{D}_{\text{bkg}}$, is common to most production categories in both Schemes 1 and 2. This observable is calculated using

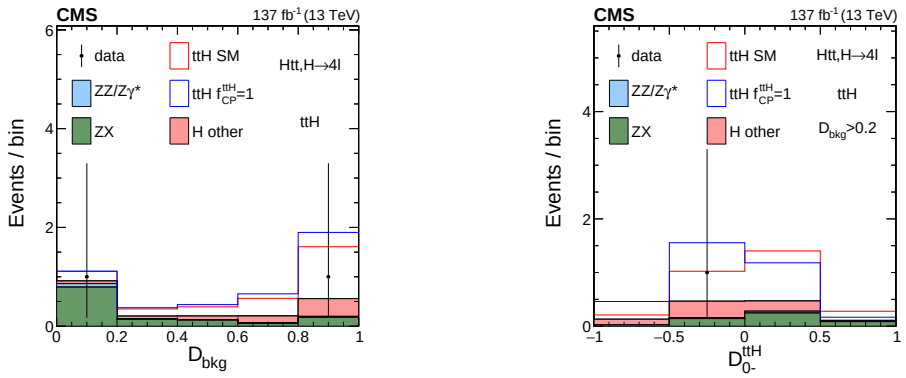

Figure 9: Distribution of the $\mathcal{D}_{\text{bkg}}$ (left) and $\mathcal{D}_{0^-}^{\text{t}\bar{\text{t}}\text{H}}$ (right), discriminants in the sum of the $\text{t}\bar{\text{t}}$H-leptonic and $\text{t}\bar{\text{t}}$H-hadronic categories in Scheme 1. The latter distribution is shown with the requirement $\mathcal{D}_{\text{bkg}} > 0.2$ in order to enhance the signal over the background contribution.

Eq. (20) and is designed to separate signal from the dominant background production of four leptons. The $\mathcal{P}_{\text{alt}}$ probability density is calculated for the dominant $\text{q}\bar{\text{q}} \to 4\ell$ background process. The signal and background probability densities include both the matrix element probability based on the four-lepton kinematic properties from MELA and the empirical $m_{4\ell}$ probability density parameterization extracted from the simulation of detector effects. In the VBF-2jet and VH-hadronic categories in Scheme 2, the observable $\mathcal{D}_{\text{bkg}}^{\text{EW}}$ is a modified version of $\mathcal{D}_{\text{bkg}}$ which includes the jet information. In this case, $\mathcal{P}_{\text{sig}}$ and $\mathcal{P}_{\text{alt}}$ still include the $m_{4\ell}$ probability parameterization and four-lepton kinematic information, but they also include kinematic information for the two associated jets. The $\mathcal{P}_{\text{alt}}$ probability density represents the EW and QCD background processes $4\ell + 2\,\text{jets}$, while $\mathcal{P}_{\text{sig}}$ represents the EW H production processes summed together, VBF, WH, and ZH. The $\mathcal{D}_{\text{bkg}}$ or $\mathcal{D}_{\text{bkg}}^{\text{EW}}$ calculation employs the SM hypothesis for the signal, while BSM kinematic information is incorporated in the observables discussed next.

4.2 Observables targeting anomalous Htt and Hgg couplings

In Scheme 1, targeting anomalous Htt and Hgg couplings, seven event categories are used. In the Untagged, VBF-1jet, VH-leptonic, and VH-hadronic categories, only one observable $\mathcal{D}_{\text{bkg}}$ is used. These categories do not provide additional information for separating CP-even and CP-odd contributions in the Htt and Hgg couplings, but are included in the fit in order to constrain the rates of the processes. The probability density parameterization of $\mathcal{D}_{\text{bkg}}$ in these categories is not sensitive to the CP structure of either Hff or HVV interactions.

There is rich kinematic information in $\text{t}\bar{\text{t}}$H production because of the sequential decay of the top quarks, as discussed further in Ref. [32]. While it is possible to construct observables, as defined in Eqs. (20) and (21), with matrix element techniques [32], we adopt a machine learning approach to account for partial reconstruction and possible permutations of the jets. A boosted decision tree (BDT) classifier is trained to separate CP-even, corresponding to the κ_{t} coupling, and CP-odd, corresponding to the $\tilde{\kappa}_{\text{t}}$ coupling, contributions independently in the $\text{t}\bar{\text{t}}$H-leptonic and $\text{t}\bar{\text{t}}$H-hadronic categories. The discriminant $\mathcal{D}_{0^-}^{\text{t}\bar{\text{t}}\text{H}}$ is obtained with this approach as the best approximation to Eq. (20), provided the full kinematic information is made available in the calculation [32]. This technique still ensures that the maximal information is retained in the discriminant and is based on the same matrix element used in simulation.

We achieve the full kinematic information in the $\mathcal{D}_{0^-}^{\text{t}\bar{\text{t}}\text{H}}$ calculation by including the following

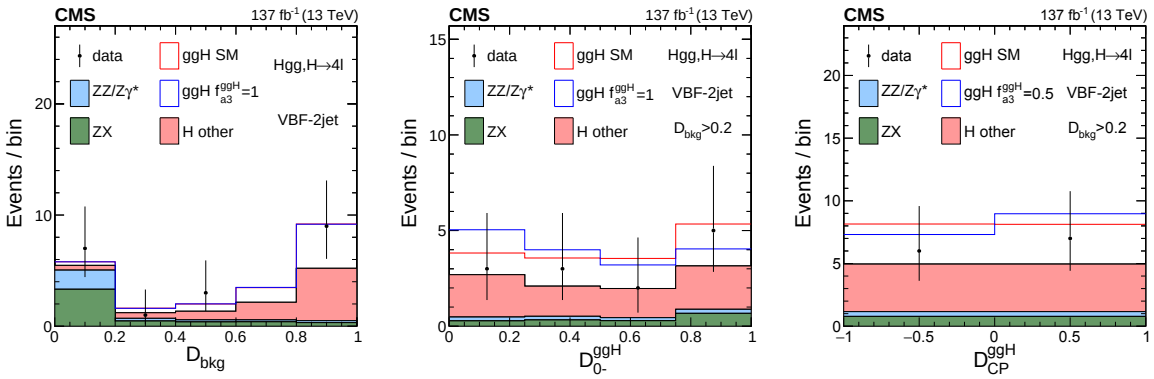

Figure 10: Distribution of the $\mathcal{D}_{\text{bkg}}$ (left), $\mathcal{D}_{0^-}^{\text{ggH}}$ (middle), and $\mathcal{D}_{\text{CP}}^{\text{ggH}}$ (right) discriminants in the VBF-2jet category in Scheme 1. The latter two distributions are shown with the requirement $\mathcal{D}_{\text{bkg}} > 0.2$ in order to enhance the signal over the background contribution.

observables in the training: the four-momenta of the reconstructed H boson and of the six jets with the largest p_{T}, as well as the b-tagging scores of the six jets for resolving their permutation. In addition, in the $\text{t}\bar{\text{t}}\text{H}$-leptonic category, the lepton multiplicity and the four-momentum of the highest-p_{T} lepton not originating from the H boson decay are used as input to the BDT classifier. It is not possible to construct the $\mathcal{D}_{\text{CP}}^{\text{t}\bar{\text{t}}\text{H}}$ discriminant, corresponding to Eq. (21), without tagging the flavors of the jets, including distinguishing quarks from antiquarks [32]. Alternatively, in the leptonic decay of both top quarks one could use the charges of the leptons, but the efficiency of such a method is very low. Therefore, in the two $\text{t}\bar{\text{t}}\text{H}$ categories, two observables are used: $\vec{x} = \{\mathcal{D}_{\text{bkg}}, \mathcal{D}_{0^-}^{\text{t}\bar{\text{t}}\text{H}}\}$. The distributions of these two discriminants are shown in Fig. 9.

The analysis of gluon fusion production with associated jets is performed in the VBF-2jet category. There are two discriminants that are sensitive to CP-even terms, corresponding to the a_2^{gg} coupling, and to CP-odd terms, corresponding to the a_3^{gg} coupling, $\mathcal{D}_{0^-}^{\text{ggH}}$ and $\mathcal{D}_{\text{CP}}^{\text{ggH}}$, following Eqs. (20) and (21), respectively. The matrix element for the gluon fusion H boson production in association with two jets includes three possible initial states: quark-quark, quark-gluon, and gluon-gluon. Only the quark-quark initial state is used to calculate these discriminants, because this configuration corresponds to the gluon scattering topology sensitive to CP properties of the Hgg coupling [32], by analogy with the weak vector boson scattering process. The jets in the other configurations, quark-gluon and gluon-gluon, are more likely to be initiated from gluon radiation or splitting and are less likely to carry information about the CP properties. For similar reasons, we include the $\mathcal{D}_{\text{2jet}}^{\text{VBF}}$ discriminant as one of the observables. This discriminant allows us to isolate the VBF-like topology of the events, which is more characteristic of the quark-quark-initiated process.

As a result, in the VBF-2jet category in Scheme 1 the observables $\vec{x} = \{\mathcal{D}_{\text{bkg}}, \mathcal{D}_{\text{2jet}}^{\text{VBF}}, \mathcal{D}_{0^-}^{\text{ggH}}, \mathcal{D}_{\text{CP}}^{\text{ggH}}\}$ are used, as summarized in Table 4. The distributions of the three observables $\mathcal{D}_{\text{bkg}}$, $\mathcal{D}_{0^-}^{\text{ggH}}$, and $\mathcal{D}_{\text{CP}}^{\text{ggH}}$ in this category are shown in Fig. 10, while the $\mathcal{D}_{\text{2jet}}^{\text{VBF}}$ observable is shown in Fig. 7. It has been shown [33, 44] that the azimuthal angle between the two jets carries information similar to $\mathcal{D}_{0^-}^{\text{ggH}}$ and $\mathcal{D}_{\text{CP}}^{\text{ggH}}$, but the latter two are better in terms of performance and practical application to parameterization in the fit discussed in Section 5.

4.3 Observables targeting anomalous HVV couplings

In Scheme 2, targeting anomalous HVV couplings, six event categories are used. Two of these categories, VBF-2jet and VH-hadronic, target full reconstruction of the associated jets in EW production of the H boson. Therefore, the full matrix element calculation using both production and decay information is employed, as discussed below and summarized in Table 4. Three other categories, Boosted, VBF-1jet, and VH-leptonic, also target EW production, but without full reconstruction of the associated particles. Therefore, in these categories matrix element calculations are not employed, and instead the transverse momentum of the H boson candidate $p_{\mathrm{T}}^{4\ell}$ is used as the second observable. Anomalous couplings in EW production lead to a harder $p_{\mathrm{T}}^{4\ell}$ spectrum. Finally, in the Untagged category, dominated by the ggH events without two associated jets, matrix element calculations using $\mathrm{H} \to \mathrm{VV} \to 4\ell$ decay information are employed.

Since we target four anomalous HVV couplings appearing in Eq. (2), namely a_2, a_3, $\kappa_1/(\Lambda_1)^2$, and $\kappa_2^{\mathrm{Z}\gamma}/(\Lambda_1^{\mathrm{Z}\gamma})^2$, optimal analysis of the $\mathrm{H} \to \mathrm{VV} \to 4\ell$ decay requires four discriminants of the type given by Eq. (20) and four discriminants of the type given by Eq. (21). In the Untagged category, the former four discriminants are defined as $\mathcal{D}_{0\mathrm{h}+}^{\mathrm{dec}}$, $\mathcal{D}_{0-}^{\mathrm{dec}}$, $\mathcal{D}_{\Lambda 1}^{\mathrm{dec}}$, and $\mathcal{D}_{\Lambda 1}^{\mathrm{Z}\gamma,\mathrm{dec}}$, respectively, where the index "dec" indicates that only the four-lepton decay information is used. Among the latter four interference discriminants, it was found that the two discriminants corresponding to the $\kappa_1/(\Lambda_1)^2$ and $\kappa_2^{\mathrm{Z}\gamma}/(\Lambda_1^{\mathrm{Z}\gamma})^2$ couplings are strongly correlated with $\mathcal{D}_{\Lambda 1}^{\mathrm{dec}}$ and $\mathcal{D}_{\Lambda 1}^{\mathrm{Z}\gamma,\mathrm{dec}}$, and therefore these two interference discriminants are not used. This observation follows from the fact that the a_1 and $\kappa_1/(\Lambda_1)^2$ or $\kappa_2^{\mathrm{Z}\gamma}/(\Lambda_1^{\mathrm{Z}\gamma})^2$ couplings correspond to the same tensor structure in Eq. (2) and differ only in the q_{V}^2 dependence. The remaining two interference discriminants, $\mathcal{D}_{\mathrm{int}}^{\mathrm{dec}}$ and $\mathcal{D}_{\mathrm{CP}}^{\mathrm{dec}}$, corresponding to the a_2 and a_3 alternative couplings, respectively, are employed in the fit.

In the VBF-2jet and VH-hadronic categories, the system of six discriminants discussed above is extended to include both production and decay information, because these categories allow full reconstruction of associated particles. The same four types of discriminants of the Untagged category following Eq. (20) are used, namely $\mathcal{D}_{0\mathrm{h}+}^{\mathrm{VBF+dec}}$, $\mathcal{D}_{0-}^{\mathrm{VBF+dec}}$, $\mathcal{D}_{\Lambda 1}^{\mathrm{VBF+dec}}$, and $\mathcal{D}_{\Lambda 1}^{\mathrm{Z}\gamma,\mathrm{VBF+dec}}$ in the VBF-2jet category, and $\mathcal{D}_{0\mathrm{h}+}^{\mathrm{VH+dec}}$, $\mathcal{D}_{0-}^{\mathrm{VH+dec}}$, $\mathcal{D}_{\Lambda 1}^{\mathrm{VH+dec}}$, and $\mathcal{D}_{\Lambda 1}^{\mathrm{Z}\gamma,\mathrm{VH+dec}}$ in the VH-hadronic category. Here the index "VBF+dec" or "VH+dec" indicates that both production and decay information is used, which means that the kinematic information from the associated jets and the four leptons are utilized in the VBF or VH matrix element calculations. In the case of the VH process, the matrix elements of the WH and ZH processes are summed. There are more interference discriminants in cases where anomalous couplings appear both in production and decay. However, using interference discriminants with production information only following Eq. (21) is the better approach if one has to limit the number of discriminants. Therefore, $\mathcal{D}_{\mathrm{int}}^{\mathrm{VBF}}$ and $\mathcal{D}_{\mathrm{CP}}^{\mathrm{VBF}}$ are used in the VBF-2jet category, and $\mathcal{D}_{\mathrm{int}}^{\mathrm{VH}}$ and $\mathcal{D}_{\mathrm{CP}}^{\mathrm{VH}}$ are used in the VH-hadronic category.

Distributions of events for the observables $\vec{x}$ in Scheme 2 are illustrated in Figs. 11–13. Here and in Figs. 9 and 10 the expected distributions are based on signal MC simulation discussed in Section 3.3 and the background estimate in Section 3.4, where cross sections of all processes, including those with the BSM couplings, are set to the SM expectations. The full list of kinematic observables employed in the fit in each category is summarized in the third column of Table 4.

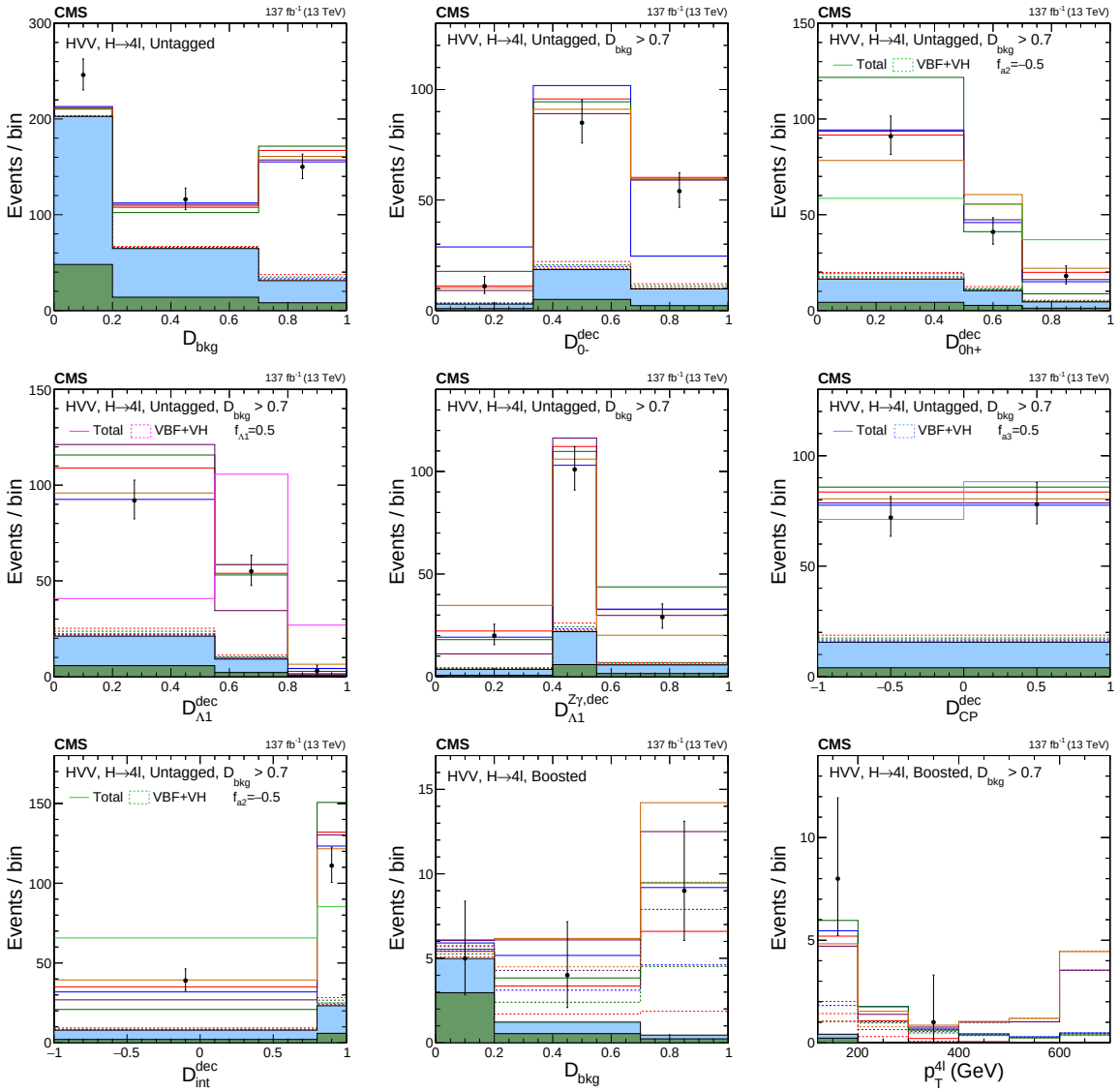

Figure 11: Distributions of events in the observables used in categorization Scheme 2. The first seven plots are in the Untagged category: The upper left plot shows $\mathcal{D}_{\text{bkg}}$. The rest of the distributions are shown with the requirement $\mathcal{D}_{\text{bkg}} > 0.7$ in order to enhance the signal over the background contribution: $\mathcal{D}_{0-}^{\text{dec}}$ (upper middle), $\mathcal{D}_{0h+}^{\text{dec}}$ (upper right), $\mathcal{D}_{\Lambda 1}^{\text{dec}}$ (middle left), $\mathcal{D}_{\Lambda 1}^{\text{Z}\gamma,\text{dec}}$ (middle middle), $\mathcal{D}_{\text{CP}}^{\text{dec}}$, and $\mathcal{D}_{\text{int}}^{\text{dec}}$. The last two plots are shown in the Boosted category: $\mathcal{D}_{\text{bkg}}$ (lower middle) and $p_{\text{T}}^{4\ell}$ with the requirement $\mathcal{D}_{\text{bkg}} > 0.7$ and overflow events included in the last bin (lower right). Observed data, background expectation, and five signal models are shown in the plots, as indicated in the legend in Fig. 7 (left). In several cases, a sixth signal model with a mixture of the SM and BSM couplings is shown and is indicated in the legend explicitly.

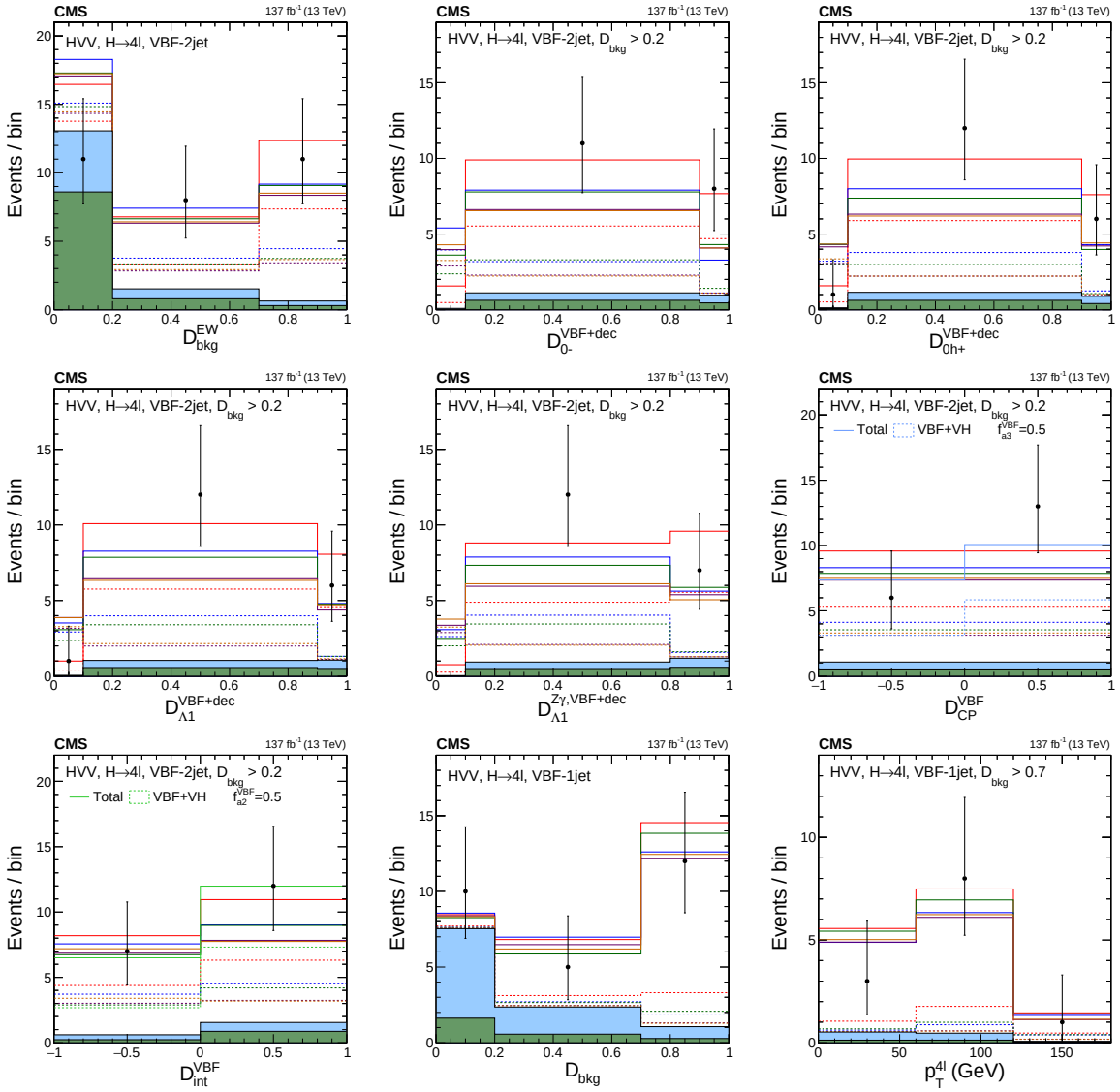

Figure 12: Distributions of events in the observables used in categorization Scheme 2. The first seven plots are in the VBF-2jet category: The upper left plot shows $\mathcal{D}_{\text{bkg}}^{\text{EW}}$. The rest of the distributions are shown with the requirement $\mathcal{D}_{\text{bkg}}^{\text{EW}} > 0.2$ in order to enhance the signal over the background contribution: $\mathcal{D}_{0-}^{\text{VBF+dec}}$ (upper middle), $\mathcal{D}_{0h+}^{\text{VBF+dec}}$ (upper right), $\mathcal{D}_{\Lambda 1}^{\text{VBF+dec}}$ (middle left), $\mathcal{D}_{\Lambda 1}^{\text{Z}\gamma,\text{VBF+dec}}$ (middle middle), $\mathcal{D}_{\text{CP}}^{\text{VBF}}$, and $\mathcal{D}_{\text{int}}^{\text{VBF}}$. The last two plots are shown in the VBF-1jet category: $\mathcal{D}_{\text{bkg}}$ (lower middle) and $p_{\text{T}}^{4\ell}$ with the requirement $\mathcal{D}_{\text{bkg}} > 0.7$ and overflow events included in the last bin (lower right). Observed data, background expectation, and five signal models are shown in the plots, as indicated in the legend in Fig. 7 (left). In several cases, a sixth signal model with a mixture of the SM and BSM couplings is shown and is indicated in the legend explicitly.

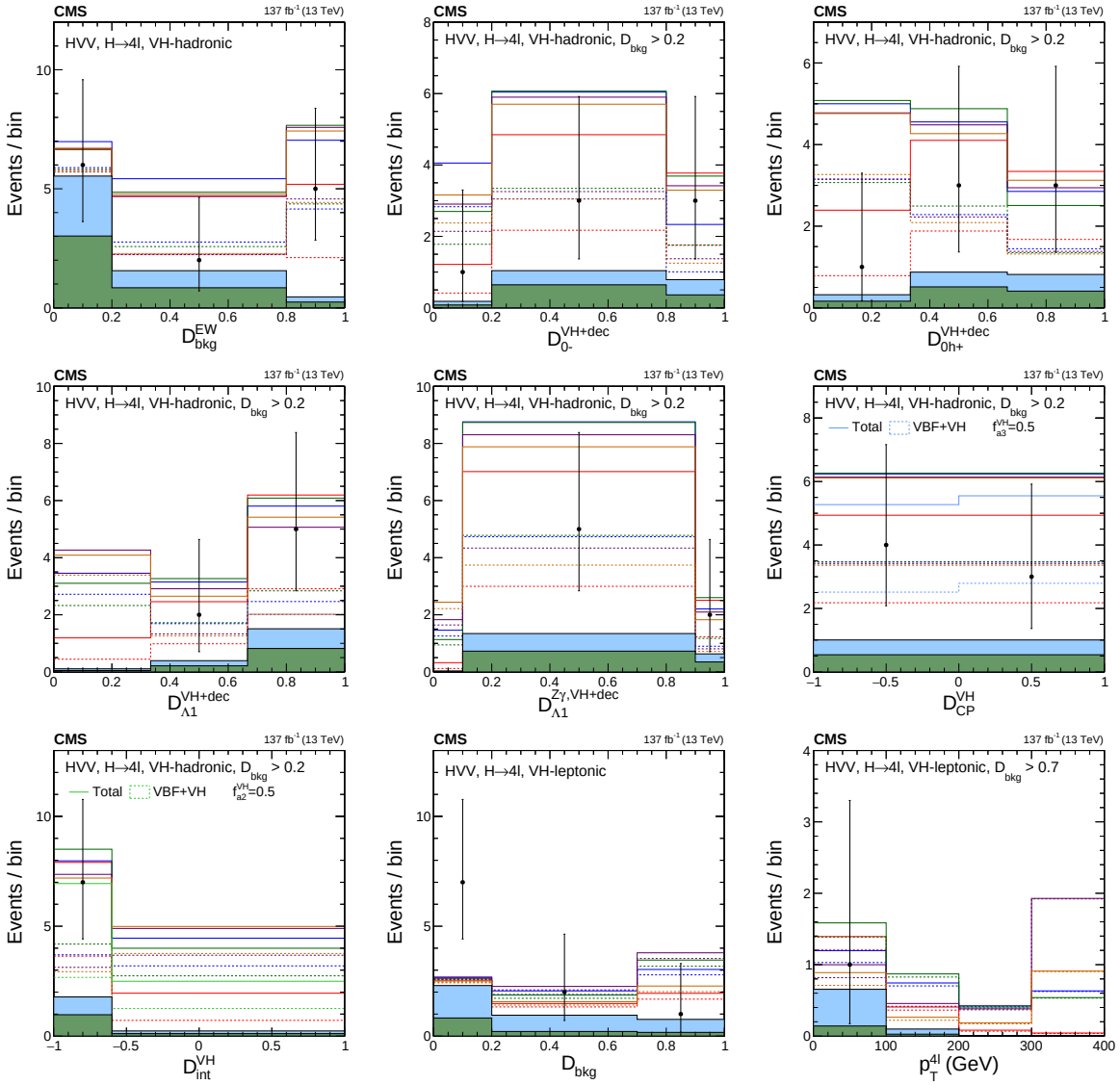

Figure 13: Distributions of events in the observables used in categorization Scheme 2. The first seven plots are in the VH-hadronic category: The upper left plot shows $\mathcal{D}_{\text{bkg}}^{\text{EW}}$. The rest of the distributions are shown with the requirement $\mathcal{D}_{\text{bkg}}^{\text{EW}} > 0.2$ in order to enhance the signal over the background contribution: $\mathcal{D}_{0-}^{\text{VH+dec}}$ (upper middle); $\mathcal{D}_{0h+}^{\text{VH+dec}}$ (upper right); $\mathcal{D}_{\Lambda 1}^{\text{VH+dec}}$ (middle left); $\mathcal{D}_{\Lambda 1}^{\text{Z}\gamma,\text{VH+dec}}$ (middle middle); $\mathcal{D}_{\text{CP}}^{\text{VH}}$, and $\mathcal{D}_{\text{int}}^{\text{VH}}$. The last two plots are shown in the VH-leptonic category: $\mathcal{D}_{\text{bkg}}$ (lower middle) and $p_{\text{T}}^{4\ell}$ with the requirement $\mathcal{D}_{\text{bkg}} > 0.7$ and overflow events included in the last bin (lower right). Observed data, background expectation, and five signal models are shown in the plots as indicated in the legend in Fig. 7 (left). In several cases, a sixth signal model with a mixture of the SM and BSM couplings is shown and is indicated in the legend explicitly.

5 Implementation of fitting and associated uncertainties

In the analysis of the Hff, Hgg, or HVV anomalous couplings, the events are split into a total of 63 (in Scheme 1, targeting Hff and Hgg) or 54 (in Scheme 2, targeting HVV) categories according to the seven or six production categories, three lepton flavor combinations (4e, 4μ, and $2e2\mu$), and three data periods (2016, 2017, and 2018). Each event is characterized by its discrete category k and set of input observables $\vec{x}$, as discussed in detail in Section 4 and summarized in Table 4. The observed distributions of events across the discriminants $\vec{x}$ are illustrated in Figs. 9–13 and are compared to the expected distributions in SM and BSM. However, quantitative characterization of these distributions requires a careful analysis of the multidimensional space of observables $\vec{x}$ and categories k, which is discussed below. Preparation of this analysis was performed in a blind way, which means that observed distributions of events were not examined until all details of the fit discussed below were finalized.

5.1 Likelihood parameterization

We perform an extended maximum likelihood fit [104] in which the probability density is normalized to the total event yield in each category k as a sum over all signal processes j and background processes i according to

$$\mathcal{P}_k(\vec{x}) = \sum_j \mu_j \mathcal{P}_{jk}^{\text{sig}}\left(\vec{x};\vec{\xi}_{jk},\vec{f}_j\right) + \sum_i \mathcal{P}_{ik}^{\text{bkg}}\left(\vec{x};\vec{\xi}_{ik}\right), \tag{22}$$

where μ_j is the ratio of the observed cross section to the SM expectation, $\vec{f}_j$ is the set of unconstrained parameters describing kinematic distributions in a given process, defined in Eqs. (15, 16, 18), and $\vec{\xi}_{jk}$ are the constrained nuisance parameters reflecting the uncertainties in the above parameterization.

In the case of the gluon fusion process, $\mu_j = \mu_{\text{ggH}}$ and $\vec{f}_j = f_{a3}^{\text{ggH}}$. The dependence on the CP-sensitive parameter f_{a3}^{ggH} appears only in the VBF-2jet category where correlation of the two associated jets is explored. Therefore, in this category a dedicated simulation of the H boson production with two associated jets with MADGRAPH5_aMC@NLO is used, and checked against the JHUGEN and MINLO simulation. The interpretation of this process in terms of fermion couplings appearing in the gluon fusion loop is discussed in Section 6.3. In cases where the SM fermions are assumed to dominate the gluon fusion loop, the μ_{ggH} and f_{a3}^{ggH} parameters are correlated to $\mu_{\text{t}\bar{\text{t}}\text{H}}$ and $f_{\text{CP}}^{\text{Htt}}$ in the $\text{t}\bar{\text{t}}\text{H}$ process through Eq. (17). A more general case, when both SM fermions and heavy BSM particles contribute to the loop, is also considered. In all cases the relationship between the Hff and Hgg couplings follows JHUGEN with the relative sign of CP-odd and CP-even coefficients opposite to that assumed in MADGRAPH5_aMC@NLO, as discussed in Ref. [33].

In the case of the $\text{t}\bar{\text{t}}\text{H}$ process, $\mu_j = \mu_{\text{t}\bar{\text{t}}\text{H}}$ and $\vec{f}_j = f_{\text{CP}}^{\text{Htt}}$. The tH production is expected to contribute about 5% of the total $\text{t}\bar{\text{t}}\text{H}$ signal in this analysis, as shown in Table 2, and, therefore, the exact treatment of this process is currently not important. This production mode depends on both HVV and Hff couplings. The anticipated small yield may be somewhat larger if the expected destructive interference between the HVV and Hff couplings in the tH process becomes constructive owing to a modification of these couplings. In this analysis, we also introduce a possible CP-odd Yukawa coupling in the tH process. We fix the sign of the a_1 coupling to be positive, and so the sign of the κ_{t} coupling allows us to float the relative sign of the HVV and Hff contributions in this process. In Scheme 1, we parameterize the tH signal strength with the

parameters $\mu_{t\bar{t}H}$, f_{CP}^{Htt}, and μ_V, defined below. There is a weak dependence of the $\mathcal{D}_{0-}$ distributions on f_{CP}^{Htt} in this channel, which we conservatively neglect. We also neglect anomalous HVV couplings in the tH parameterization because their effect is negligible with the current constraints from analysis of the VBF and VH events. In Scheme 2, where we do not have a dedicated category for the top quark coupling measurements, we neglect the dependence of the tH process on the HVV couplings because this would have a negligible effect on the results and unnecessarily complicate the fit parameterization.

For EW processes (VBF, ZH, WH), the common unconstrained parameters of interest are $\mu_j = \mu_V$ and $\vec{f}_j = \left(f_{a3}, f_{a2}, f_{\Lambda 1}, f_{\Lambda 1}^{Z\gamma}\right)$ in Approach 1 or $\vec{f}_j = (f_{a3}, f_{a2}, f_{\Lambda 1})$ in Approach 2, when using categorization Scheme 2 for fitting HVV couplings. We simplify treatment of the EW processes in categorization Scheme 1 when fitting for *CP*-violating Hgg or Htt couplings and allow only the *CP*-violating f_{a3} parameter in $\vec{f}_j$. When all anomalous couplings are set to zero, the signal strength μ_V is equal to the ratio of the cross sections of all EW processes (VBF, ZH, WH) to the SM expectation. In the case of $f_{ai} = 1$, this ratio is corrected by the factor $(\alpha_{ii}/\alpha_{11})$ as quoted in Table 1 for decay cross sections, and the inverse of this factor for the EW production cross sections, due to the evolution of the cross sections with anomalous couplings.

It has been shown that there is no sensitivity to the anomalous couplings in the $b\bar{b}H$ process [32] and it is parameterized with the signal strength $\mu_j = \mu_{b\bar{b}H}$. Depending on the fit implementation discussed in Section 6, this signal strength may be correlated with those in other channels, such as μ_{ggH} or $\mu_{t\bar{t}H}$. The exact treatment of this process is expected to have negligible effect on the results, because it cannot be distinguished kinematically from other dominant processes and its relative contribution in each kinematic region is expected to be negligibly small, as shown in Tables 2 and 3.

The background processes i in Eq. (22) include the $q\bar{q} \to 4\ell$, $gg \to 4\ell$, and EW processes, all of which are estimated with simulation, but receive additional constraints from sidebands in data. The EW background includes vector boson scattering and VVV processes, which are the background counterparts of the VBF and VH processes. We also include the $t\bar{t}VV$ and $t\bar{t}V$ processes in this background contribution, which are important in the study of the $t\bar{t}H$ signal process. Interference of the signal and background processes is negligible in the analysis of the on-shell H boson production. The Z + X background contribution models Z+jets and other related processes with lepton misidentification and is estimated from the control regions in the data as discussed in Section 3.4. All signal j and background i processes contributing to Eq. (22) and their expected yields are shown in Tables 2 and 3.

The signal and background probability distributions $\mathcal{P}_{jk}^{sig}$ and $\mathcal{P}_{ik}^{bkg}$ appearing in Eq. (22) are binned multidimensional histograms (templates) of observables $\vec{x}$ listed in Table 4. The binning of these templates has been optimized for memory and speed of computer calculations, expected population of events across those bins, and retaining kinematic information. In particular, the large number of discriminants used in the Untagged, VBF-2jet, and VH-hadronic categories in Scheme 2, requires careful optimization of the binning employed in analysis. In these categories, two bins are used in the two interference discriminants and three bins are used in the other five discriminants, which corresponds to a total of 972 bins in the seven-dimensional (7D) distribution. However, the bins with a very low yield of expected events for all contributions are merged, and the expected symmetry in the distribution of the $\mathcal{D}_{CP}$ observable is enforced. As a result, the total number of independent bins depends on the category, but does not exceed 400 in any of the categories. Even though only a limited number of bins is used in each dimension, the 7D distribution retains substantial kinematic information that is nearly

optimal for all anomalous couplings targeted in this analysis. This has been validated against a dedicated analysis targeting one anomalous coupling at a time with a much larger number of bins in each dimension for a smaller number of discriminants, as employed in Refs. [16, 17]. This nearly optimal performance is realized in large respect due to the optimal population of events across the range of discriminant values by construction of the MELA approach.

The $\mathcal{P}^{\text{sig}}_{jk}$ and $\mathcal{P}^{\text{bkg}}_{ik}$ probabilities depend on the parameters $\vec{\xi}_{jk}$ and $\vec{f}_j$ and are therefore interpolated between various templates as a function of these parameters. The $\vec{\xi}_{jk}$ reflect systematic uncertainties either in the normalization or shape of both signal and background templates and an analytical linear interpolation is adopted. The $\vec{f}_j$ parameters require nontrivial analytical interpolation of the signal templates, which is discussed in more detail below.

5.2 Signal parameterization

In the signal production and decay processes, the same anomalous couplings could appear either on both the production and decay sides simultaneously, as in the case of HVV couplings in EW production and $\mathrm{H} \to \mathrm{VV} \to 4\ell$ decay, or only on one side (production or decay). This is illustrated in Eq. (14), with $\left(\sum_{il} \alpha^{(j)}_{il} a_i a_l\right)$ appearing on the production side and $\left(\sum_{mn} \alpha^{(f)}_{mn} a_m a_n\right)$ appearing on the decay side. We absorb the width Γ_{H} in Eq. (14) into the overall signal strength and parameterize the kinematic dependence in the signal probability density on the ratio of couplings through $\vec{f}_j$ in the following way.

In the case of HVV anomalous couplings, we have either $L = 5$ couplings in Approach 1 or $L = 4$ couplings in Approach 2, which we can parameterize with four or three components of $\vec{f}_j$, defined above, and $f_{a1} = (1 - |f_{a2}| - |f_{a3}| - |f_{\Lambda 1}| - |f^{\mathrm{Z}\gamma}_{\Lambda 1}|)$. Let us denote these as f_l with $l = 1, 2, 3, 4, 5$. For the ggH and $\mathrm{t\bar{t}H}$ processes, when we consider anomalous couplings on the production side, we have only two parameters $f_l = (1 - |f^{\mathrm{ggH}}_{a3}|)$ and f^{ggH}_{a3}, or $(1 - |f^{\mathrm{Htt}}_{\mathrm{CP}}|)$ and $f^{\mathrm{Htt}}_{\mathrm{CP}}$, and $L = 2$. When developing the expression in Eq. (14), one gets a polynomial in the couplings $a_l \propto \sqrt{|f_l|}\ \mathrm{sign}(f_l)$ following Eq. (19), which is either quartic ($C = 4$), in the case of the EW processes, or quadratic ($C = 2$), when the couplings appear only on the decay or production side. Parameterization of the anomalous coupling dependence of the $\mathcal{P}^{\text{sig}}_{jk}$ probability density in Eq. (22) is different in these two cases.

This leads to the following general expression for the probability density of the EW processes with $C = 4$

$$\mathcal{P}^{\text{sig}}_{jk}\left(\vec{x}; \vec{\xi}_{jk}, \vec{f}_j\right) \propto \sum_{l \le m \le n \le p = 1}^{L} \mathcal{P}^{\text{sig}}_{jk,lmnp}\left(\vec{x}; \vec{\xi}_{jk}\right) \sqrt{|f_l\, f_m\, f_n\, f_p|}\ \mathrm{sign}(f_l\, f_m\, f_n\, f_p)\,. \tag{23}$$

The following general expression applies to the probability density of the processes with $C = 2$

$$\mathcal{P}^{\text{sig}}_{jk}\left(\vec{x}; \vec{\xi}_{jk}, \vec{f}_j\right) \propto \sum_{l \le m = 1}^{L} \mathcal{P}^{\text{sig}}_{jk,lm}\left(\vec{x}; \vec{\xi}_{jk}\right) \sqrt{|f_l\, f_m|}\ \mathrm{sign}(f_l\, f_m)\,. \tag{24}$$

In both Eqs. (23) and (24), only the kinematic dependence on $\vec{f}_j$ is expressed, while the overall normalization can be absorbed into μ_j or accounted for as part of the cross section measurement.

In the general case, there are $(C + L - 1)!/(C!(L - 1)!)$ terms in either Eq. (23) or Eq. (24). This leads to 70 terms in Eq. (23) when we measure four anomalous HVV couplings in production

and decay ($L = 5$, $C = 4$), 15 terms in Eq. (24) when we measure four anomalous HVV couplings in decay only ($L = 5$, $C = 2$), and three terms in Eq. (24) when we measure Hgg or Htt couplings in production only ($L = 2$, $C = 2$). When both HVV (in decay) and Hgg or Htt (in production) couplings are measured at the same time in a given process, the number of terms is multiplied ($15 \times 3 = 45$), since the two probabilities factorize.

The $\mathcal{P}^{\text{sig}}_{jk,lm(np)}$ templates are extracted from simulation, discussed in Section 3.3, typically using from three to twelve samples generated with various $\vec{f}_j$ values chosen to map different points of phase-space well and reweighted with the MELA package to cover all possibilities with $(C+L-1)!/(C!(L-1)!)$ combinations of couplings. In parameterizing the signal templates $\mathcal{P}^{\text{sig}}_{jk,lm(np)}$, it is important to ensure that the expected number of events in every bin of the probability densities, defined in Eqs. (23) and (24), remains nonnegative at all possible values of $\vec{f}_j$, because a negative yield would cause the likelihood function used for the final fit to become ill-defined.

To detect a negative event yield, we first minimize Eq. (23) or Eq. (24), which are polynomials in $\sqrt{|f_l|}$, by finding where the gradient is zero. For Eq. (24), which is quadratic, this is a simple problem in linear algebra. Equation (23) is quartic, so its gradient is a system of cubic equations, which cannot be solved exactly for $L > 1$. We use the HOM4PS program [105–107] to numerically solve the system of equations. If we find the minimum to be negative, we adjust the estimated $\mathcal{P}^{\text{sig}}_{jk,lmnp}$ until the yield is always positive. This adjustment is made using the statistical uncertainty on $\mathcal{P}^{\text{sig}}_{jk,lmnp}$ through a cutting planes algorithm [108] implemented using the GUROBI program [109]. In all cases, it is found that only small modifications to the initial estimates of $\mathcal{P}^{\text{sig}}_{jk,lmnp}$ are needed.

The parameterization in Eqs. (23) and (24) is written in the self-consistent full-amplitude approach. In the EFT interpretation of the amplitude fit, the series in powers of $|f_{ai}|^{1/2}$ corresponds to terms of different dimension, as discussed in Section 2.3. For example, in Eq. (23) the term with f_{a1}^2 corresponds to the SM-like contribution with dimension-four operators, while $f_{a1}^{3/2}|f_{ai}|^{1/2}$ corresponds to interference between the SM amplitude and the dimension-six contributions in the EFT expansion. Assuming that $f_{a1} \sim 1$ and all f_{ai} are small, all other terms could in principle be neglected as a test of EFT validity. In practice, however, neglecting those terms can easily lead to a negative probability in certain points in the phase space of observables, which invalidates the maximum likelihood fit. This does not necessarily mean that the EFT approach is not valid. This happens because the sizable interference terms can lead to a negative partial sum in Eq. (23), especially in the optimized multidimensional space of observables that are sensitive to such interference effects. Therefore, in practice, the fits presented in Section 6 do not allow one to place constraints without the full series shown in Eqs. (23) and (24).

5.3 Likelihood fit

The final constraints on parameters μ_j and $\vec{f}_j$ are placed using the profile likelihood method implemented in the ROOFIT toolkit [110] within the ROOT [111] framework. The extended likelihood function is constructed using the probability densities in Eq. (22), with each event characterized by the discrete category k and observables $\vec{x}$. The likelihood $\mathcal{L}$ is maximized with respect to the nuisance parameters $\vec{\xi}_{jk}$ describing the systematic uncertainties discussed below, and μ_j and $\vec{f}_j$ parameters of interest. The allowed 68 and 95% CL intervals are defined using the profile likelihood function, $-2\Delta \ln \mathcal{L} = 1.00$ and 3.84, for which exact coverage is expected in the asymptotic limit [112].

The reinterpretation of the primary μ_j and $\vec{f}_j$ results in terms of couplings is performed with the help of Eq. (14) to relate signal strength μ_j to couplings and Eqs. (16–18) to relate $\vec{f}_j$ to coupling ratios. In this way the couplings directly enter the parameterization in Eq. (22). However, without further constraints on the H boson width, such a fit would not provide useful constraints on the coupling size. Therefore, in the total width Γ_{H} parameterization in Eq. (14), we assume that there are no unobserved or undetected H boson decays. We express the width Γ_{H} as the sum of partial decay widths of nine H boson decay modes dominant in the SM, $\mathrm{H} \to \mathrm{b\bar{b}}$ being the largest and $\mathrm{H} \to \mu^+\mu^-$ being the smallest. Each partial decay width is scaled as a function of anomalous couplings following the parameterization in Ref. [33].

5.4 Systematic uncertainties

Several systematic uncertainties are considered in the set of constrained parameters $\vec{\xi}_{jk}$. The relative expected yields in different categories and the template shapes describing probability distributions in Eq. (22) are varied within either theoretical or experimental uncertainties. All results reported at 68 and 95% CL are dominated by statistical uncertainties. All systematic uncertainties are treated as correlated between different time periods, except for the jet-related uncertainties, which originate from statistically independent sources, and luminosity uncertainties, which are partially correlated [113–115].

The theoretical uncertainties considered are PDF parameterization, factorization and renormalization scales, the hadronization scale used in PYTHIA, and the underlying event variations. The underlying event modeling uncertainty is determined by varying initial- and final-state radiation scales between 0.25 and 4 times their nominal value. The effects of the modeling of hadronization are determined by simulating additional events with the variation of the nominal PYTHIA tune described in Section 3. Experimental uncertainties involve jet energy calibration and b-quark-tagging efficiency uncertainties, which are only relevant when production categories are considered, and lepton efficiency and momentum uncertainties, which are similar for the different processes and categories. In the estimation of the $\mathrm{Z}+\mathrm{X}$ background, the flavor composition of QCD-evolved jets misidentified as leptons may be different in the $\mathrm{Z}+1\ell$ and $\mathrm{Z}+2\ell$ control regions, and together with the statistical uncertainty in the $\mathrm{Z}+2\ell$ region, this uncertainty accounts for about a $\pm 30\%$ variation in the $\mathrm{Z}+\mathrm{X}$ background.

The normalization of the background processes derived from the MC simulation is affected by a 1.8% uncertainty in the integrated luminosity. However, all results are found to be insensitive to luminosity or theoretical constraints on the nonresonant $\mathrm{ZZ}/\mathrm{Z}\gamma^* \to 4\ell$ background. Even though the theoretical cross section is one of the constraints in the fit, the wide sideband included in the range $105 < m_{4\ell} < 140\,\mathrm{GeV}$ constrains this nearly flat background from the data, with nearly identical results when the theoretical constraints are removed. The main distinguishing feature of this background is the dominant contribution of the $\mathrm{Z}\gamma^*$ intermediate state, which allows effective separation of the already small background from signal using kinematic information.

6 Results

The signal strength μ_j and the set of parameters $\vec{f}_j$ describing the tensor structure of interactions are constrained in each production process and decay $\mathrm{H} \to \mathrm{ZZ}$ / $\mathrm{Z}\gamma^*$ / $\gamma^*\gamma^* \to 4\ell$. In the following, we describe the measurement of f_{a3}^{ggH} in the ggH process, $f_{\mathrm{CP}}^{\mathrm{Htt}}$ in the $\mathrm{t\bar{t}H}$ and tH processes, and the combination of the two where the top quark contributes to the gluon fusion loop. We then report measurements of $\left(f_{a2}, f_{a3}, f_{\Lambda 1}, f_{\Lambda 1}^{\mathrm{Z}\gamma}\right)$ in the VBF and VH processes along

Table 5: Constraints on the f_{a3}^{ggH} and f_{CP}^{Htt} parameters with the best fit values and allowed 68% CL (quoted uncertainties) and 95% CL (within square brackets) intervals, limited to the physical range of $[-1, 1]$. The f_{CP}^{Htt} constraints obtained in this work are combined with those in the $H \to \gamma\gamma$ channel [26]. The interpretation of the f_{a3}^{ggH} result under the assumption of the top quark dominance in the gluon fusion loop are presented in terms of the f_{CP}^{Htt} parameter, where either ggH or its combination with tH and $t\bar{t}H$ results are shown.

Parameter	Scenario	Observed	Expected
f_{a3}^{ggH}	ggH ($H \to 4\ell$)	$-0.04^{+1.04}_{-0.96}$ $[-1, 1]$	0 ± 1 $[-1, 1]$
f_{CP}^{Htt}	tH & $t\bar{t}H$ ($H \to 4\ell$)	$\pm(0.88^{+0.12}_{-1.88})$ $[-1, 1]$	0 ± 1 $[-1, 1]$
	tH & $t\bar{t}H$ ($H \to \gamma\gamma$) [26]	0.00 ± 0.33 $[-0.67, 0.67]$	0.00 ± 0.49 $[-0.82, 0.82]$
	tH & $t\bar{t}H$ ($H \to 4\ell$ & $\gamma\gamma$)	0.00 ± 0.33 $[-0.67, 0.67]$	0.00 ± 0.48 $[-0.81, 0.81]$
	ggH ($H \to 4\ell$)	$-0.01^{+1.01}_{-0.99}$ $[-1, 1]$	0 ± 1 $[-1, 1]$
	ggH & tH & $t\bar{t}H$ ($H \to 4\ell$)	$-0.56^{+1.56}_{-0.44}$ $[-1, 1]$	0.00 ± 0.47 $[-1, 1]$
	ggH & tH & $t\bar{t}H$ ($H \to 4\ell$ & $\gamma\gamma$)	$-0.04^{+0.38}_{-0.36}$ $[-0.69, 0.68]$	0.00 ± 0.30 $[-0.70, 0.70]$

with the $H \to 4\ell$ decay in all production processes, following Approach 1 with the coupling relationship $a_i^{WW} = a_i^{ZZ}$. We also report measurements of $(f_{a2}, f_{a3}, f_{\Lambda 1})$ following Approach 2 within SMEFT, discussed in Section 2. These results are interpreted in terms of constraints on the Hff, Hgg, and HVV operators. While all operators could potentially be constrained in a joint analysis of all H boson decay modes, in this paper we analyze only the $H \to 4\ell$ decay mode, and perform a combination with the tH and $t\bar{t}H$ processes in the $H \to \gamma\gamma$ decay mode. Therefore, for the purpose of illustration, we make further assumptions on how certain couplings, to which this analysis is not sensitive, are related. For example, we must make certain assumptions about the relationship between the Hbb, Hcc, $H\tau\tau$, and $H\mu\mu$ couplings and other couplings. These assumptions are discussed in each of the applications presented below.

6.1 Constraints on Hgg couplings

The measurement of anomalous couplings of the H boson to gluons is presented in Fig. 14 and Table 5. Since the direct couplings of the H boson to SM fermions in the gluon fusion loop and to potentially new particles appearing in the loop can not be resolved using this measurement alone, both effects are characterized with two parameters, f_{a3}^{ggH} and μ_{ggH}. The signal strength μ_{ggH}, which is the ratio of the measured cross section of the gluon fusion process to that expected in the SM, is profiled when the f_{a3}^{ggH} results are reported. The measurement of the f_{a3}^{ggH} is consistent with zero, as expected in the SM. This can be clearly seen from the $\mathcal{D}_{CP}^{ggH}$ and $\mathcal{D}_{0^-}^{ggH}$ distributions in Fig. 10. The measured value of $\mu_{ggH} = 0.86^{+0.13}_{-0.11}$ is consistent with that reported in Ref. [78] without the fit for the *CP* structure of interactions. The values of μ_{ggH} and f_{a3}^{ggH} are uncorrelated. The signal strength of the VBF and VH processes μ_V and their *CP* properties f_{a3} are also profiled when this measurement is performed. This measurement is also performed simultaneously in a fit with the $t\bar{t}H$ process with the $\mu_{t\bar{t}H}$ and f_{CP}^{Htt} parameters unconstrained, as discussed below. The tH process is always included with the $t\bar{t}H$ process with its signal strength expressed through the $\mu_{t\bar{t}H}$, μ_V, and f_{CP}^{Htt} parameters.

The parameters f_{a3}^{ggH} and μ_{ggH} are equivalent to the measurement of the *CP*-even and *CP*-odd couplings on the production side, while the HVV couplings on the decay side are constrained

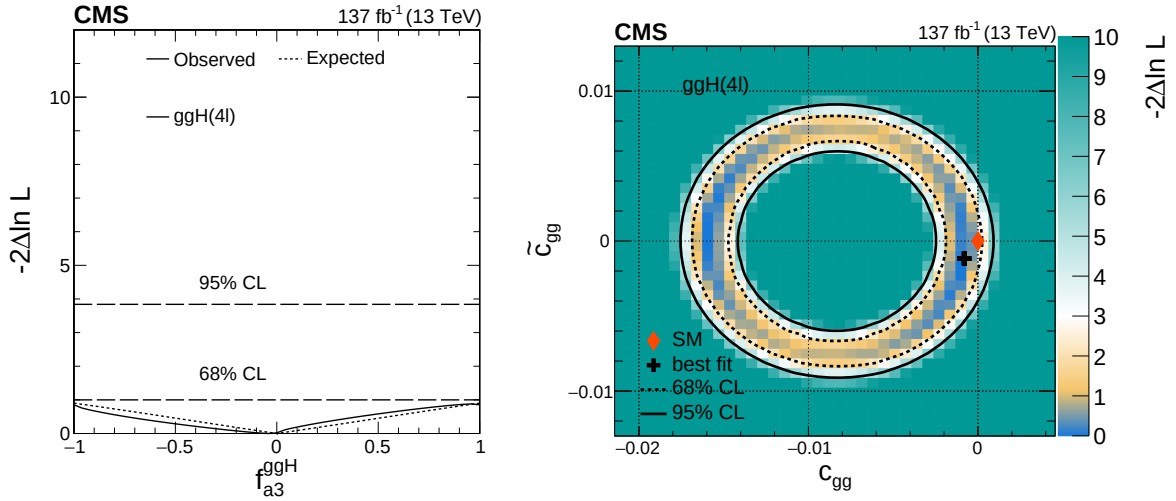

Figure 14: Constraints on the anomalous H boson couplings to gluons in the ggH process using the $H \to 4\ell$ decay. Left: Observed (solid) and expected (dashed) likelihood scans of the *CP*-sensitive parameter f_{a3}^{ggH}. The dashed horizontal lines show 68 and 95% CL. Right: Observed confidence level intervals on the c_{gg} and $\tilde{c}_{gg}$ couplings reinterpreted from the f_{a3}^{ggH} and μ_{ggH} measurement with f_{a3} and μ_V profiled, and with $\kappa_t = \kappa_b = 1$. The dashed and solid lines show the 68 and 95% CL exclusion regions in two dimensions, respectively.

from the simultaneous measurement of the VBF and VH processes with f_{a3} and μ_V profiled. The c_{gg} and $\tilde{c}_{gg}$ couplings, introduced in Eqs. (12) and (13), can be extracted from the above measurements. We follow the parameterization of the cross section and the total width from Ref. [33], where c_{gg}, $\tilde{c}_{gg}$, κ_t, $\tilde{\kappa}_t$, κ_b, and $\tilde{\kappa}_b$ contribute. Since it is not possible to disentangle all these couplings in a single process, we fix $\kappa_t = \kappa_b = 1$ and $\tilde{\kappa}_t = \tilde{\kappa}_b = 0$ to the SM expectation and leave c_{gg} and $\tilde{c}_{gg}$, which describe possible BSM contribution in the loop, unconstrained. The small contribution of the $H \to \gamma\gamma$ and $Z\gamma$ decays to the total width is assumed to be SM-like.

The resulting constraints on c_{gg} and $\tilde{c}_{gg}$ are shown in Fig. 14, right. The general features of these constraints are the following. The pure signal strength measurement μ_{ggH}, available even without the fit for f_{a3}^{ggH}, provides a constraint in the form of a ring on a two-parameter plane in Fig. 14, right. The measurement of f_{a3}^{ggH} resolves the areas within this ring. Since the sensitivity of the f_{a3}^{ggH} measurement is currently just under 68% CL, this resolution is not strong. The H boson width dependence on c_{gg} and $\tilde{c}_{gg}$ is relatively weak and does not alter this logic considerably. The results are consistent with the SM expectation.

As mentioned earlier, it is not possible to resolve the loop contributions from the SM or BSM particles in this measurement. Therefore, the deviations of the SM-like Yukawa couplings κ_t and κ_b from unit values are absorbed into the effective c_{gg} measurement, and the *CP*-odd Yukawa couplings $\tilde{\kappa}_t$ and $\tilde{\kappa}_b$ are absorbed into the effective $\tilde{c}_{gg}$ measurement, together with possible contributions from BSM particles. However, re-interpretation of these results is possible in terms of the independent Yukawa couplings and effective point-like gluon couplings in combination with the $t\bar{t}H$ and tH modes, as discussed below.

6.2 Constraints on Htt couplings

The measurement of anomalous couplings of the H boson to top quarks is presented in Fig. 15 and Table 5. First, the measurements of f_{CP}^{Htt} from the $t\bar{t}H$ and tH processes only are reported.

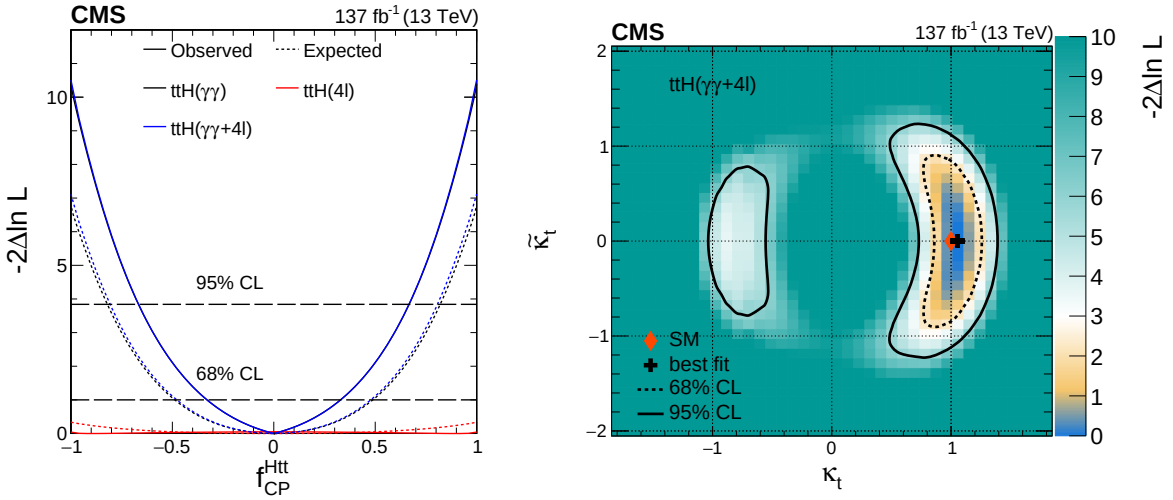

Figure 15: Constraints on the anomalous H boson couplings to top quarks in the $t\bar{t}H$ and tH processes using the $H \to \gamma\gamma$ [26] and $H \to 4\ell$ decays. Left: Observed (solid) and expected (dashed) likelihood scans of f_{CP}^{Htt} in the $t\bar{t}H$ and tH processes in the $H \to 4\ell$ (red), $\gamma\gamma$ (black), and combined (blue) channels, where the combination is done without relating the signal strengths in the two processes. The dashed horizontal lines show 68 and 95% CL. Right: Observed confidence level intervals on the κ_t and $\tilde{\kappa}_t$ couplings reinterpreted from the f_{CP}^{Htt}, $\mu_{t\bar{t}H}$, and μ_V measurements in the combined fit of the $H \to 4\ell$ and $\gamma\gamma$ channels, with the signal strengths in the two channels related through the couplings as discussed in text. The dashed and solid lines show the 68 and 95% CL exclusion regions in two dimensions, respectively.

The signal strength $\mu_{t\bar{t}H}$, which is the ratio of the measured cross section of the $t\bar{t}H$ process to that expected in the SM, is profiled when the f_{CP}^{Htt} results are reported. The measured value of $\mu_{t\bar{t}H} = 0.17^{+0.70}_{-0.17}$ is consistent with that reported in Ref. [78] without the fit for the CP structure of interactions. In both cases we observe downward fluctuations in the signal yield compared to expectation, but these fluctuations are not statistically significant. There is no significant linear correlation between $\mu_{t\bar{t}H}$ and f_{CP}^{Htt}. The signal strength of the VBF and VH processes μ_V, ggH process μ_{ggH}, and their CP properties f_{a3} and f_{a3}^{ggH} are also profiled when this measurement is performed. This analysis of the $t\bar{t}H$ and tH processes is not sensitive to the sign of f_{CP}^{Htt}. However, for later combination with the ggH measurement, presented above, under the assumption of the top quark dominance in the gluon fusion loop, symmetric constraints on f_{CP}^{Htt} are reported.

The observed best fit f_{CP}^{Htt} value gives preference to the CP-odd Yukawa coupling. This comes from the negative value of the $\mathcal{D}_{0^-}^{t\bar{t}H}$ discriminant for the one observed signal-like event in Fig. 9. However, this result is statistically consistent with the pure CP-even Yukawa coupling expected in the SM. With just about two signal $t\bar{t}H$ events and many fewer tH events expected to appear in the fit in the $H \to 4\ell$ channel under the assumption of the SM cross section, according to Table 2, the expected confidence sensitivity on the f_{CP}^{Htt} constraints is low. Nonetheless, the very high signal purity in the $H \to 4\ell$ channel makes every observed event candidate carry a large statistical weight. The importance of including the CP measurements in the $t\bar{t}H$ and tH production modes also becomes evident when combination with ggH is performed. There is a significant gain in such a combination beyond a simple addition of independent measurements, as discussed in Section 6.3.

The CMS experiment recently reported the measurement of the f_{CP}^{Htt} parameter in the $t\bar{t}H$ and tH production processes with the decay $H \to \gamma\gamma$ [26] (shown also in Table 5). In that measurement, the signal strength $\mu_{t\bar{t}H}^{\gamma\gamma}$ parameter is profiled, while the signal strengths in other production processes are fixed to the SM expectation. However, there is a very weak correlation of the measurement in the $t\bar{t}H$ and tH processes with parameters in the other production mechanisms. Therefore, we proceed with a combination of the f_{CP}^{Htt} measurements in the $H \to 4\ell$ and $\gamma\gamma$ channels, where we correlate their common systematic uncertainties, but not the signal strengths of the processes. In particular, we do not relate the $\mu_{t\bar{t}H}$ and $\mu_{t\bar{t}H}^{\gamma\gamma}$ signal strengths because they could be affected differently by the particles appearing in the loops responsible for the $H \to \gamma\gamma$ decay. The results of this combination are presented in Fig. 15 and Table 5. The measured signal strength in the $H \to 4\ell$ channel is $\mu_{t\bar{t}H} = 0.04^{+0.76}_{-0.04}$, uncorrelated with f_{CP}^{Htt}, while $\mu_{t\bar{t}H}^{\gamma\gamma} = 1.23^{+0.33}_{-0.24}$ and the correlation with f_{CP}^{Htt} is $+0.20$. The pure pseudoscalar hypothesis of the H boson corresponding to $f_{CP}^{Htt} = 1$ in the case of the *CP*-odd Yukawa interaction is excluded at 3.2 standard deviations, while the expected exclusion is 2.7 standard deviations. Below, we also present an interpretation of these results where the signal strengths in the two H boson decay channels are related through the couplings.

In the above measurements, the f_{CP}^{Htt} parameter has the same meaning in both the $H \to 4\ell$ and $\gamma\gamma$ channels. In order to make an EFT coupling interpretation of the results, we have to make a further assumption that no BSM particles contribute to the loop in the $H \to \gamma\gamma$ decay. Without this or a similar assumption, the signal strength in the $H \to \gamma\gamma$ decay cannot be interpreted without ambiguity. We further re-parameterize the cross section following Ref. [33] with the couplings κ_t and $\tilde{\kappa}_t$, and fix $\kappa_b = 1$ and $\tilde{\kappa}_b = 0$. The bottom quark coupling makes a very small contribution to the loop in the $H \to \gamma\gamma$ decay, but it makes a large contribution to the total decay width, where we assume that there are no unobserved or undetected H boson decays. In order to simplify the fit, we do not allow anomalous HVV couplings, and the measurement of the signal strength μ_V constrains the contribution of the a_1 coupling in the loop. The f_{a3}^{ggH} and μ_{ggH} parameters are profiled in this fit.

The observed confidence level intervals on the κ_t and $\tilde{\kappa}_t$ couplings from the combined fit of the $H \to 4\ell$ and $\gamma\gamma$ channels are shown in Fig. 15. There is no linear correlation between the values of κ_t and $\tilde{\kappa}_t$. As was the case for the $(c_{gg}, \tilde{c}_{gg})$ measurement in Fig. 14, the pure yield measurement in the $t\bar{t}H$ process would constrain a ring in the two-dimensional plane. However, the *CP*-sensitive measurement of f_{CP}^{Htt} disfavors the values away from $\tilde{\kappa}_t = 0$. Moreover, the sign ambiguity between the κ_t and $-\kappa_t$ values cannot be resolved in the $t\bar{t}H$ channel alone. With the inclusion of the tH process, the negative values of κ_t are disfavored because strong constructive interference between the amplitudes induced by the HVV and Htt couplings would result in enhanced tH yield, inconsistent with the data. Therefore, the sign of κ_t is defined in reference to the tree-level HVV coupling a_1. But, the sign ambiguity between the $\tilde{\kappa}_t$ and $-\tilde{\kappa}_t$ values cannot be resolved in this fit, unless information from the other channels is incorporated, such as information from the gluon fusion loop discussed below.

6.3 Constraints on Htt and Hgg couplings in combination

First, we consider the ggH process under the assumption of top quark dominance in the gluon fusion loop. The measurement of anomalous couplings of the H boson to top quarks for this case is presented in Fig. 16 and Table 5. Similar to the case of the $H \to \gamma\gamma$ loop discussed above, the cross section of the ggH process, normalized to the SM expectation, is parameterized

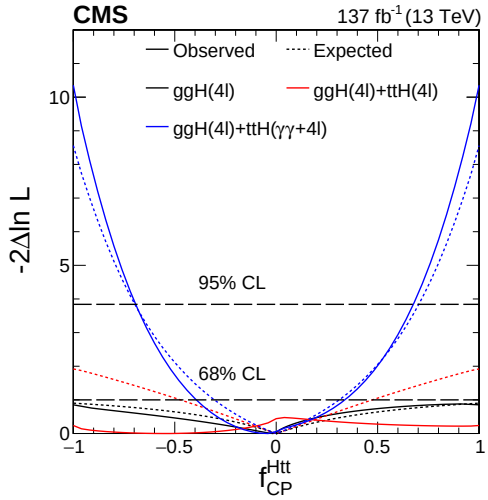

Figure 16: Constraints on the anomalous H boson couplings to top quarks in the $t\bar{t}H$, tH, and ggH processes combined, assuming top quark dominance in the gluon fusion loop, using the $H \to 4\ell$ and $\gamma\gamma$ decays. Observed (solid) and expected (dashed) likelihood scans of f_{CP}^{Htt} are shown in the ggH process with $H \to 4\ell$ (black), $t\bar{t}H$, tH, and ggH processes combined with $H \to 4\ell$ (red), and in the $t\bar{t}H$, tH, and ggH processes with $H \to 4\ell$ and the $t\bar{t}H$ and tH processes with $\gamma\gamma$ combined (blue). Combination is done by relating the signal strengths in the three processes through the couplings in the loops in both production and decay, as discussed in the text. The dashed horizontal lines show 68 and 95% CL exclusion.

following Ref. [33] to account for *CP*-odd Yukawa couplings as follows:

$$\frac{\sigma(ggH)}{\sigma_{SM}} = \kappa_f^2 + 2.38\tilde{\kappa}_f^2, \tag{25}$$

where we set $\kappa_f = \kappa_t = \kappa_b$ and $\tilde{\kappa}_f = \tilde{\kappa}_t = \tilde{\kappa}_b$. Equation (25) sets the relationship between f_{CP}^{Htt} and f_{a3}^{ggH}, reported in Fig. 14 and Table 5, according to Eq. (17).

Constraints on f_{CP}^{Htt} are also shown for the combination of the $t\bar{t}H$, tH, and ggH processes with $H \to 4\ell$ in Fig. 16 and Table 5. The combination of the $H \to 4\ell$ and $\gamma\gamma$ channels with $t\bar{t}H$, tH, and ggH processes proceeds in a similar manner and is also shown in Fig. 16 and Table 5. In this case, we do not allow anomalous HVV couplings, and the measurement of the signal strength μ_V constrains the contribution of the a_1 coupling in the $H \to \gamma\gamma$ loop.

The gain in this combination of the ggH and tH & $t\bar{t}H$ processes is beyond the simple addition of the two constraints. While in the ggH and $t\bar{t}H$ analyses the signal strengths of the two processes are independent, they could be related under the assumption of top quark dominance in the loop using Eq. (25). As discussed in Section 2, *CP*-odd coupling predicts rather different cross sections in the two processes: $\sigma(\tilde{\kappa}_f = 1)/\sigma(\kappa_f = 1)$ is 2.38 in the gluon fusion process dominated by the top quark loop and 0.391 in the $t\bar{t}H$ process. This means that the ratio differs by a factor of 6.09 for $f_{CP}^{Htt} = 1$ when compared to SM ($f_{CP}^{Htt} = 0$). This correlation enhances the sensitivity in the f_{CP}^{Htt} measurement. For example, the combined sensitivity from tH and $t\bar{t}H$ (with either $H \to 4\ell$ alone or together with $H \to \gamma\gamma$), and ggH is significantly improved compared to separate analyses, and the result is not just a simple addition of two independent results, as shown in Fig. 16 and Table 5. This effect also enhances correlation between f_{CP}^{Htt} and the yield parameters. In the full combination, the measured signal strength is $\mu_{t\bar{t}H} = 0.70^{+0.30}_{-0.25}$ and the correlation with f_{CP}^{Htt} is +0.96.

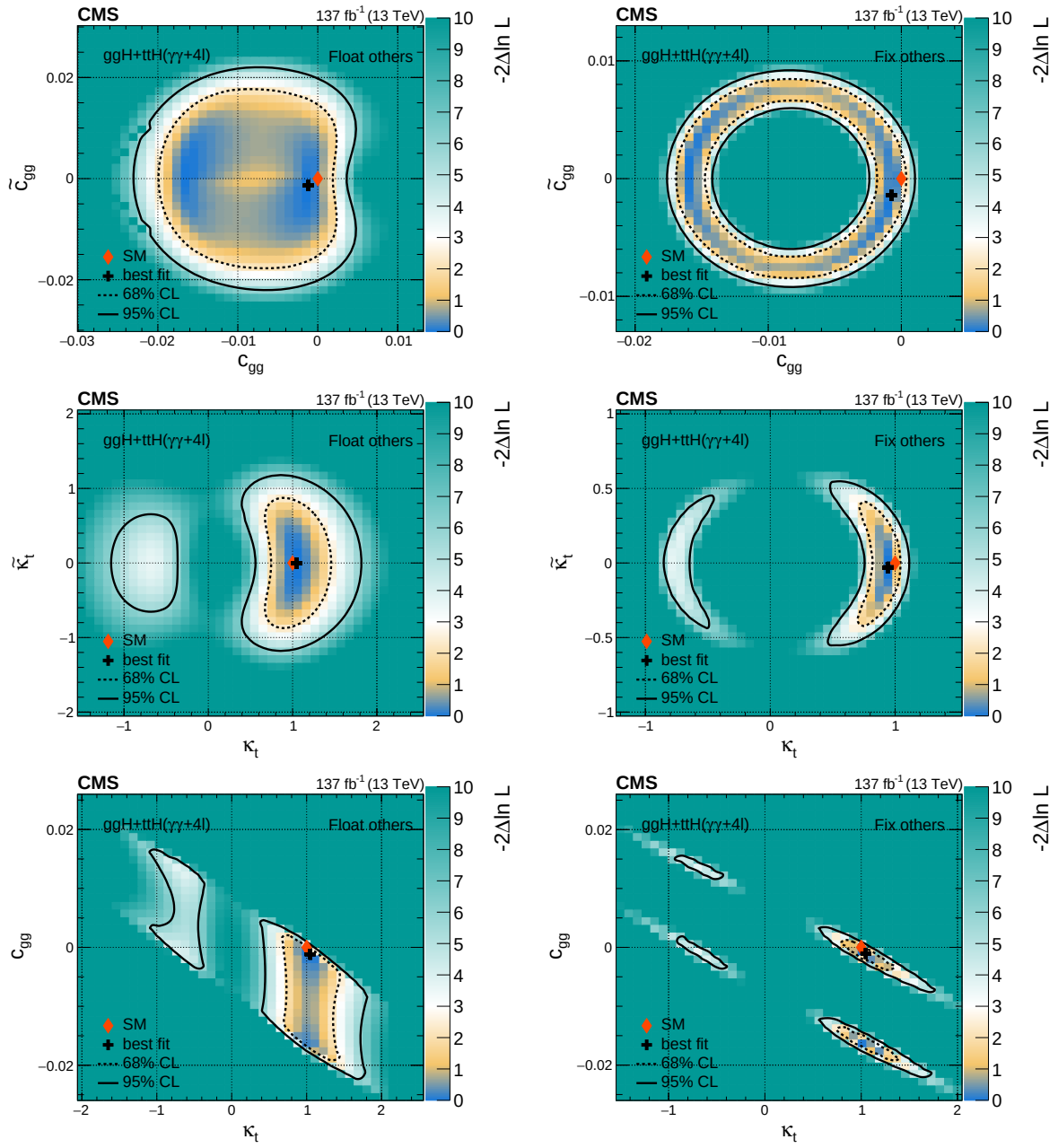

Figure 17: Constraints on the anomalous H boson couplings c_{gg}, $\tilde{c}_{gg}$, κ_t, and $\tilde{\kappa}_t$ in the $t\bar{t}H$, tH, and ggH processes combined, using the $H \to 4\ell$ and $\gamma\gamma$ decays. The constraints are shown for the pairs of parameters: c_{gg} and $\tilde{c}_{gg}$ (upper), κ_t and $\tilde{\kappa}_t$ (middle), κ_t and c_{gg} (lower), and with the other two parameters either profiled (left) or fixed to the SM expectation (right). The dashed and solid lines show the 68 and 95% CL exclusion regions in two dimensions, respectively.

Finally, we present the reinterpretation of the f_{a3}^{ggH}, f_{CP}^{Htt}, and signal strength measurements in terms of constraints on c_{gg}, $\tilde{c}_{gg}$, κ_t, and $\tilde{\kappa}_t$. In this fit, it is assumed that $\kappa_b = \kappa_c = \kappa_\mu = 1$ and $\tilde{\kappa}_b = \tilde{\kappa}_c = \tilde{\kappa}_\mu = 0$ in the fermion coupling contribution to the loops and in the decay width parameterization [33]. The gluon fusion loop is parameterized in terms of point-like couplings c_{gg} and $\tilde{c}_{gg}$, and the top and bottom quark contributions. These point-like and top couplings can be resolved in combination with the $t\bar{t}H$ and tH production processes. The $H \to \gamma\gamma$ loop is parameterized with the top and bottom quark and with the W contributions. One cannot generally relate the point-like couplings in this loop and in the gluon fusion loop, and they are assumed to be zero in $H \to \gamma\gamma$. The measurement of the signal strength μ_V constrains the contributions of the a_1 coupling, affecting the W contribution to the $H \to \gamma\gamma$ loop and tH process, and anomalous HVV couplings are not allowed. By convention, the a_1 coupling is constrained to be positive, which sets the relative sign of κ_t. It is assumed that there are no unobserved or undetected H boson decays.

The constraints are shown in Fig. 17, where the likelihood scans are plotted for the pairs of parameters: (c_{gg}, $\tilde{c}_{gg}$), (κ_t, $\tilde{\kappa}_t$), and (κ_t, c_{gg}), with the other two parameters either profiled or fixed to the SM expectation. On the likelihood scan of (c_{gg}, $\tilde{c}_{gg}$) with the other parameters fixed, the appearance is generally similar to the scan shown in Fig. 14. This is because the addition of the $t\bar{t}H$ and tH processes does not alter the results much with their couplings fixed to the SM. However, with the other parameters affecting the gluon fusion loop left floating, the contours are washed out, as one would expect with more degrees of freedom in a fit.

On the likelihood scan of (κ_t, $\tilde{\kappa}_t$) with the other parameters profiled, one can observe the effects similar to that in Fig. 15. This is because the ggH process does not bring additional constraints due to uncertainties with the point-like interactions, but may introduce additional modifications to the fit parameters. However, with the point-like interactions c_{gg} and $\tilde{c}_{gg}$ set to zero, constraints on the κ_t and $\tilde{\kappa}_t$ couplings appear tighter as a result of the combination of information from the $t\bar{t}H$, tH, and ggH processes. In both cases, the general features remain similar to Fig. 15, such as pure yield measurements leading to constraints within a ring, *CP*-sensitive measurements resolving areas within this ring, and the tH process leading to the exclusion of negative values of κ_t. However, in this case, ambiguity between the positive and negative values of $\tilde{\kappa}_t$ can be resolved with the inclusion of the ggH process, where the $\mathcal{D}_{CP}^{ggH}$ discriminant carries information sensitive to the sign.

On the likelihood scan of (κ_t, c_{gg}) with the other parameters fixed, we observe a resolved fourfold ambiguity of the best fit ranges. Within each range, there is a large correlation between the two parameters. This happens because the point-like interaction c_{gg} is equivalent to a BSM heavy quark Q contribution to the loop. It is hard to distinguish between such a new heavy quark and the heavy top quark. The two amplitudes add constructively, leading to a large anticorrelation. The rate of the gluon fusion process would be roughly proportional to $(\kappa_t + \alpha\,\kappa_Q)^2$ with $\alpha \sim 1$. Given that the $t\bar{t}H$ rate constrains $\kappa_t \sim \pm 1$, the ggH rate would constrain (κ_t, κ_Q) to four discrete sets of values around $(+1, 0)$, $(+1, -2)$, $(-1, 0)$, and $(-1, +2)$. The presence of the tH process shifts the preferred negative κ_t solutions away from -1 and makes it less likely than the $+1$ value for the reasons discussed above. However, the local minimum near $\kappa_Q \sim -2$, corresponding to $c_{gg} \sim -0.017$, cannot be excluded, even though the global minimum is at $c_{gg} = -0.001$, close to the null SM expectation. In the case with the other parameters profiled, the constraints on the (κ_t, c_{gg}) plane get washed out further, as expected in a fit with more degrees of freedom. In this case, the *CP*-odd amplitudes can compensate for some effects of the *CP*-even ones. However, some sensitivity is retained because *CP*-sensitive measurements constrain the relative contribution of *CP*-odd amplitudes.

Table 6: Summary of constraints on the anomalous HVV coupling parameters with the best fit values and allowed 68 and 95% CL intervals. Three scenarios are shown for each parameter: with three other anomalous HVV couplings set to zero (first), with three other anomalous HVV couplings left unconstrained (second), in Approach 1 with the relationship $a_i^{WW} = a_i^{ZZ}$ in both cases; and with two other anomalous HVV couplings left unconstrained (third), in Approach 2 within SMEFT with the symmetry relationship of couplings set in Eqs. (3–7). The $f_{\Lambda 1}^{Z\gamma}$ parameter is not independent in the latter scenario.

Parameter	Scenario		Observed	Expected
f_{a3}	Approach 1	best fit	0.00004	0.00000
	f_{a2} =$f_{\Lambda 1}$ =$f_{\Lambda 1}^{Z\gamma}$ =0	68% CL	$[-0.00007, 0.00044]$	$[-0.00081, 0.00081]$
		95% CL	$[-0.00055, 0.00168]$	$[-0.00412, 0.00412]$
	Approach 1	best fit	-0.00805	0.00000
	float f_{a2},$f_{\Lambda 1}$,$f_{\Lambda 1}^{Z\gamma}$	68% CL	$[-0.02656, 0.00034]$	$[-0.00086, 0.00086]$
		95% CL	$[-0.07191, 0.00990]$	$[-0.00423, 0.00422]$
	Approach 2	best fit	0.00005	0.0000
	float f_{a2},$f_{\Lambda 1}$	68% CL	$[-0.00010, 0.00061]$	$[-0.0012, 0.0012]$
		95% CL	$[-0.00072, 0.00218]$	$[-0.0057, 0.0057]$
f_{a2}	Approach 1	best fit	0.00020	0.0000
	f_{a3} =$f_{\Lambda 1}$ =$f_{\Lambda 1}^{Z\gamma}$ =0	68% CL	$[-0.00010, 0.00109]$	$[-0.0012, 0.0014]$
		95% CL	$[-0.00078, 0.00368]$	$[-0.0075, 0.0073]$
	Approach 1	best fit	-0.24679	0.0000
	float f_{a3},$f_{\Lambda 1}$,$f_{\Lambda 1}^{Z\gamma}$	68% CL	$[-0.41087, -0.15149]$ $\cup[-0.00008, 0.00065]$	$[-0.0017, 0.0014]$
		95% CL	$[-0.66842, -0.08754]$ $\cup[-0.00091, 0.00309]$	$[-0.0082, 0.0073]$
	Approach 2	best fit	-0.00002	0.0000
	float f_{a3},$f_{\Lambda 1}$	68% CL	$[-0.00178, 0.00103]$	$[-0.0060, 0.0033]$
		95% CL	$[-0.00694, 0.00536]$	$[-0.0206, 0.0131]$
$f_{\Lambda 1}$	Approach 1	best fit	0.00004	0.00000
	f_{a3} =f_{a2} =$f_{\Lambda 1}^{Z\gamma}$ =0	68% CL	$[-0.00002, 0.00022]$	$[-0.00016, 0.00026]$
		95% CL	$[-0.00014, 0.00060]$	$[-0.00069, 0.00110]$
	Approach 1	best fit	0.18629	0.00000
	float f_{a3},f_{a2},$f_{\Lambda 1}^{Z\gamma}$	68% CL	$[-0.00002, 0.00019]$ $\cup[0.07631, 0.27515]$	$[-0.00017, 0.00036]$
		95% CL	$[-0.00523, 0.35567]$	$[-0.00076, 0.00134]$
	Approach 2	best fit	0.00012	0.0000
	float f_{a3},f_{a2}	68% CL	$[-0.00021, 0.00141]$	$[-0.0013, 0.0030]$
		95% CL	$[-0.00184, 0.00443]$	$[-0.0056, 0.0102]$
$f_{\Lambda 1}^{Z\gamma}$	Approach 1	best fit	-0.00001	0.0000
	f_{a3} =f_{a2} =$f_{\Lambda 1}$ =0	68% CL	$[-0.00099, 0.00057]$	$[-0.0026, 0.0020]$
		95% CL	$[-0.00387, 0.00301]$	$[-0.0096, 0.0082]$
	Approach 1	best fit	-0.02884	0.0000
	float f_{a3},f_{a2},$f_{\Lambda 1}$	68% CL	$[-0.09000, -0.00534]$ $\cup[-0.00068, 0.00078]$	$[-0.0027, 0.0026]$
		95% CL	$[-0.29091, 0.03034]$	$[-0.0099, 0.0096]$

6.4 Constraints on HVV couplings

The measurement of anomalous couplings of the H boson to EW vector bosons in Approach 1 with the relationship $a_i^{WW} = a_i^{ZZ}$ is presented in Fig. 18 and Table 6. Figure 18 shows the observed and expected likelihood scans in the simultaneous measurement of f_{a3}, f_{a2}, $f_{\Lambda 1}$, and $f_{\Lambda 1}^{Z\gamma}$, where the *CP*-sensitive parameter f_{a3}^{ggH} and the signal strength parameters μ_V and μ_{ggH} are profiled, and where we relate $\mu_{t\bar{t}H}$ and f_{CP}^{Htt} to μ_{ggH} and f_{a3}^{ggH} assuming top quark dominance in the loop. The results are shown for each coupling separately, with the other three anomalous couplings either set to zero or left unconstrained in the fit. Figure 19 shows the same results presented as two-dimensional contours, where all couplings discussed above are left unconstrained. In all cases, the likelihood scans are limited to the physical range of $|f_{a3}| + |f_{a2}| + |f_{\Lambda 1}| + |f_{\Lambda 1}^{Z\gamma}| < 1$.

There are several features visible on these plots. First, the results with all other couplings constrained to zero exhibit narrow minima near $f_{ai} = 0$ in both the expected and the observed scans. This effect comes from utilizing production information. The anomalous coupling terms in Eq. (2) are multiplied by a factor of q_i^2, which is larger in VBF and VH production than in $H \to 4\ell$ decay. As a result, the cross section in VBF and VH production increases quickly with f_{ai}. At the same time, the constraints above $f_{ai} \sim 0.02$ are dominated by the decay information from $H \to 4\ell$.

However, when all four anomalous couplings are allowed to float independently, the best fit value is $(f_{a3}, f_{a2}, f_{\Lambda 1}, f_{\Lambda 1}^{Z\gamma}) = (-0.00805, -0.24679, 0.18629, -0.02884)$. This global minimum is driven by the decay information from $H \to 4\ell$ and is only slightly preferred to the local minimum at $(0,0,0,0)$, with a difference in $-2\ln(\mathcal{L})$ of 0.05 between the SM value and the global minimum. The local minimum at $(0,0,0,0)$ is still evident in the four-dimensional distribution and its projections on each parameter, and is driven by the production information, as discussed above for the fits with one parameter. Owing to what appears to be a statistical fluctuation in the observed data when the $-2\ln(\mathcal{L})$ minima obtained from the decay and from the production kinematics differ, the observed constraints appear weaker than expected. However, the results are still statistically consistent with the SM and with the expected constraints in the SM. Should the global minimum nonetheless persist away from $(0,0,0,0)$ with more data, it will be interesting to study consistency of the constraints from the VBF and VH production and from the $H \to 4\ell$ decay. The production and decay test different ranges of q_i^2, as discussed above. If the q_i^2 growth is truncated in the VBF and VH production due to lower-energy BSM effects, the decay information becomes more important.

6.5 Constraints on HVV couplings within $SU(2) \times U(1)$ symmetry

The above studies of the H boson couplings to EW vector bosons are repeated following Approach 2 within SMEFT with the symmetries in Eqs. (3–7). In this case, the $f_{\Lambda 1}^{Z\gamma}$ parameter is not independent. Therefore, constraints on the three parameters f_{a3}, f_{a2}, $f_{\Lambda 1}$, and the signal strength are obtained in this scenario following the same approach as above. These constraints are shown in Fig. 20 and Table 6. The measured signal strength is $\mu_V = 1.10^{+0.50}_{-0.42}$. The observed correlation coefficients are shown in Table 7. Keeping only linear terms and dropping terms with order greater than one for anomalous couplings does not allow us to make a reasonable likelihood scan, since the probability density goes negative, as discussed in Section 2.3.

Since the relationship of the HWW and HZZ couplings does not affect the measurement of the f_{a3} parameter in the $H \to 4\ell$ decay, the constraints from the decay information in the wider range of f_{a3} in Approach 2 are unaffected compared to Approach 1, when other couplings are

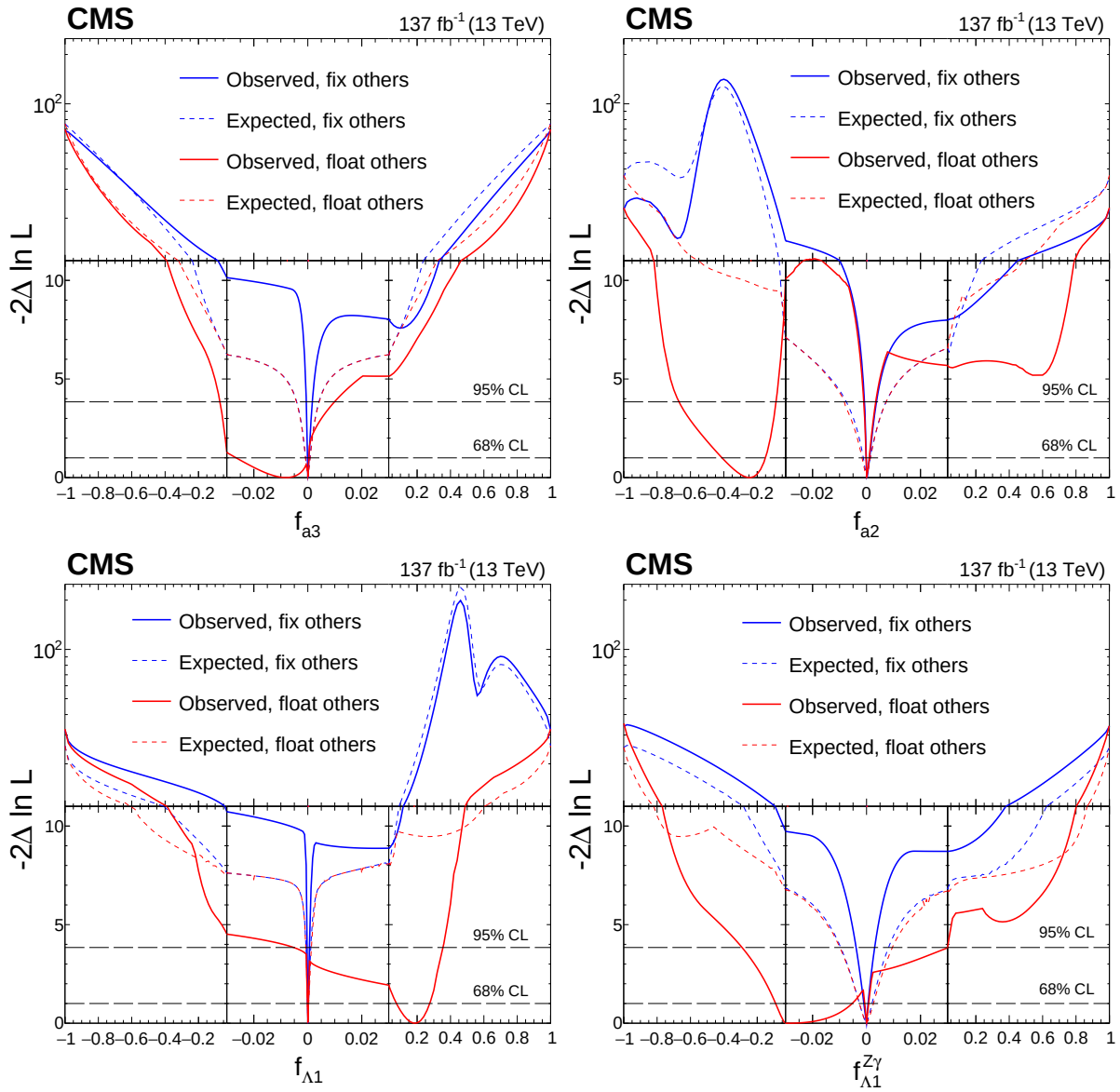

Figure 18: Observed (solid) and expected (dashed) likelihood scans of f_{a3} (upper left), f_{a2} (upper right), $f_{\Lambda 1}$ (lower left), and $f_{\Lambda 1}^{Z\gamma}$ (lower right) in Approach 1 with the coupling relationship $a_i^{WW} = a_i^{ZZ}$. The results are shown for each coupling fraction separately with the other three anomalous coupling fractions either set to zero or left unconstrained in the fit. In all cases, the signal strength parameters have been left unconstrained. The dashed horizontal lines show the 68 and 95% CL regions. For better visibility of all features, the x and y axes are presented with variable scales. On the linear-scale x axis, a zoom is applied in the range -0.03 to 0.03. The y axis is shown in linear or logarithmic scale for values of $-2\ln\mathcal{L}$ below or above 11, respectively.

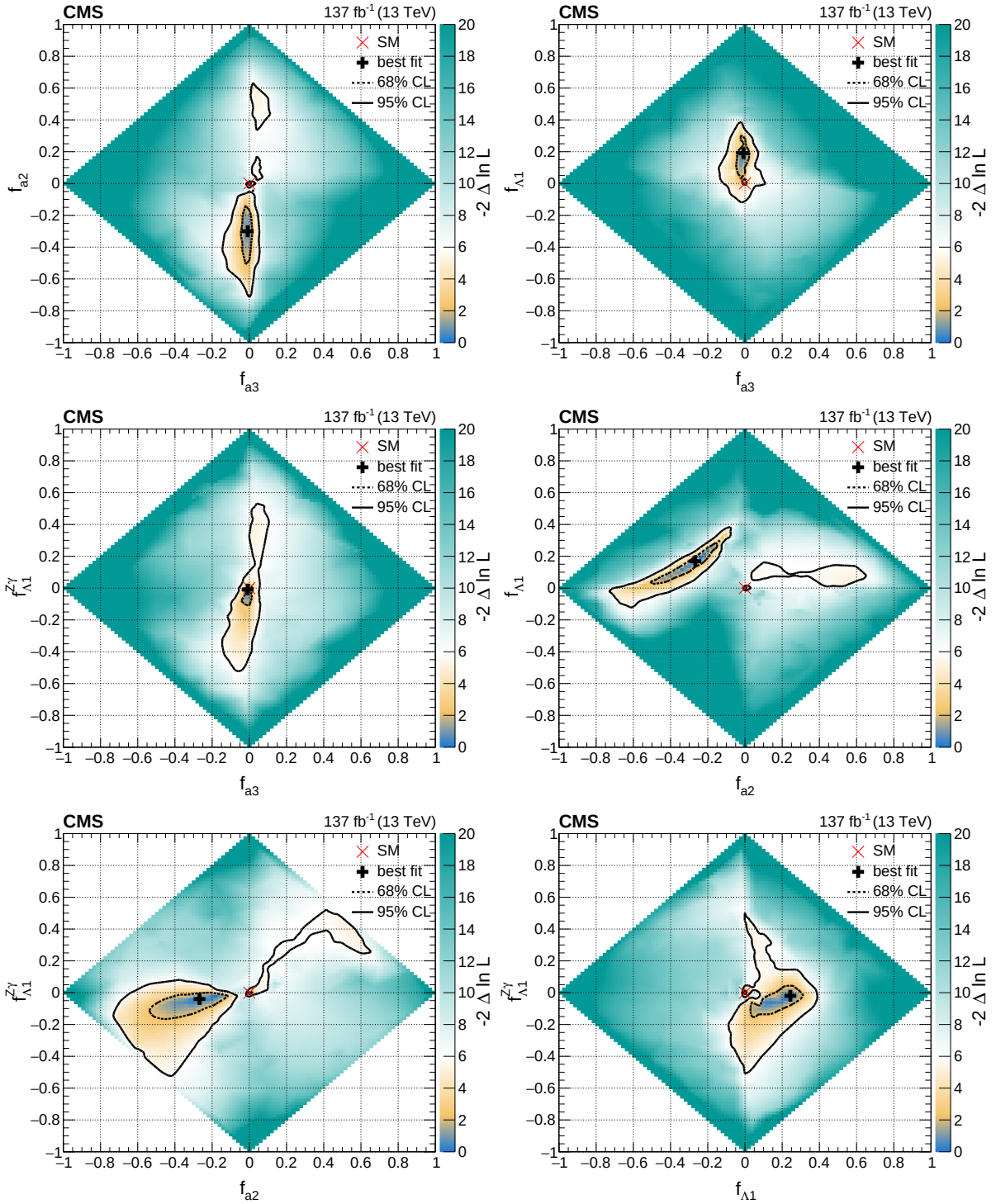

Figure 19: Observed two-dimensional likelihood scans of the four coupling parameters f_{a3}, f_{a2}, $f_{\Lambda 1}$, and $f_{\Lambda 1}^{Z\gamma}$ in Approach 1 with the coupling relationship $a_i^{WW} = a_i^{ZZ}$. In each case, the other two anomalous couplings along with the signal strength parameters have been left unconstrained. The 68 and 95% CL regions are presented as contours with dashed and solid black lines, respectively. The best fit values and the SM expectations are indicated by markers.

Table 7: The observed correlation coefficients of the signal strength μ_V and the f_{a3}, f_{a2}, $f_{\Lambda 1}$ parameters in Approach 2 within SMEFT with the symmetry relationship of couplings set in Eqs. (3–7).

Parameter	Observed correlation			
	μ_V	f_{a3}	f_{a2}	$f_{\Lambda 1}$
μ_V	1	-0.242	-0.060	-0.025
f_{a3}		1	-0.082	$+0.008$
f_{a2}			1	-0.763
$f_{\Lambda 1}$				1

fixed to zero. However, with one less parameter to float, the constraints are modified somewhat when all other couplings are left unconstrained. The modified relationship between the HWW and HZZ couplings also leads to some modification of constraints using production information in the narrow range of f_{a3}. On the other hand, the f_{a2} and $f_{\Lambda 1}$ parameters are modified substantially because the $f_{\Lambda 1}^{Z\gamma}$ information gets absorbed into these measurements through symmetry relationships.

The measurement of the signal strength μ_V and the f_{a3}, f_{a2}, $f_{\Lambda 1}$ parameters can be reinterpreted in terms of the δc_z, c_{zz}, $c_{z\Box}$, and $\tilde{c}_{zz}$ coupling strength parameters. Observed one- and two-dimensional constraints from a simultaneous fit of SMEFT parameters are shown in Figs. 21 and 22. The c_{gg} and $\tilde{c}_{gg}$ couplings are left unconstrained. A summary of all constraints on the Htt, Hgg, and HVV coupling parameters in the Higgs basis of SMEFT, including the correlation coefficients, is shown in Table 8. The results in this table are taken from Sections 6.3 and 6.5, as measured in the tH, $t\bar{t}H$, ggH, and EW processes.

The above interpretation of HVV results in terms of the δc_z, c_{zz}, $c_{z\Box}$, and $\tilde{c}_{zz}$ couplings can be extended into an interpretation in terms of the couplings in the Warsaw SMEFT basis [28]. In this basis, nine operators are considered: $c_{H\Box}$, c_{HD}, c_{HW} , c_{HWB}, c_{HB}, $c_{H\tilde{W}}$, $c_{H\tilde{W}B}$, $c_{H\tilde{B}}$, and δ_v, where the latter is a linear combination of additional Warsaw basis operators [71]. However, not all nine of these operators are independent. First of all, consideration of Eq. (3) leads to δ_v expression as a linear combination of c_{HD} and c_{HWB}. Four constraints on the couplings $a_2^{\gamma\gamma,Z\gamma}$ and $a_3^{\gamma\gamma,Z\gamma}$ lead to only one of the three operators c_{HW} , c_{HWB}, and c_{HB} being independent, and only one of $c_{H\tilde{W}}$, $c_{H\tilde{W}B}$, and $c_{H\tilde{B}}$ being independent. Therefore, we obtain only four independent constraints, the same number as in the Higgs basis. We note that the couplings of the Z boson to fermions are fixed to those expected in the SM because those are well constrained from prior measurements and this constraint is already included in our primary measurements. Even though some of the above EFT operators may affect couplings of the Z boson, their effect must be compensated by the other EFT operators not affecting the H boson couplings directly. With the above constraints, we use the tools in Refs. [33, 71] to relate operators in the Higgs and Warsaw bases. Since it is arbitrary which one of the three operators is considered to be independent, we present results with all three choices in each case. The results can be found in Table 9, where three other independent couplings are left unconstrained for each measurement.

7 Summary

In this paper, a comprehensive study of *CP*-violation, anomalous couplings, and the tensor structure of H boson interactions with electroweak gauge bosons, gluons, and fermions, using

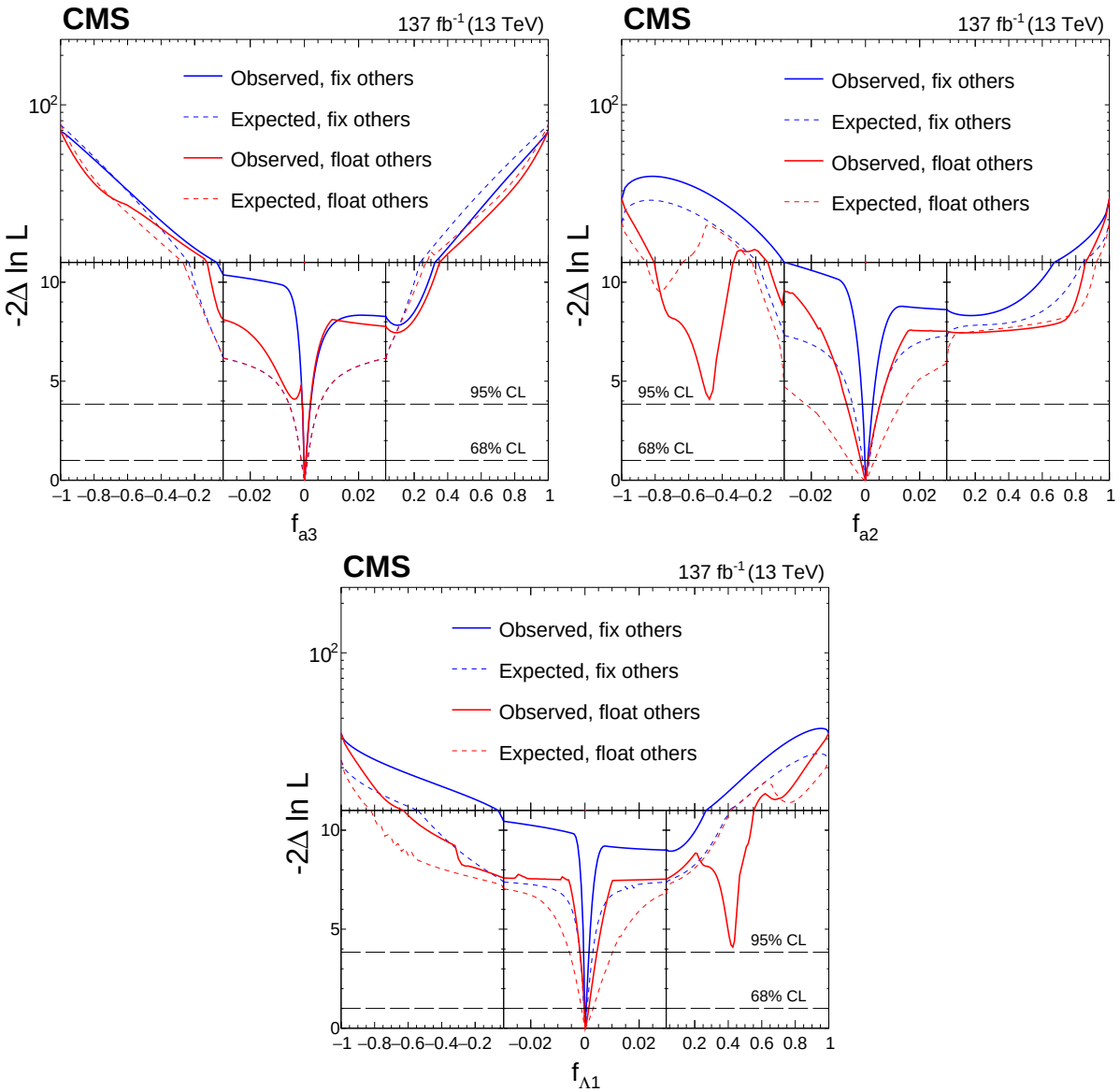

Figure 20: Observed (solid) and expected (dashed) likelihood scans of f_{a3} (upper left), f_{a2} (upper right), and $f_{\Lambda 1}$ (lower) in Approach 2 within SMEFT with the symmetry relationship of couplings set in Eqs. (3–7). The results are shown for each coupling separately with the other anomalous coupling fractions either set to zero or left unconstrained in the fit. In all cases, the signal strength parameters have been left unconstrained. The dashed horizontal lines show the 68 and 95% CL regions. For better visibility of all features, the x and y axes are presented with variable scales. On the linear-scale x axis, a zoom is applied in the range -0.03 to 0.03. The y axis is shown in linear or logarithmic scale for values of $-2\ln\mathcal{L}$ below or above 11, respectively.

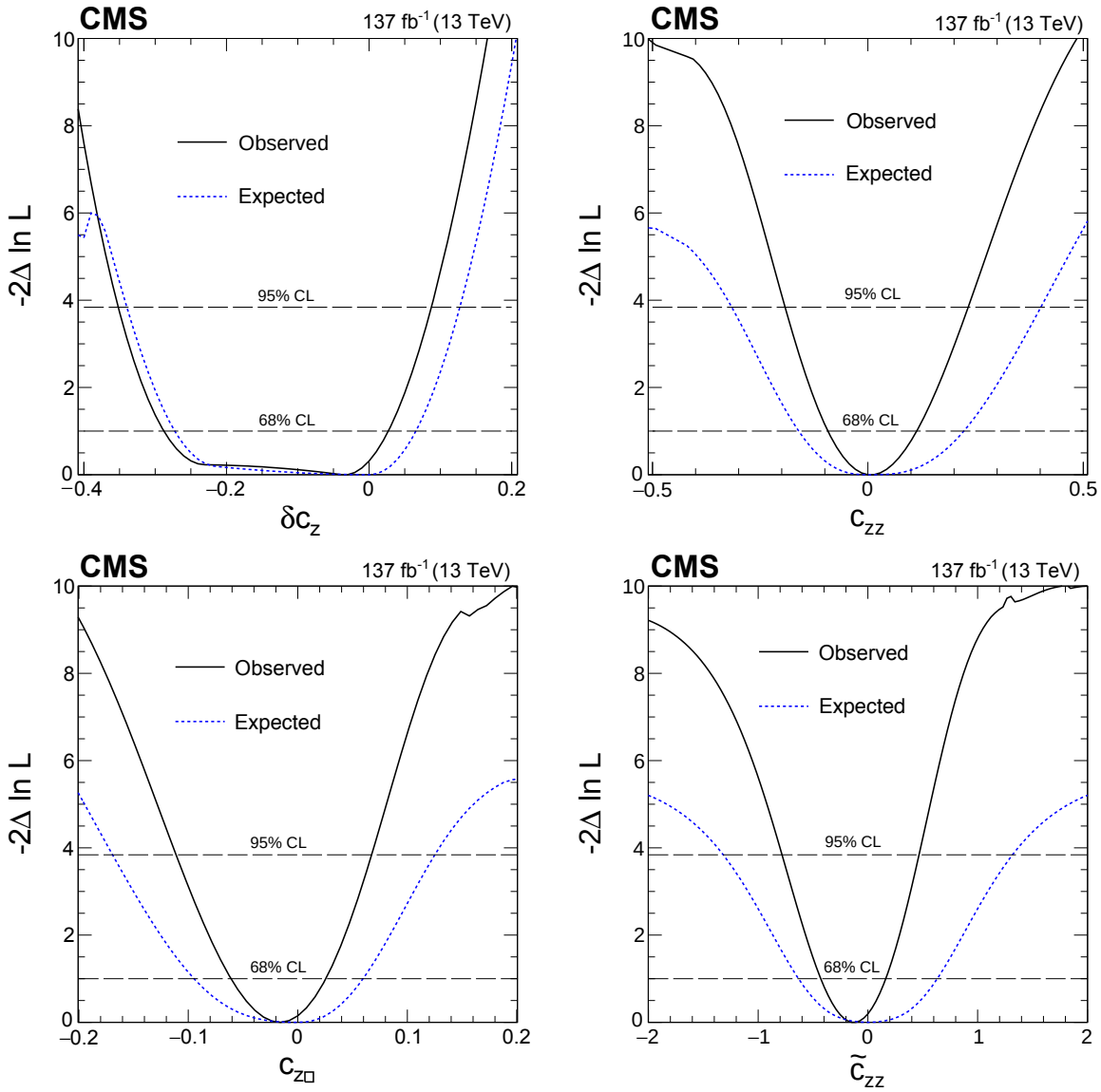

Figure 21: Observed (solid) and expected (dashed) constraints from a simultaneous fit of the SMEFT parameters δc_z (upper left), c_{zz} (upper right), $c_{z\Box}$ (lower left), and $\tilde{c}_{zz}$ (lower right) with the c_{gg} and $\tilde{c}_{gg}$ couplings left unconstrained.

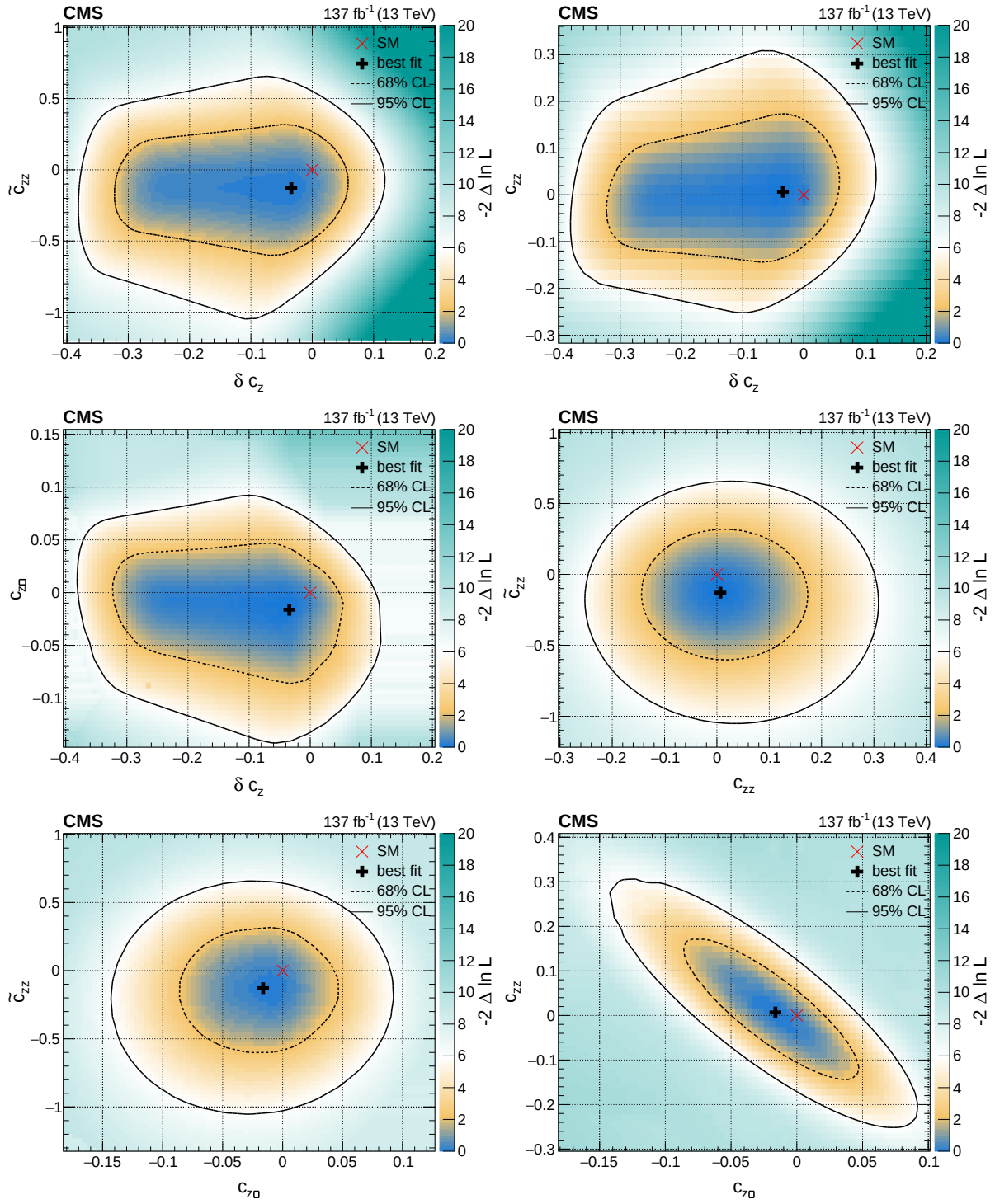

Figure 22: Observed two-dimensional constraints from a simultaneous fit of the SMEFT parameters δc_z, c_{zz}, $c_{z\Box}$, and $\tilde{c}_{zz}$ with the c_{gg} and $\tilde{c}_{gg}$ couplings left unconstrained.

Table 8: Summary of constraints on the Htt, Hgg, and HVV coupling parameters in the Higgs basis of SMEFT. The observed correlation coefficients are presented for the Htt & Hgg and HVV couplings in the fit configurations discussed in text and shown in Figs. 17 and 22, respectively.

Channels	Coupling	Observed	Expected	Observed correlation			
				c_{gg}	$\tilde{c}_{gg}$	κ_t	$\tilde{\kappa}_t$
tH & $t\bar{t}$H & ggH	c_{gg}	$-0.0012^{+0.0022}_{-0.0174}$	$0.0000^{+0.0019}_{-0.0196}$	1	−0.050	−0.941	+0.029
	$\tilde{c}_{gg}$	$-0.0017^{+0.0160}_{-0.0130}$	$0.0000^{+0.0138}_{-0.0138}$		1	+0.046	−0.568
	κ_t	$1.05^{+0.25}_{-0.20}$	$1.00^{+0.34}_{-0.26}$			1	+0.168
	$\tilde{\kappa}_t$	$-0.01^{+0.69}_{-0.67}$	$0.00^{+0.71}_{-0.71}$				1
				δc_z	c_{zz}	$c_{z\Box}$	$\tilde{c}_{zz}$
VBF & VH & H → 4ℓ	δc_z	$-0.03^{+0.06}_{-0.25}$	$0.00^{+0.07}_{-0.27}$	1	+0.241	−0.060	−0.009
	c_{zz}	$0.01^{+0.11}_{-0.10}$	$0.00^{+0.22}_{-0.16}$		1	−0.884	+0.058
	$c_{z\Box}$	$-0.02^{+0.04}_{-0.04}$	$0.00^{+0.06}_{-0.09}$			1	+0.020
	$\tilde{c}_{zz}$	$-0.11^{+0.30}_{-0.31}$	$0.00^{+0.63}_{-0.63}$				1

Table 9: Summary of constraints on the HVV coupling parameters in the Warsaw basis of SMEFT. For each coupling constraint reported, three other independent operators are left unconstrained, where only one of the three operators c_{HW}, c_{HWB}, and c_{HB} is independent, and only one of $c_{H\tilde{W}}$, $c_{H\tilde{W}B}$, and $c_{H\tilde{B}}$ is independent.

Channels	Coupling	Observed	Expected
VBF & VH & H → 4ℓ	$c_{H\Box}$	$0.04^{+0.43}_{-0.45}$	$0.00^{+0.75}_{-0.93}$
	c_{HD}	$-0.73^{+0.97}_{-4.21}$	$0.00^{+1.06}_{-4.60}$
	c_{HW}	$0.01^{+0.18}_{-0.17}$	$0.00^{+0.39}_{-0.28}$
	c_{HWB}	$0.01^{+0.20}_{-0.18}$	$0.00^{+0.42}_{-0.31}$
	c_{HB}	$0.00^{+0.05}_{-0.05}$	$0.00^{+0.03}_{-0.08}$
	$c_{H\tilde{W}}$	$-0.23^{+0.51}_{-0.52}$	$0.00^{+1.11}_{-1.11}$
	$c_{H\tilde{W}B}$	$-0.25^{+0.56}_{-0.57}$	$0.00^{+1.21}_{-1.21}$
	$c_{H\tilde{B}}$	$-0.06^{+0.15}_{-0.16}$	$0.00^{+0.33}_{-0.33}$

all accessible production mechanisms and the H → 4ℓ decay mode, is presented. The results are based on the 2016–2018 data from pp collisions recorded with the CMS detector during Run 2 of the LHC, corresponding to an integrated luminosity of 137 fb^{-1} at a center-of-mass energy of 13 TeV. These results significantly surpass our results from Run 1 [13] in both precision and extent of coverage. The improvements result not only from a significantly increased sample of H bosons, but also from a detailed analysis of kinematic distributions of the particles associated with the H boson production in addition to kinematic distributions in its decay. These results also surpass our earlier studies of on-shell production of the H boson in this decay channel with a partial Run 2 dataset [16, 17].

The parameterization of the H boson production and decay processes is based on a scattering amplitude or, equivalently, an effective field theory Lagrangian, with operators up to dimension six. Additional symmetries and prior measurements allow us to reduce the number of independent parameters and make a connection to the standard model effective field theory (SMEFT) formulation. Dedicated Monte Carlo programs and matrix-element re-weighting

techniques provide modeling of all kinematic effects in the production and decay of the H boson, with any variation of parameters of the scattering amplitude and with full simulation of detector effects. Each production process of the H boson is identified using the kinematic features of its associated particles. The matrix element likelihood approach (MELA) is employed to construct observables that are optimal for the measurement of the targeted anomalous couplings in each process, including *CP*-sensitive observables. A maximum likelihood fit allows a simultaneous measurement of up to five HVV, two Hgg, and two Htt couplings.

For the first time, we present a complete dedicated study of *CP* properties in the H boson coupling to gluons through a loop of heavy particles using the *CP*-sensitive observables, while separating the electroweak and strong boson fusion processes. An interpretation of the loop contribution is made both with and without an assumption of top quark dominance, which allows a new heavy particle to contribute. In both cases, combination with the *CP*-sensitive measurement of the Htt coupling in the $\mathrm{t\bar{t}H}$ and tH processes allows either simultaneous or separate measurements of the two effective point-like Hgg couplings and the two Htt couplings, both *CP*-odd and *CP*-even. For the $\mathrm{t\bar{t}H}$ and tH processes, results in the $\mathrm{H} \to 4\ell$ channel are combined with those in the $\mathrm{H} \to \gamma\gamma$ channel [26]. This is the first comprehensive study of *CP* properties in the Hgg and Htt couplings from a simultaneous measurement of the ggH, $\mathrm{t\bar{t}H}$, and tH processes.

Also for the first time, we present the measurement of *CP* properties and the tensor structure of the H boson's interactions with two electroweak bosons with up to five parameters measured simultaneously. The HVV coupling is analyzed in VBF and VH production and in $\mathrm{H} \to \mathrm{VV} \to 4\ell$ decay. The measurements are performed with two approaches. In the first approach, more lenient symmetry considerations are applied, which allow a less restrictive interpretation of results. In the second approach, $\mathrm{SU(2)}\times\mathrm{U(1)}$ symmetry is invoked and the formulation becomes equivalent to SMEFT. The operator basis is chosen to coincide with the couplings of the mass eigenstates, which allows us to minimize the number of independent parameters. A translation of the SMEFT results to the Warsaw basis is also presented for easier comparison with other results.

In all cases, we first present results in terms of the total cross section of a process and the fractional contribution of each anomalous coupling. These results are further re-interpreted in terms of direct constraints on the couplings by applying certain assumptions about the H boson total width. Each of the measurements presented here is limited by statistical precision and is consistent with the expectations for the standard model Higgs boson.

Acknowledgments

We thank Markus Schulze for optimizing the JHUGEN Monte Carlo simulation program and matrix element library for this analysis. We thank Amitabh Basu for guidance on implementing the cutting planes algorithm and Tianran Chen for updating the HOM4PS program for this analysis and providing support. We are grateful to the members of the LHC Higgs and EFT Working Groups for stimulating the development of several phenomenological aspects of this work, among which is relating the EFT operator bases for the Higgs boson couplings.

We congratulate our colleagues in the CERN accelerator departments for the excellent performance of the LHC and thank the technical and administrative staffs at CERN and at other CMS institutes for their contributions to the success of the CMS effort. In addition, we gratefully acknowledge the computing centers and personnel of the Worldwide LHC Computing Grid and other centers for delivering so effectively the computing infrastructure essential to our analy-

ses. We also acknowledge the Maryland Advanced Research Computing Center (MARCC) for providing computing resources essential for this analysis. Finally, we acknowledge the enduring support for the construction and operation of the LHC, the CMS detector, and the supporting computing infrastructure provided by the following funding agencies: the Austrian Federal Ministry of Education, Science and Research and the Austrian Science Fund; the Belgian Fonds de la Recherche Scientifique, and Fonds voor Wetenschappelijk Onderzoek; the Brazilian Funding Agencies (CNPq, CAPES, FAPERJ, FAPERGS, and FAPESP); the Bulgarian Ministry of Education and Science; CERN; the Chinese Academy of Sciences, Ministry of Science and Technology, and National Natural Science Foundation of China; the Ministerio de Ciencia Tecnología e Innovación (MINCIENCIAS), Colombia; the Croatian Ministry of Science, Education and Sport, and the Croatian Science Foundation; the Research and Innovation Foundation, Cyprus; the Secretariat for Higher Education, Science, Technology and Innovation, Ecuador; the Ministry of Education and Research, Estonian Research Council via PRG780, PRG803 and PRG445 and European Regional Development Fund, Estonia; the Academy of Finland, Finnish Ministry of Education and Culture, and Helsinki Institute of Physics; the Institut National de Physique Nucléaire et de Physique des Particules / CNRS, and Commissariat à l'Énergie Atomique et aux Énergies Alternatives / CEA, France; the Bundesministerium für Bildung und Forschung, the Deutsche Forschungsgemeinschaft (DFG), under Germany's Excellence Strategy – EXC 2121 "Quantum Universe" – 390833306, and under project number 400140256 - GRK2497, and Helmholtz-Gemeinschaft Deutscher Forschungszentren, Germany; the General Secretariat for Research and Technology, Greece; the National Research, Development and Innovation Fund, Hungary; the Department of Atomic Energy and the Department of Science and Technology, India; the Institute for Studies in Theoretical Physics and Mathematics, Iran; the Science Foundation, Ireland; the Istituto Nazionale di Fisica Nucleare, Italy; the Ministry of Science, ICT and Future Planning, and National Research Foundation (NRF), Republic of Korea; the Ministry of Education and Science of the Republic of Latvia; the Lithuanian Academy of Sciences; the Ministry of Education, and University of Malaya (Malaysia); the Ministry of Science of Montenegro; the Mexican Funding Agencies (BUAP, CINVESTAV, CONACYT, LNS, SEP, and UASLP-FAI); the Ministry of Business, Innovation and Employment, New Zealand; the Pakistan Atomic Energy Commission; the Ministry of Science and Higher Education and the National Science Center, Poland; the Fundação para a Ciência e a Tecnologia, Portugal; JINR, Dubna; the Ministry of Education and Science of the Russian Federation, the Federal Agency of Atomic Energy of the Russian Federation, Russian Academy of Sciences, the Russian Foundation for Basic Research, and the National Research Center "Kurchatov Institute"; the Ministry of Education, Science and Technological Development of Serbia; the Secretaría de Estado de Investigación, Desarrollo e Innovación, Programa Consolider-Ingenio 2010, Plan Estatal de Investigación Científica y Técnica y de Innovación 2017–2020, research project IDI-2018-000174 del Principado de Asturias, and Fondo Europeo de Desarrollo Regional, Spain; the Ministry of Science, Technology and Research, Sri Lanka; the Swiss Funding Agencies (ETH Board, ETH Zurich, PSI, SNF, UniZH, Canton Zurich, and SER); the Ministry of Science and Technology, Taipei; the Thailand Center of Excellence in Physics, the Institute for the Promotion of Teaching Science and Technology of Thailand, Special Task Force for Activating Research and the National Science and Technology Development Agency of Thailand; the Scientific and Technical Research Council of Turkey, and Turkish Atomic Energy Authority; the National Academy of Sciences of Ukraine; the Science and Technology Facilities Council, UK; the US Department of Energy, and the US National Science Foundation.

Individuals have received support from the Marie-Curie program and the European Research Council and Horizon 2020 Grant, contract Nos. 675440, 724704, 752730, 765710, and 824093 (European Union); the Leventis Foundation; the Alfred P. Sloan Foundation; the Alexander

von Humboldt Foundation; the Belgian Federal Science Policy Office; the Fonds pour la Formation à la Recherche dans l'Industrie et dans l'Agriculture (FRIA-Belgium); the Agentschap voor Innovatie door Wetenschap en Technologie (IWT-Belgium); the F.R.S.-FNRS and FWO (Belgium) under the "Excellence of Science – EOS" – be.h project n. 30820817; the Beijing Municipal Science & Technology Commission, No. Z191100007219010; the Ministry of Education, Youth and Sports (MEYS) of the Czech Republic; the Lendület ("Momentum") Program and the János Bolyai Research Scholarship of the Hungarian Academy of Sciences, the New National Excellence Program ÚNKP, the NKFIA research grants 123842, 123959, 124845, 124850, 125105, 128713, 128786, and 129058 (Hungary); the Council of Scientific and Industrial Research, India; the National Science Center (Poland), contracts Opus 2014/15/B/ST2/03998 and 2015/19/B/ST2/02861; the National Priorities Research Program by Qatar National Research Fund; the Ministry of Science and Higher Education, project no. 0723-2020-0041 (Russia); the Programa de Excelencia María de Maeztu, and the Programa Severo Ochoa del Principado de Asturias; the Thalis and Aristeia programs cofinanced by EU-ESF, and the Greek NSRF; the Rachadapisek Sompot Fund for Postdoctoral Fellowship, Chulalongkorn University, and the Chulalongkorn Academic into Its 2nd Century Project Advancement Project (Thailand); the Kavli Foundation; the Nvidia Corporation; the SuperMicro Corporation; the Welch Foundation, contract C-1845; and the Weston Havens Foundation (USA).

References

[1] ATLAS Collaboration, "Observation of a new particle in the search for the Standard Model Higgs boson with the ATLAS detector at the LHC", *Phys. Lett. B* **716** (2012) 1, doi:10.1016/j.physletb.2012.08.020, arXiv:1207.7214.

[2] CMS Collaboration, "Observation of a new boson at a mass of 125 GeV with the CMS experiment at the LHC", *Phys. Lett. B* **716** (2012) 30, doi:10.1016/j.physletb.2012.08.021, arXiv:1207.7235.

[3] CMS Collaboration, "Observation of a new boson with mass near 125 GeV in pp collisions at $\sqrt{s} = 7$ and 8 TeV", *JHEP* **06** (2013) 081, doi:10.1007/JHEP06(2013)081, arXiv:1303.4571.

[4] S. L. Glashow, "Partial-symmetries of weak interactions", *Nucl. Phys.* **22** (1961) 579, doi:10.1016/0029-5582(61)90469-2.

[5] F. Englert and R. Brout, "Broken symmetry and the mass of gauge vector mesons", *Phys. Rev. Lett.* **13** (1964) 321, doi:10.1103/PhysRevLett.13.321.

[6] P. W. Higgs, "Broken symmetries, massless particles and gauge fields", *Phys. Lett.* **12** (1964) 132, doi:10.1016/0031-9163(64)91136-9.

[7] P. W. Higgs, "Broken symmetries and the masses of gauge bosons", *Phys. Rev. Lett.* **13** (1964) 508, doi:10.1103/PhysRevLett.13.508.

[8] G. S. Guralnik, C. R. Hagen, and T. W. B. Kibble, "Global conservation laws and massless particles", *Phys. Rev. Lett.* **13** (1964) 585, doi:10.1103/PhysRevLett.13.585.

[9] S. Weinberg, "A model of leptons", *Phys. Rev. Lett.* **19** (1967) 1264, doi:10.1103/PhysRevLett.19.1264.

[10] A. Salam, "Weak and electromagnetic interactions", in *Elementary particle physics: relativistic groups and analyticity*, N. Svartholm, ed., p. 367. Almqvist & Wiksell, Stockholm, 1968. Proceedings of the eighth Nobel symposium.

[11] CMS Collaboration, "On the mass and spin-parity of the Higgs boson candidate via its decays to Z boson pairs", *Phys. Rev. Lett.* **110** (2013) 081803, doi:10.1103/PhysRevLett.110.081803, arXiv:1212.6639.

[12] CMS Collaboration, "Measurement of the properties of a Higgs boson in the four-lepton final state", *Phys. Rev. D* **89** (2014) 092007, doi:10.1103/PhysRevD.89.092007, arXiv:1312.5353.

[13] CMS Collaboration, "Constraints on the spin-parity and anomalous HVV couplings of the Higgs boson in proton collisions at 7 and 8 TeV", *Phys. Rev. D* **92** (2015) 012004, doi:10.1103/PhysRevD.92.012004, arXiv:1411.3441.

[14] CMS Collaboration, "Limits on the Higgs boson lifetime and width from its decay to four charged leptons", *Phys. Rev. D* **92** (2015) 072010, doi:10.1103/PhysRevD.92.072010, arXiv:1507.06656.

[15] CMS Collaboration, "Combined search for anomalous pseudoscalar HVV couplings in VH ($H \to b\bar{b}$) production and $H \to VV$ decay", *Phys. Lett. B* **759** (2016) 672, doi:10.1016/j.physletb.2016.06.004, arXiv:1602.04305.

[16] CMS Collaboration, "Constraints on anomalous Higgs boson couplings using production and decay information in the four-lepton final state", *Phys. Lett. B* **775** (2017) 1, doi:10.1016/j.physletb.2017.10.021, arXiv:1707.00541.

[17] CMS Collaboration, "Measurements of the Higgs boson width and anomalous HVV couplings from on-shell and off-shell production in the four-lepton final state", *Phys. Rev. D* (2019) 112003, doi:10.1103/PhysRevD.99.112003, arXiv:1901.00174.

[18] CMS Collaboration, "Constraints on anomalous *HVV* couplings from the production of Higgs bosons decaying to τ lepton pairs", *Phys. Rev. D* **100** (2019) 112002, doi:10.1103/PhysRevD.100.112002, arXiv:1903.06973.

[19] ATLAS Collaboration, "Evidence for the spin-0 nature of the Higgs boson using ATLAS data", *Phys. Lett. B* **726** (2013) 120, doi:10.1016/j.physletb.2013.08.026, arXiv:1307.1432.

[20] ATLAS Collaboration, "Study of the spin and parity of the Higgs boson in diboson decays with the ATLAS detector", *Eur. Phys. J. C* **75** (2015) 476, doi:10.1140/epjc/s10052-015-3685-1, arXiv:1506.05669.

[21] ATLAS Collaboration, "Test of CP invariance in vector-boson fusion production of the Higgs boson using the Optimal Observable method in the ditau decay channel with the ATLAS detector", *Eur. Phys. J. C* **76** (2016) 658, doi:10.1140/epjc/s10052-016-4499-5, arXiv:1602.04516.

[22] ATLAS Collaboration, "Measurement of inclusive and differential cross sections in the $H \to ZZ^* \to 4\ell$ decay channel in pp collisions at $\sqrt{s} = 13i$ TeV with the ATLAS detector", *JHEP* **10** (2017) 132, doi:10.1007/JHEP10(2017)132, arXiv:1708.02810.

[23] ATLAS Collaboration, "Measurement of the Higgs boson coupling properties in the $H \to ZZ^* \to 4\ell$ decay channel at $\sqrt{s}$ = 13 TeV with the ATLAS detector", *JHEP* **03** (2018) 095, doi:10.1007/JHEP03(2018)095, arXiv:1712.02304.

[24] ATLAS Collaboration, "Measurements of Higgs boson properties in the diphoton decay channel with 36 fb^{-1} of pp collision data at $\sqrt{s} = 13$ TeV with the ATLAS detector", *Phys. Rev. D* **98** (2018) 052005, doi:10.1103/PhysRevD.98.052005, arXiv:1802.04146.

[25] ATLAS Collaboration, "Test of CP invariance in vector-boson fusion production of the Higgs boson in the H $\to \tau\tau$ channel in proton−proton collisions at $\sqrt{s}$ = 13 TeV with the ATLAS detector", *Phys. Lett. B* **805** (2020) 135426, doi:10.1016/j.physletb.2020.135426, arXiv:2002.05315.

[26] CMS Collaboration, "Measurements of t$\bar{\text{t}}H$ Production and the CP Structure of the Yukawa Interaction between the Higgs Boson and Top Quark in the Diphoton Decay Channel", *Phys. Rev. Lett.* **125** (2020) 061801, doi:10.1103/PhysRevLett.125.061801, arXiv:2003.10866.

[27] ATLAS Collaboration, "*CP* Properties of Higgs Boson Interactions with Top Quarks in the $t\bar{t}H$ and tH Processes Using $H \to \gamma\gamma$ with the ATLAS Detector", *Phys. Rev. Lett.* **125** (2020) 061802, doi:10.1103/PhysRevLett.125.061802, arXiv:2004.04545.

[28] LHC Higgs Cross Section Working Group, "Handbook of LHC Higgs cross sections: 4. deciphering the nature of the Higgs sector", *CERN* (2016) doi:10.23731/CYRM-2017-002, arXiv:1610.07922.

[29] Y. Gao et al., "Spin determination of single-produced resonances at hadron colliders", *Phys. Rev. D* **81** (2010) 075022, doi:10.1103/PhysRevD.81.075022, arXiv:1001.3396.

[30] S. Bolognesi et al., "Spin and parity of a single-produced resonance at the LHC", *Phys. Rev. D* **86** (2012) 095031, doi:10.1103/PhysRevD.86.095031, arXiv:1208.4018.

[31] I. Anderson et al., "Constraining anomalous HVV interactions at proton and lepton colliders", *Phys. Rev. D* **89** (2014) 035007, doi:10.1103/PhysRevD.89.035007, arXiv:1309.4819.

[32] A. V. Gritsan, R. Röntsch, M. Schulze, and M. Xiao, "Constraining anomalous Higgs boson couplings to the heavy flavor fermions using matrix element techniques", *Phys. Rev. D* **94** (2016) 055023, doi:10.1103/PhysRevD.94.055023, arXiv:1606.03107.

[33] A. V. Gritsan et al., "New features in the JHU generator framework: constraining Higgs boson properties from on-shell and off-shell production", *Phys. Rev. D* **102** (2020) 056022, doi:10.1103/PhysRevD.102.056022, arXiv:2002.09888.

[34] ATLAS Collaboration, "Higgs boson production cross-section measurements and their EFT interpretation in the 4ℓ decay channel at $\sqrt{s}$ =13 TeV with the ATLAS detector", *Eur. Phys. J. C* **80** (2020) 957, doi:10.1140/epjc/s10052-020-8227-9, arXiv:2004.03447. [Erratum: doi:10.1140/epjc/s10052-020-08644-x].

[35] ATLAS Collaboration, "Measurements of the Higgs boson inclusive and differential fiducial cross sections in the 4ℓ decay channel at $\sqrt{s}$ = 13 TeV", *Eur. Phys. J. C* **80** (2020) 942, doi:10.1140/epjc/s10052-020-8223-0, arXiv:2004.03969.

[36] C. A. Nelson, "Correlation between decay planes in Higgs boson decays into a W Pair (into a Z Pair)", *Phys. Rev. D* **37** (1988) 1220, doi:10.1103/PhysRevD.37.1220.

[37] A. Soni and R. M. Xu, "Probing CP violation via Higgs decays to four leptons", *Phys. Rev. D* **48** (1993) 5259, doi:10.1103/PhysRevD.48.5259, arXiv:hep-ph/9301225.

[38] D. Chang, W.-Y. Keung, and I. Phillips, "CP odd correlation in the decay of neutral Higgs boson into ZZ, W^+W^-, or $t\bar{t}$", *Phys. Rev. D* **48** (1993) 3225, doi:10.1103/PhysRevD.48.3225, arXiv:hep-ph/9303226.

[39] V. D. Barger et al., "Higgs bosons: Intermediate mass range at e+ e- colliders", *Phys. Rev. D* **49** (1994) 79, doi:10.1103/PhysRevD.49.79, arXiv:hep-ph/9306270.

[40] T. Arens and L. M. Sehgal, "Energy spectra and energy correlations in the decay $H \to ZZ \to \mu^+\mu^-\mu^+\mu^-$", *Z. Phys. C* **66** (1995) 89, doi:10.1007/BF01496583, arXiv:hep-ph/9409396.

[41] S. Bar-Shalom et al., "Large tree level CP violation in $e^+e^- \to t\bar{t}H^0$ in the two Higgs doublet model", *Phys. Rev. D* **53** (1996) 1162, doi:10.1103/PhysRevD.53.1162, arXiv:hep-ph/9508314.

[42] J. F. Gunion and X.-G. He, "Determining the CP nature of a neutral Higgs boson at the LHC", *Phys. Rev. Lett.* **76** (1996) 4468, doi:10.1103/PhysRevLett.76.4468, arXiv:hep-ph/9602226.

[43] T. Han and J. Jiang, "CP violating ZZH coupling at e^+e^- linear colliders", *Phys. Rev. D* **63** (2001) 096007, doi:10.1103/PhysRevD.63.096007, arXiv:hep-ph/0011271.

[44] T. Plehn, D. L. Rainwater, and D. Zeppenfeld, "Determining the structure of Higgs couplings at the LHC", *Phys. Rev. Lett.* **88** (2002) 051801, doi:10.1103/PhysRevLett.88.051801, arXiv:hep-ph/0105325.

[45] S. Y. Choi, D. J. Miller, M. M. Mühlleitner, and P. M. Zerwas, "Identifying the Higgs spin and parity in decays to Z pairs", *Phys. Lett. B* **553** (2003) 61, doi:10.1016/S0370-2693(02)03191-X, arXiv:hep-ph/0210077.

[46] C. P. Buszello, I. Fleck, P. Marquard, and J. J. van der Bij, "Prospective analysis of spin- and CP-sensitive variables in $H \to ZZ \to \ell_1^+\ell_1^-\ell_2^+\ell_2^-$ at the LHC", *Eur. Phys. J. C* **32** (2004) 209, doi:10.1140/epjc/s2003-01392-0, arXiv:hep-ph/0212396.

[47] V. Hankele, G. Klamke, D. Zeppenfeld, and T. Figy, "Anomalous Higgs boson couplings in vector boson fusion at the CERN LHC", *Phys. Rev. D* **74** (2006) 095001, doi:10.1103/PhysRevD.74.095001, arXiv:hep-ph/0609075.

[48] E. Accomando et al., "Workshop on CP studies and non-standard Higgs physics", (2006). arXiv:hep-ph/0608079.

[49] R. M. Godbole, D. J. Miller, and M. M. Mühlleitner, "Aspects of CP violation in the HZZ coupling at the LHC", *JHEP* **12** (2007) 031, doi:10.1088/1126-6708/2007/12/031, arXiv:0708.0458.

[50] K. Hagiwara, Q. Li, and K. Mawatari, "Jet angular correlation in vector-boson fusion processes at hadron colliders", *JHEP* **07** (2009) 101, doi:10.1088/1126-6708/2009/07/101, arXiv:0905.4314.

[51] A. De Rújula et al., "Higgs look-alikes at the LHC", *Phys. Rev. D* **82** (2010) 013003, doi:10.1103/PhysRevD.82.013003, arXiv:1001.5300.

[52] N. D. Christensen, T. Han, and Y. Li, "Testing CP violation in ZZH interactions at the LHC", *Phys. Lett. B* **693** (2010) 28, doi:10.1016/j.physletb.2010.08.008, arXiv:1005.5393.

[53] J. S. Gainer, K. Kumar, I. Low, and R. Vega-Morales, "Improving the sensitivity of Higgs boson searches in the golden channel", *JHEP* **11** (2011) 027, doi:10.1007/JHEP11(2011)027, arXiv:1108.2274.

[54] J. Ellis, D. S. Hwang, V. Sanz, and T. You, "A fast track towards the 'Higgs' spin and parity", *JHEP* **11** (2012) 134, doi:10.1007/JHEP11(2012)134, arXiv:1208.6002.

[55] Y. Chen, N. Tran, and R. Vega-Morales, "Scrutinizing the Higgs signal and background in the 2e2μ golden channel", *JHEP* **01** (2013) 182, doi:10.1007/JHEP01(2013)182, arXiv:1211.1959.

[56] J. S. Gainer et al., "Geolocating the Higgs boson candidate at the LHC", *Phys. Rev. Lett.* **111** (2013) 041801, doi:10.1103/PhysRevLett.111.041801, arXiv:1304.4936.

[57] P. Artoisenet et al., "A framework for Higgs characterisation", *JHEP* **11** (2013) 043, doi:10.1007/JHEP11(2013)043, arXiv:1306.6464.

[58] M. Chen et al., "Role of interference in unraveling the ZZ couplings of the newly discovered boson at the LHC", *Phys. Rev. D* **89** (2014) 034002, doi:10.1103/PhysRevD.89.034002, arXiv:1310.1397.

[59] Y. Chen and R. Vega-Morales, "Extracting Effective Higgs Couplings in the Golden Channel", *JHEP* **04** (2014) 057, doi:10.1007/JHEP04(2014)057, arXiv:1310.2893.

[60] J. S. Gainer et al., "Beyond geolocating: Constraining higher dimensional operators in $H \to 4\ell$ with off-shell production and more", *Phys. Rev. D* **91** (2015) 035011, doi:10.1103/PhysRevD.91.035011, arXiv:1403.4951.

[61] M. Gonzalez-Alonso, A. Greljo, G. Isidori, and D. Marzocca, "Pseudo-observables in Higgs decays", *Eur. Phys. J. C* **75** (2015) 128, doi:10.1140/epjc/s10052-015-3345-5, arXiv:1412.6038.

[62] M. J. Dolan, P. Harris, M. Jankowiak, and M. Spannowsky, "Constraining *CP*-violating Higgs sectors at the LHC using gluon fusion", *Phys. Rev. D* **90** (2014) 073008, doi:10.1103/PhysRevD.90.073008, arXiv:1406.3322.

[63] F. Demartin et al., "Higgs characterisation at NLO in QCD: CP properties of the top-quark Yukawa interaction", *Eur. Phys. J. C* **74** (2014) 3065, doi:10.1140/epjc/s10052-014-3065-2, arXiv:1407.5089.

[64] M. R. Buckley and D. Goncalves, "Boosting the Direct CP Measurement of the Higgs-Top Coupling", *Phys. Rev. Lett.* **116** (2016) 091801, doi:10.1103/PhysRevLett.116.091801, arXiv:1507.07926.

[65] A. Greljo, G. Isidori, J. M. Lindert, and D. Marzocca, "Pseudo-observables in electroweak Higgs production", *Eur. Phys. J. C* **76** (2016) 158, doi:10.1140/epjc/s10052-016-4000-5, arXiv:1512.06135.

[66] I. Brivio, T. Corbett, and M. Trott, "The Higgs width in the SMEFT", *JHEP* **10** (2019) 056, doi:10.1007/JHEP10(2019)056, arXiv:1906.06949.

[67] S. Weinberg, "Baryon and lepton nonconserving processes", *Phys. Rev. Lett.* **43** (1979) 1566, doi:10.1103/PhysRevLett.43.1566.

[68] W. Buchmuller and D. Wyler, "Effective Lagrangian analysis of new interactions and flavor conservation", *Nucl. Phys. B* **268** (1986) 621, doi:10.1016/0550-3213(86)90262-2.

[69] C. N. Leung, S. T. Love, and S. Rao, "Low-energy manifestations of a new interaction scale: operator analysis", *Z. Phys. C* **31** (1986) 433, doi:10.1007/BF01588041.

[70] A. Dedes et al., "Feynman rules for the standard model effective field theory in R_ξ -gauges", *JHEP* **06** (2017) 143, doi:10.1007/JHEP06(2017)143, arXiv:1704.03888.

[71] A. Falkowski et al., "Rosetta: an operator basis translator for Standard Model effective field theory", *Eur. Phys. J. C* **75** (2015) 583, doi:10.1140/epjc/s10052-015-3806-x, arXiv:1508.05895.

[72] Particle Data Group, P. A. Zyla et al., "Review of particle physics", *Prog. Theor. Exp. Phys.* **2020** (2020) 083C01, doi:10.1093/ptep/ptaa104.

[73] P. Sikivie, L. Susskind, M. B. Voloshin, and V. I. Zakharov, "Isospin Breaking in Technicolor Models", *Nucl. Phys. B* **173** (1980) 189, doi:10.1016/0550-3213(80)90214-X.

[74] CMS Collaboration, "The CMS experiment at the CERN LHC", *JINST* **3** (2008) S08004, doi:10.1088/1748-0221/3/08/S08004.

[75] CMS Collaboration, "Performance of the CMS Level-1 trigger in proton-proton collisions at $\sqrt{s} = 13$ TeV", *JINST* **15** (2020) P10017, doi:10.1088/1748-0221/15/10/P10017, arXiv:2006.10165.

[76] CMS Collaboration, "The CMS trigger system", *JINST* **12** (2017) P01020, doi:10.1088/1748-0221/12/01/P01020, arXiv:1609.02366.

[77] CMS Collaboration, "Measurements of properties of the Higgs boson decaying into the four-lepton final state in pp collisions at $\sqrt{s} = 13$ TeV", *JHEP* **11** (2017) 047, doi:10.1007/JHEP11(2017)047, arXiv:1706.09936.

[78] CMS Collaboration, "Measurements of production cross sections of the Higgs boson in the four-lepton final state in proton-proton collisions at $\sqrt{s} = 13$ TeV", (2021). arXiv:2103.04956. Submitted to *Eur. Phys. J. C*.

[79] CMS Collaboration, "Particle-flow reconstruction and global event description with the CMS detector", *JINST* **12** (2017) P10003, doi:10.1088/1748-0221/12/10/P10003, arXiv:1706.04965.

[80] M. Cacciari, G. P. Salam, and G. Soyez, "The anti-k_T jet clustering algorithm", *JHEP* **04** (2008) 063, doi:10.1088/1126-6708/2008/04/063, arXiv:0802.1189.

[81] M. Cacciari, G. P. Salam, and G. Soyez, "FastJet user manual", *Eur. Phys. J. C* **72** (2012) 1896, doi:10.1140/epjc/s10052-012-1896-2, arXiv:1111.6097.

[82] CMS Collaboration, "Identification of heavy-flavour jets with the CMS detector in pp collisions at 13 TeV", *JINST* **13** (2018) P05011, doi:10.1088/1748-0221/13/05/P05011, arXiv:1712.07158.

[83] T. Sjöstrand et al., "An introduction to PYTHIA 8.2", *Comput. Phys. Commun.* **191** (2015) 159, doi:10.1016/j.cpc.2015.01.024, arXiv:1410.3012.

[84] CMS Collaboration, "Event generator tunes obtained from underlying event and multiparton scattering measurements", *Eur. Phys. J. C* **76** (2016) 155, doi:10.1140/epjc/s10052-016-3988-x, arXiv:1512.00815.

[85] CMS Collaboration, "Extraction and validation of a new set of CMS PYTHIA8 tunes from underlying-event measurements", *Eur. Phys. J. C* **80** (2020) 4, doi:10.1140/epjc/s10052-019-7499-4, arXiv:1903.12179.

[86] NNPDF Collaboration, "Unbiased global determination of parton distributions and their uncertainties at NNLO and at LO", *Nucl. Phys. B* **855** (2012) 153, doi:10.1016/j.nuclphysb.2011.09.024, arXiv:1107.2652.

[87] GEANT4 Collaboration, "GEANT4 — a simulation toolkit", *Nucl. Instrum. Meth. A* **506** (2003) 250, doi:10.1016/S0168-9002(03)01368-8.

[88] J. M. Campbell and R. K. Ellis, "MCFM for the Tevatron and the LHC", *Nucl. Phys. Proc. Suppl.* **205-206** (2010) 10, doi:10.1016/j.nuclphysbps.2010.08.011, arXiv:1007.3492.

[89] S. Frixione, P. Nason, and C. Oleari, "Matching NLO QCD computations with parton shower simulations: the POWHEG method", *JHEP* **11** (2007) 070, doi:10.1088/1126-6708/2007/11/070, arXiv:0709.2092.

[90] E. Bagnaschi, G. Degrassi, P. Slavich, and A. Vicini, "Higgs production via gluon fusion in the POWHEG approach in the SM and in the MSSM", *JHEP* **02** (2012) 088, doi:10.1007/JHEP02(2012)088, arXiv:1111.2854.

[91] P. Nason and C. Oleari, "NLO Higgs boson production via vector-boson fusion matched with shower in POWHEG", *JHEP* **02** (2010) 037, doi:10.1007/JHEP02(2010)037, arXiv:0911.5299.

[92] G. Luisoni, P. Nason, C. Oleari, and F. Tramontano, "$HW^{\pm}/HZ$ + 0 and 1 jet at NLO with the POWHEG BOX interfaced to GoSam and their merging within MiNLO", *JHEP* **10** (2013) 083, doi:10.1007/JHEP10(2013)083, arXiv:1306.2542.

[93] H. B. Hartanto, B. Jager, L. Reina, and D. Wackeroth, "Higgs boson production in association with top quarks in the POWHEG BOX", *Phys. Rev. D* **91** (2015) 094003, doi:10.1103/PhysRevD.91.094003, arXiv:1501.04498.

[94] J. Alwall et al., "The automated computation of tree-level and next-to-leading order differential cross sections, and their matching to parton shower simulations", *JHEP* **07** (2014) 079, doi:10.1007/JHEP07(2014)079, arXiv:1405.0301.

[95] K. Hamilton, P. Nason, and G. Zanderighi, "MINLO: multi-scale improved NLO", *JHEP* **10** (2012) 155, doi:10.1007/JHEP10(2012)155, arXiv:1206.3572.

[96] CMS Collaboration, "A measurement of the Higgs boson mass in the diphoton decay channel", *Phys. Lett. B* **805** (2020) 135425, doi:10.1016/j.physletb.2020.135425, arXiv:2002.06398.

[97] M. Grazzini, S. Kallweit, and D. Rathlev, "ZZ production at the LHC: fiducial cross sections and distributions in NNLO QCD", *Phys. Lett. B* **750** (2015) 407, doi:10.1016/j.physletb.2015.09.055, arXiv:1507.06257.

[98] J. M. Campbell, R. K. Ellis, and C. Williams, "Vector boson pair production at the LHC", *JHEP* **07** (2011) 018, doi:10.1007/JHEP07(2011)018, arXiv:1105.0020.

[99] J. M. Campbell, R. K. Ellis, and C. Williams, "Bounding the Higgs width at the LHC using full analytic results for $gg \to e^- e^+ \mu^- \mu^+$", *JHEP* **04** (2014) 060, doi:10.1007/JHEP04(2014)060, arXiv:1311.3589.

[100] J. M. Campbell and R. K. Ellis, "Higgs constraints from vector boson fusion and scattering", *JHEP* **04** (2015) 030, doi:10.1007/JHEP04(2015)030, arXiv:1502.02990.

[101] S. Catani and M. Grazzini, "An NNLO subtraction formalism in hadron collisions and its application to Higgs boson production at the LHC", *Phys. Rev. Lett.* **98** (2007) 222002, doi:10.1103/PhysRevLett.98.222002, arXiv:hep-ph/0703012.

[102] M. Grazzini, "NNLO predictions for the Higgs boson signal in the $H \to WW \to \ell\nu\ell\nu$ and $H \to ZZ \to 4\ell$ decay channels", *JHEP* **02** (2008) 043, doi:10.1088/1126-6708/2008/02/043, arXiv:0801.3232.

[103] M. Grazzini and H. Sargsyan, "Heavy-quark mass effects in Higgs boson production at the LHC", *JHEP* **09** (2013) 129, doi:10.1007/JHEP09(2013)129, arXiv:1306.4581.

[104] R. J. Barlow, "Extended maximum likelihood", *Nucl. Instrum. Meth. A* **297** (1990) 496, doi:10.1016/0168-9002(90)91334-8.

[105] T. Chen and T.-Y. Li, "Homotopy continuation method for solving systems of nonlinear and polynomial equations", *Commun. Inf. Syst.* **15** (2015) 119, doi:10.4310/CIS.2015.v15.n2.a1.

[106] T. Chen, T.-L. Lee, and T.-Y. Li, "Hom4PS-3: A parallel numerical solver for systems of polynomial equations based on polyhedral homotopy continuation methods", in *Proceedings of the Mathematical Software—ICMS 2014*, p. 183. 2014. doi:10.1007/978-3-662-44199-2_30.

[107] T. Chen, T.-L. Lee, and T.-Y. Li, "Mixed cell computation in Hom4PS-3", *J. Symb. Comput.* **79, Part 3** (2017) 516, doi:10.1016/j.jsc.2016.07.017.

[108] A. S. Nemirovsky and D. B. Yudin, "Problem complexity and method efficiency in optimization.". Wiley, 1983.

[109] Gurobi Optimization, LLC, "Gurobi optimizer reference manual", 2018. http://www.gurobi.com.

[110] W. Verkerke and D. P. Kirkby, "The RooFit toolkit for data modeling", in *Proceedings of the 13th International Conference for Computing in High-Energy and Nuclear Physics (CHEP03)*. 2003. arXiv:physics/0306116. [eConf C0303241, MOLT007].

[111] R. Brun and F. Rademakers, "ROOT: An object oriented data analysis framework", *Nucl. Instrum. Meth. A* **389** (1997) 81, doi:10.1016/S0168-9002(97)00048-X.

[112] S. S. Wilks, "The large-sample distribution of the likelihood ratio for testing composite hypotheses", *Annals Math. Statist.* **9** (1938) 60, doi:10.1214/aoms/1177732360.

[113] CMS Collaboration, "CMS luminosity measurements for the 2016 data taking period", CMS Physics Analysis Summary CMS-PAS-LUM-17-001, 2017.

[114] CMS Collaboration, "CMS luminosity measurement for the 2017 data taking period at $\sqrt{s} = 13$ TeV", CMS Physics Analysis Summary CMS-PAS-LUM-17-004, 2018.

[115] CMS Collaboration, "CMS luminosity measurement for the 2018 data-taking period at $\sqrt{s} = 13$ TeV", CMS Physics Analysis Summary CMS-PAS-LUM-18-002, 2019.

A The CMS Collaboration

Yerevan Physics Institute, Yerevan, Armenia
A.M. Sirunyan†, A. Tumasyan

Institut für Hochenergiephysik, Wien, Austria
W. Adam, J.W. Andrejkovic, T. Bergauer, S. Chatterjee, M. Dragicevic, A. Escalante Del Valle, R. Frühwirth[1], M. Jeitler[1], N. Krammer, L. Lechner, D. Liko, I. Mikulec, P. Paulitsch, F.M. Pitters, J. Schieck[1], R. Schöfbeck, M. Spanring, S. Templ, W. Waltenberger, C.-E. Wulz[1]

Institute for Nuclear Problems, Minsk, Belarus
V. Chekhovsky, A. Litomin, V. Makarenko

Universiteit Antwerpen, Antwerpen, Belgium
M.R. Darwish[2], E.A. De Wolf, X. Janssen, T. Kello[3], A. Lelek, H. Rejeb Sfar, P. Van Mechelen, S. Van Putte, N. Van Remortel

Vrije Universiteit Brussel, Brussel, Belgium
F. Blekman, E.S. Bols, J. D'Hondt, J. De Clercq, M. Delcourt, H. El Faham, S. Lowette, S. Moortgat, A. Morton, D. Müller, A.R. Sahasransu, S. Tavernier, W. Van Doninck, P. Van Mulders

Université Libre de Bruxelles, Bruxelles, Belgium
D. Beghin, B. Bilin, B. Clerbaux, G. De Lentdecker, L. Favart, A. Grebenyuk, A.K. Kalsi, K. Lee, M. Mahdavikhorrami, I. Makarenko, L. Moureaux, L. Pétré, A. Popov, N. Postiau, E. Starling, L. Thomas, M. Vanden Bemden, C. Vander Velde, P. Vanlaer, D. Vannerom, L. Wezenbeek

Ghent University, Ghent, Belgium
T. Cornelis, D. Dobur, J. Knolle, L. Lambrecht, G. Mestdach, M. Niedziela, C. Roskas, A. Samalan, K. Skovpen, T.T. Tran, M. Tytgat, W. Verbeke, B. Vermassen, M. Vit

Université Catholique de Louvain, Louvain-la-Neuve, Belgium
A. Bethani, G. Bruno, F. Bury, C. Caputo, P. David, C. Delaere, I.S. Donertas, A. Giammanco, K. Jaffel, V. Lemaitre, K. Mondal, J. Prisciandaro, A. Taliercio, M. Teklishyn, P. Vischia, S. Wertz, S. Wuyckens

Centro Brasileiro de Pesquisas Fisicas, Rio de Janeiro, Brazil
G.A. Alves, C. Hensel, A. Moraes

Universidade do Estado do Rio de Janeiro, Rio de Janeiro, Brazil
W.L. Aldá Júnior, M. Alves Gallo Pereira, M. Barroso Ferreira Filho, H. BRANDAO MALBOUISSON, W. Carvalho, J. Chinellato[4], E.M. Da Costa, G.G. Da Silveira[5], D. De Jesus Damiao, S. Fonseca De Souza, D. Matos Figueiredo, C. Mora Herrera, K. Mota Amarilo, L. Mundim, H. Nogima, P. Rebello Teles, A. Santoro, S.M. Silva Do Amaral, A. Sznajder, M. Thiel, F. Torres Da Silva De Araujo, A. Vilela Pereira

Universidade Estadual Paulista [a], Universidade Federal do ABC [b], São Paulo, Brazil
C.A. Bernardes[a,a], L. Calligaris[a], T.R. Fernandez Perez Tomei[a], E.M. Gregores[a,b], D.S. Lemos[a], P.G. Mercadante[a,b], S.F. Novaes[a], Sandra S. Padula[a]

Institute for Nuclear Research and Nuclear Energy, Bulgarian Academy of Sciences, Sofia, Bulgaria
A. Aleksandrov, G. Antchev, R. Hadjiiska, P. Iaydjiev, M. Misheva, M. Rodozov, M. Shopova, G. Sultanov

University of Sofia, Sofia, Bulgaria
A. Dimitrov, T. Ivanov, L. Litov, B. Pavlov, P. Petkov, A. Petrov

Beihang University, Beijing, China
T. Cheng, W. Fang[3], Q. Guo, T. Javaid[6], M. Mittal, H. Wang, L. Yuan

Department of Physics, Tsinghua University, Beijing, China
M. Ahmad, G. Bauer, C. Dozen[7], Z. Hu, J. Martins[8], Y. Wang, K. Yi[9,10]

Institute of High Energy Physics, Beijing, China
E. Chapon, G.M. Chen[6], H.S. Chen[6], M. Chen, F. Iemmi, A. Kapoor, D. Leggat, H. Liao, Z.-A. LIU[6], V. Milosevic, F. Monti, R. Sharma, J. Tao, J. Thomas-wilsker, J. Wang, H. Zhang, S. Zhang[6], J. Zhao

State Key Laboratory of Nuclear Physics and Technology, Peking University, Beijing, China
A. Agapitos, Y. Ban, C. Chen, Q. Huang, A. Levin, Q. Li, X. Lyu, Y. Mao, S.J. Qian, D. Wang, Q. Wang, J. Xiao

Sun Yat-Sen University, Guangzhou, China
M. Lu, Z. You

Institute of Modern Physics and Key Laboratory of Nuclear Physics and Ion-beam Application (MOE) - Fudan University, Shanghai, China
X. Gao[3], H. Okawa

Zhejiang University, Hangzhou, China
Z. Lin, R. Pan, M. Xiao

Universidad de Los Andes, Bogota, Colombia
C. Avila, A. Cabrera, C. Florez, J. Fraga, A. Sarkar, M.A. Segura Delgado

Universidad de Antioquia, Medellin, Colombia
J. Mejia Guisao, F. Ramirez, J.D. Ruiz Alvarez, C.A. Salazar González

University of Split, Faculty of Electrical Engineering, Mechanical Engineering and Naval Architecture, Split, Croatia
D. Giljanovic, N. Godinovic, D. Lelas, I. Puljak

University of Split, Faculty of Science, Split, Croatia
Z. Antunovic, M. Kovac, T. Sculac

Institute Rudjer Boskovic, Zagreb, Croatia
V. Brigljevic, D. Ferencek, D. Majumder, M. Roguljic, A. Starodumov[11], T. Susa

University of Cyprus, Nicosia, Cyprus
A. Attikis, E. Erodotou, A. Ioannou, G. Kole, M. Kolosova, S. Konstantinou, J. Mousa, C. Nicolaou, F. Ptochos, P.A. Razis, H. Rykaczewski, H. Saka

Charles University, Prague, Czech Republic
M. Finger[12], M. Finger Jr.[12], A. Kveton

Escuela Politecnica Nacional, Quito, Ecuador
E. Ayala

Universidad San Francisco de Quito, Quito, Ecuador
E. Carrera Jarrin

Academy of Scientific Research and Technology of the Arab Republic of Egypt, Egyptian Network of High Energy Physics, Cairo, Egypt
H. Abdalla[13], A.A. Abdelalim[14,15]

Center for High Energy Physics (CHEP-FU), Fayoum University, El-Fayoum, Egypt
A. Lotfy, M.A. Mahmoud

National Institute of Chemical Physics and Biophysics, Tallinn, Estonia
S. Bhowmik, A. Carvalho Antunes De Oliveira, R.K. Dewanjee, K. Ehataht, M. Kadastik, C. Nielsen, J. Pata, M. Raidal, L. Tani, C. Veelken

Department of Physics, University of Helsinki, Helsinki, Finland
P. Eerola, L. Forthomme, H. Kirschenmann, K. Osterberg, M. Voutilainen

Helsinki Institute of Physics, Helsinki, Finland
S. Bharthuar, E. Brücken, F. Garcia, J. Havukainen, M.S. Kim, R. Kinnunen, T. Lampén, K. Lassila-Perini, S. Lehti, T. Lindén, M. Lotti, L. Martikainen, J. Ott, H. Siikonen, E. Tuominen, J. Tuominiemi

Lappeenranta University of Technology, Lappeenranta, Finland
P. Luukka, H. Petrow, T. Tuuva

IRFU, CEA, Université Paris-Saclay, Gif-sur-Yvette, France
C. Amendola, M. Besancon, F. Couderc, M. Dejardin, D. Denegri, J.L. Faure, F. Ferri, S. Ganjour, A. Givernaud, P. Gras, G. Hamel de Monchenault, P. Jarry, B. Lenzi, E. Locci, J. Malcles, J. Rander, A. Rosowsky, M.Ö. Sahin, A. Savoy-Navarro[16], M. Titov, G.B. Yu

Laboratoire Leprince-Ringuet, CNRS/IN2P3, Ecole Polytechnique, Institut Polytechnique de Paris, Palaiseau, France
S. Ahuja, F. Beaudette, M. Bonanomi, A. Buchot Perraguin, P. Busson, A. Cappati, C. Charlot, O. Davignon, B. Diab, G. Falmagne, S. Ghosh, R. Granier de Cassagnac, A. Hakimi, I. Kucher, M. Nguyen, C. Ochando, P. Paganini, J. Rembser, R. Salerno, J.B. Sauvan, Y. Sirois, A. Zabi, A. Zghiche

Université de Strasbourg, CNRS, IPHC UMR 7178, Strasbourg, France
J.-L. Agram[17], J. Andrea, D. Apparu, D. Bloch, G. Bourgatte, J.-M. Brom, E.C. Chabert, C. Collard, D. Darej, J.-C. Fontaine[17], U. Goerlach, C. Grimault, A.-C. Le Bihan, E. Nibigira, P. Van Hove

Institut de Physique des 2 Infinis de Lyon (IP2I), Villeurbanne, France
E. Asilar, S. Beauceron, C. Bernet, G. Boudoul, C. Camen, A. Carle, N. Chanon, D. Contardo, P. Depasse, H. El Mamouni, J. Fay, S. Gascon, M. Gouzevitch, B. Ille, Sa. Jain, I.B. Laktineh, H. Lattaud, A. Lesauvage, M. Lethuillier, L. Mirabito, S. Perries, K. Shchablo, V. Sordini, L. Torterotot, G. Touquet, M. Vander Donckt, S. Viret

Georgian Technical University, Tbilisi, Georgia
A. Khvedelidze[12], I. Lomidze, Z. Tsamalaidze[12]

RWTH Aachen University, I. Physikalisches Institut, Aachen, Germany
L. Feld, K. Klein, M. Lipinski, D. Meuser, A. Pauls, M.P. Rauch, N. Röwert, J. Schulz, M. Teroerde

RWTH Aachen University, III. Physikalisches Institut A, Aachen, Germany
D. Eliseev, M. Erdmann, P. Fackeldey, B. Fischer, S. Ghosh, T. Hebbeker, K. Hoepfner, F. Ivone, H. Keller, L. Mastrolorenzo, M. Merschmeyer, A. Meyer, G. Mocellin, S. Mondal, S. Mukherjee,

D. Noll, A. Novak, T. Pook, A. Pozdnyakov, Y. Rath, H. Reithler, J. Roemer, A. Schmidt, S.C. Schuler, A. Sharma, S. Wiedenbeck, S. Zaleski

RWTH Aachen University, III. Physikalisches Institut B, Aachen, Germany
C. Dziwok, G. Flügge, W. Haj Ahmad[18], O. Hlushchenko, T. Kress, A. Nowack, C. Pistone, O. Pooth, D. Roy, H. Sert, A. Stahl[19], T. Ziemons

Deutsches Elektronen-Synchrotron, Hamburg, Germany
H. Aarup Petersen, M. Aldaya Martin, P. Asmuss, I. Babounikau, S. Baxter, O. Behnke, A. Bermúdez Martínez, S. Bhattacharya, A.A. Bin Anuar, K. Borras[20], V. Botta, D. Brunner, A. Campbell, A. Cardini, C. Cheng, F. Colombina, S. Consuegra Rodríguez, G. Correia Silva, V. Danilov, L. Didukh, G. Eckerlin, D. Eckstein, L.I. Estevez Banos, O. Filatov, E. Gallo[21], A. Geiser, A. Giraldi, A. Grohsjean, M. Guthoff, A. Jafari[22], N.Z. Jomhari, H. Jung, A. Kasem[20], M. Kasemann, H. Kaveh, C. Kleinwort, D. Krücker, W. Lange, J. Lidrych, K. Lipka, W. Lohmann[23], R. Mankel, I.-A. Melzer-Pellmann, J. Metwally, A.B. Meyer, M. Meyer, J. Mnich, A. Mussgiller, Y. Otarid, D. Pérez Adán, D. Pitzl, A. Raspereza, B. Ribeiro Lopes, J. Rübenach, A. Saggio, A. Saibel, M. Savitskyi, M. Scham, V. Scheurer, C. Schwanenberger[21], A. Singh, R.E. Sosa Ricardo, D. Stafford, N. Tonon, O. Turkot, M. Van De Klundert, R. Walsh, D. Walter, Y. Wen, K. Wichmann, L. Wiens, C. Wissing, S. Wuchterl

University of Hamburg, Hamburg, Germany
R. Aggleton, S. Bein, L. Benato, A. Benecke, P. Connor, K. De Leo, M. Eich, F. Feindt, A. Fröhlich, C. Garbers, E. Garutti, P. Gunnellini, J. Haller, A. Hinzmann, G. Kasieczka, R. Klanner, R. Kogler, T. Kramer, V. Kutzner, J. Lange, T. Lange, A. Lobanov, A. Malara, A. Nigamova, K.J. Pena Rodriguez, O. Rieger, P. Schleper, M. Schröder, J. Schwandt, D. Schwarz, J. Sonneveld, H. Stadie, G. Steinbrück, A. Tews, B. Vormwald, I. Zoi

Karlsruher Institut fuer Technologie, Karlsruhe, Germany
J. Bechtel, T. Berger, E. Butz, R. Caspart, T. Chwalek, W. De Boer†, A. Dierlamm, A. Droll, K. El Morabit, N. Faltermann, M. Giffels, J.o. Gosewisch, A. Gottmann, F. Hartmann[19], C. Heidecker, U. Husemann, I. Katkov[24], P. Keicher, R. Koppenhöfer, S. Maier, M. Metzler, S. Mitra, Th. Müller, M. Neukum, A. Nürnberg, G. Quast, K. Rabbertz, J. Rauser, D. Savoiu, M. Schnepf, D. Seith, I. Shvetsov, H.J. Simonis, R. Ulrich, J. Van Der Linden, R.F. Von Cube, M. Wassmer, M. Weber, S. Wieland, R. Wolf, S. Wozniewski, S. Wunsch

Institute of Nuclear and Particle Physics (INPP), NCSR Demokritos, Aghia Paraskevi, Greece
G. Anagnostou, P. Asenov, G. Daskalakis, T. Geralis, A. Kyriakis, D. Loukas, A. Stakia

National and Kapodistrian University of Athens, Athens, Greece
M. Diamantopoulou, D. Karasavvas, G. Karathanasis, P. Kontaxakis, C.K. Koraka, A. Manousakis-katsikakis, A. Panagiotou, I. Papavergou, N. Saoulidou, K. Theofilatos, E. Tziaferi, K. Vellidis, E. Vourliotis

National Technical University of Athens, Athens, Greece
G. Bakas, K. Kousouris, I. Papakrivopoulos, G. Tsipolitis, A. Zacharopoulou

University of Ioánnina, Ioánnina, Greece
I. Evangelou, C. Foudas, P. Gianneios, P. Katsoulis, P. Kokkas, N. Manthos, I. Papadopoulos, J. Strologas

MTA-ELTE Lendület CMS Particle and Nuclear Physics Group, Eötvös Loránd University,

Budapest, Hungary
M. Csanad, K. Farkas, M.M.A. Gadallah[25], S. Lökös[26], P. Major, K. Mandal, A. Mehta, G. Pasztor, A.J. Rádl, O. Surányi, G.I. Veres

Wigner Research Centre for Physics, Budapest, Hungary
M. Bartók[27], G. Bencze, C. Hajdu, D. Horvath[28], F. Sikler, V. Veszpremi, G. Vesztergombi[†]

Institute of Nuclear Research ATOMKI, Debrecen, Hungary
S. Czellar, J. Karancsi[27], J. Molnar, Z. Szillasi, D. Teyssier

Institute of Physics, University of Debrecen, Debrecen, Hungary
P. Raics, Z.L. Trocsanyi[29], G. Zilizi

Eszterhazy Karoly University, Karoly Robert Campus, Gyongyos, Hungary
T. Csorgo[30], F. Nemes[30], T. Novak

Indian Institute of Science (IISc), Bangalore, India
J.R. Komaragiri, D. Kumar, L. Panwar, P.C. Tiwari

National Institute of Science Education and Research, HBNI, Bhubaneswar, India
S. Bahinipati[31], D. Dash, C. Kar, P. Mal, T. Mishra, V.K. Muraleedharan Nair Bindhu[32], A. Nayak[32], P. Saha, N. Sur, S.K. Swain, D. Vats[32]

Panjab University, Chandigarh, India
S. Bansal, S.B. Beri, V. Bhatnagar, G. Chaudhary, S. Chauhan, N. Dhingra[33], R. Gupta, A. Kaur, M. Kaur, S. Kaur, P. Kumari, M. Meena, K. Sandeep, J.B. Singh, A.K. Virdi

University of Delhi, Delhi, India
A. Ahmed, A. Bhardwaj, B.C. Choudhary, M. Gola, S. Keshri, A. Kumar, M. Naimuddin, P. Priyanka, K. Ranjan, A. Shah

Saha Institute of Nuclear Physics, HBNI, Kolkata, India
M. Bharti[34], R. Bhattacharya, S. Bhattacharya, D. Bhowmik, S. Dutta, S. Dutta, B. Gomber[35], M. Maity[36], S. Nandan, P. Palit, P.K. Rout, G. Saha, B. Sahu, S. Sarkar, M. Sharan, B. Singh[34], S. Thakur[34]

Indian Institute of Technology Madras, Madras, India
P.K. Behera, S.C. Behera, P. Kalbhor, A. Muhammad, R. Pradhan, P.R. Pujahari, A. Sharma, A.K. Sikdar

Bhabha Atomic Research Centre, Mumbai, India
D. Dutta, V. Jha, V. Kumar, D.K. Mishra, K. Naskar[37], P.K. Netrakanti, L.M. Pant, P. Shukla

Tata Institute of Fundamental Research-A, Mumbai, India
T. Aziz, S. Dugad, M. Kumar, U. Sarkar

Tata Institute of Fundamental Research-B, Mumbai, India
S. Banerjee, R. Chudasama, M. Guchait, S. Karmakar, S. Kumar, G. Majumder, K. Mazumdar, S. Mukherjee

Indian Institute of Science Education and Research (IISER), Pune, India
K. Alpana, S. Dube, B. Kansal, S. Pandey, A. Rane, A. Rastogi, S. Sharma

Department of Physics, Isfahan University of Technology, Isfahan, Iran
H. Bakhshiansohi[38], M. Zeinali[39]

Institute for Research in Fundamental Sciences (IPM), Tehran, Iran
S. Chenarani[40], S.M. Etesami, M. Khakzad, M. Mohammadi Najafabadi

University College Dublin, Dublin, Ireland
M. Grunewald

INFN Sezione di Bari [a], Università di Bari [b], Politecnico di Bari [c], Bari, Italy
M. Abbrescia[a,b], R. Aly[a,b,41], C. Aruta[a,b], A. Colaleo[a], D. Creanza[a,c], N. De Filippis[a,c], M. De Palma[a,b], A. Di Florio[a,b], A. Di Pilato[a,b], W. Elmetenawee[a,b], L. Fiore[a], A. Gelmi[a,b], M. Gul[a], G. Iaselli[a,c], M. Ince[a,b], S. Lezki[a,b], G. Maggi[a,c], M. Maggi[a], I. Margjeka[a,b], V. Mastrapasqua[a,b], J.A. Merlin[a], S. My[a,b], S. Nuzzo[a,b], A. Pellecchia[a,b], A. Pompili[a,b], G. Pugliese[a,c], A. Ranieri[a], G. Selvaggi[a,b], L. Silvestris[a], F.M. Simone[a,b], R. Venditti[a], P. Verwilligen[a]

INFN Sezione di Bologna [a], Università di Bologna [b], Bologna, Italy
G. Abbiendi[a], C. Battilana[a,b], D. Bonacorsi[a,b], L. Borgonovi[a], L. Brigliadori[a], R. Campanini[a,b], P. Capiluppi[a,b], A. Castro[a,b], F.R. Cavallo[a], M. Cuffiani[a,b], G.M. Dallavalle[a], T. Diotalevi[a,b], F. Fabbri[a], A. Fanfani[a,b], P. Giacomelli[a], L. Giommi[a,b], C. Grandi[a], L. Guiducci[a,b], S. Lo Meo[a,42], L. Lunerti[a,b], S. Marcellini[a], G. Masetti[a], F.L. Navarria[a,b], A. Perrotta[a], F. Primavera[a,b], A.M. Rossi[a,b], T. Rovelli[a,b], G.P. Siroli[a,b]

INFN Sezione di Catania [a], Università di Catania [b], Catania, Italy
S. Albergo[a,b,43], S. Costa[a,b,43], A. Di Mattia[a], R. Potenza[a,b], A. Tricomi[a,b,43], C. Tuve[a,b]

INFN Sezione di Firenze [a], Università di Firenze [b], Firenze, Italy
G. Barbagli[a], A. Cassese[a], R. Ceccarelli[a,b], V. Ciulli[a,b], C. Civinini[a], R. D'Alessandro[a,b], E. Focardi[a,b], G. Latino[a,b], P. Lenzi[a,b], M. Lizzo[a,b], M. Meschini[a], S. Paoletti[a], R. Seidita[a,b], G. Sguazzoni[a], L. Viliani[a]

INFN Laboratori Nazionali di Frascati, Frascati, Italy
L. Benussi, S. Bianco, D. Piccolo

INFN Sezione di Genova [a], Università di Genova [b], Genova, Italy
M. Bozzo[a,b], F. Ferro[a], R. Mulargia[a,b], E. Robutti[a], S. Tosi[a,b]

INFN Sezione di Milano-Bicocca [a], Università di Milano-Bicocca [b], Milano, Italy
A. Benaglia[a], F. Brivio[a,b], F. Cetorelli[a,b], V. Ciriolo[a,b,19], F. De Guio[a,b], M.E. Dinardo[a,b], P. Dini[a], S. Gennai[a], A. Ghezzi[a,b], P. Govoni[a,b], L. Guzzi[a,b], M. Malberti[a], S. Malvezzi[a], A. Massironi[a], D. Menasce[a], L. Moroni[a], M. Paganoni[a,b], D. Pedrini[a], S. Ragazzi[a,b], N. Redaelli[a], T. Tabarelli de Fatis[a,b], D. Valsecchi[a,b,19], D. Zuolo[a,b]

INFN Sezione di Napoli [a], Università di Napoli 'Federico II' [b], Napoli, Italy, Università della Basilicata [c], Potenza, Italy, Università G. Marconi [d], Roma, Italy
S. Buontempo[a], F. Carnevali[a,b], N. Cavallo[a,c], A. De Iorio[a,b], F. Fabozzi[a,c], A.O.M. Iorio[a,b], L. Lista[a,b], S. Meola[a,d,19], P. Paolucci[a,19], B. Rossi[a], C. Sciacca[a,b]

INFN Sezione di Padova [a], Università di Padova [b], Padova, Italy, Università di Trento [c], Trento, Italy
P. Azzi[a], N. Bacchetta[a], D. Bisello[a,b], P. Bortignon[a], A. Bragagnolo[a,b], R. Carlin[a,b], P. Checchia[a], T. Dorigo[a], U. Dosselli[a], F. Gasparini[a,b], U. Gasparini[a,b], S.Y. Hoh[a,b], L. Layer[a,44], M. Margoni[a,b], A.T. Meneguzzo[a,b], J. Pazzini[a,b], M. Presilla[a,b], P. Ronchese[a,b], R. Rossin[a,b], F. Simonetto[a,b], G. Strong[a], M. Tosi[a,b], H. YARAR[a,b], M. Zanetti[a,b], P. Zotto[a,b], A. Zucchetta[a,b], G. Zumerle[a,b]

INFN Sezione di Pavia [a], Università di Pavia [b], Pavia, Italy
C. Aime'[a,b], A. Braghieri[a], S. Calzaferri[a,b], D. Fiorina[a,b], P. Montagna[a,b], S.P. Ratti[a,b], V. Re[a], C. Riccardi[a,b], P. Salvini[a], I. Vai[a], P. Vitulo[a,b]

INFN Sezione di Perugia [a], Università di Perugia [b], Perugia, Italy
G.M. Bilei[a], D. Ciangottini[a,b], L. Fanò[a,b], P. Lariccia[a,b], M. Magherini[b], G. Mantovani[a,b], V. Mariani[a,b], M. Menichelli[a], F. Moscatelli[a], A. Piccinelli[a,b], A. Rossi[a,b], A. Santocchia[a,b], D. Spiga[a], T. Tedeschi[a,b]

INFN Sezione di Pisa [a], Università di Pisa [b], Scuola Normale Superiore di Pisa [c], Pisa Italy, Università di Siena [d], Siena, Italy
P. Azzurri[a], G. Bagliesi[a], V. Bertacchi[a,c], L. Bianchini[a], T. Boccali[a], E. Bossini[a,b], R. Castaldi[a], M.A. Ciocci[a,b], R. Dell'Orso[a], M.R. Di Domenico[a,d], S. Donato[a], A. Giassi[a], M.T. Grippo[a], F. Ligabue[a,c], E. Manca[a,c], G. Mandorli[a,c], A. Messineo[a,b], F. Palla[a], S. Parolia[a,b], G. Ramirez-Sanchez[a,c], A. Rizzi[a,b], G. Rolandi[a,c], S. Roy Chowdhury[a,c], A. Scribano[a], N. Shafiei[a,b], P. Spagnolo[a], R. Tenchini[a], G. Tonelli[a,b], N. Turini[a,d], A. Venturi[a], P.G. Verdini[a]

INFN Sezione di Roma [a], Sapienza Università di Roma [b], Rome, Italy
M. Campana[a,b], F. Cavallari[a], M. Cipriani[a,b], D. Del Re[a,b], E. Di Marco[a], M. Diemoz[a], E. Longo[a,b], P. Meridiani[a], G. Organtini[a,b], F. Pandolfi[a], R. Paramatti[a,b], C. Quaranta[a,b], S. Rahatlou[a,b], C. Rovelli[a], F. Santanastasio[a,b], L. Soffi[a], R. Tramontano[a,b]

INFN Sezione di Torino [a], Università di Torino [b], Torino, Italy, Università del Piemonte Orientale [c], Novara, Italy
N. Amapane[a,b], R. Arcidiacono[a,c], S. Argiro[a,b], M. Arneodo[a,c], N. Bartosik[a], R. Bellan[a,b], A. Bellora[a,b], J. Berenguer Antequera[a,b], C. Biino[a], N. Cartiglia[a], S. Cometti[a], M. Costa[a,b], R. Covarelli[a,b], N. Demaria[a], B. Kiani[a,b], F. Legger[a], C. Mariotti[a], S. Maselli[a], E. Migliore[a,b], E. Monteil[a,b], M. Monteno[a], M.M. Obertino[a,b], G. Ortona[a], L. Pacher[a,b], N. Pastrone[a], M. Pelliccioni[a], G.L. Pinna Angioni[a,b], M. Ruspa[a,c], R. Salvatico[a,b], K. Shchelina[a,b], F. Siviero[a,b], V. Sola[a], A. Solano[a,b], D. Soldi[a,b], A. Staiano[a], M. Tornago[a,b], D. Trocino[a,b], A. Vagnerini

INFN Sezione di Trieste [a], Università di Trieste [b], Trieste, Italy
S. Belforte[a], V. Candelise[a,b], M. Casarsa[a], F. Cossutti[a], A. Da Rold[a,b], G. Della Ricca[a,b], G. Sorrentino[a,b], F. Vazzoler[a,b]

Kyungpook National University, Daegu, Korea
S. Dogra, C. Huh, B. Kim, D.H. Kim, G.N. Kim, J. Kim, J. Lee, S.W. Lee, C.S. Moon, Y.D. Oh, S.I. Pak, B.C. Radburn-Smith, S. Sekmen, Y.C. Yang

Chonnam National University, Institute for Universe and Elementary Particles, Kwangju, Korea
H. Kim, D.H. Moon

Hanyang University, Seoul, Korea
B. Francois, T.J. Kim, J. Park

Korea University, Seoul, Korea
S. Cho, S. Choi, Y. Go, B. Hong, K. Lee, K.S. Lee, J. Lim, J. Park, S.K. Park, J. Yoo

Kyung Hee University, Department of Physics, Seoul, Republic of Korea
J. Goh, A. Gurtu

Sejong University, Seoul, Korea
H.S. Kim, Y. Kim

Seoul National University, Seoul, Korea
J. Almond, J.H. Bhyun, J. Choi, S. Jeon, J. Kim, J.S. Kim, S. Ko, H. Kwon, H. Lee, S. Lee, B.H. Oh, M. Oh, S.B. Oh, H. Seo, U.K. Yang, I. Yoon

University of Seoul, Seoul, Korea
W. Jang, D. Jeon, D.Y. Kang, Y. Kang, J.H. Kim, S. Kim, B. Ko, J.S.H. Lee, Y. Lee, I.C. Park, Y. Roh, M.S. Ryu, D. Song, I.J. Watson, S. Yang

Yonsei University, Department of Physics, Seoul, Korea
S. Ha, H.D. Yoo

Sungkyunkwan University, Suwon, Korea
Y. Jeong, H. Lee, Y. Lee, I. Yu

College of Engineering and Technology, American University of the Middle East (AUM), Egaila, Kuwait
T. Beyrouthy, Y. Maghrbi

Riga Technical University, Riga, Latvia
V. Veckalns[45]

Vilnius University, Vilnius, Lithuania
M. Ambrozas, A. Juodagalvis, A. Rinkevicius, G. Tamulaitis, A. Vaitkevicius

National Centre for Particle Physics, Universiti Malaya, Kuala Lumpur, Malaysia
N. Bin Norjoharuddeen, W.A.T. Wan Abdullah, M.N. Yusli, Z. Zolkapli

Universidad de Sonora (UNISON), Hermosillo, Mexico
J.F. Benitez, A. Castaneda Hernandez, M. León Coello, J.A. Murillo Quijada, A. Sehrawat, L. Valencia Palomo

Centro de Investigacion y de Estudios Avanzados del IPN, Mexico City, Mexico
G. Ayala, H. Castilla-Valdez, I. Heredia-De La Cruz[46], R. Lopez-Fernandez, C.A. Mondragon Herrera, D.A. Perez Navarro, A. Sanchez-Hernandez

Universidad Iberoamericana, Mexico City, Mexico
S. Carrillo Moreno, C. Oropeza Barrera, M. Ramirez-Garcia, F. Vazquez Valencia

Benemerita Universidad Autonoma de Puebla, Puebla, Mexico
I. Pedraza, H.A. Salazar Ibarguen, C. Uribe Estrada

University of Montenegro, Podgorica, Montenegro
J. Mijuskovic[47], N. Raicevic

University of Auckland, Auckland, New Zealand
D. Krofcheck

University of Canterbury, Christchurch, New Zealand
S. Bheesette, P.H. Butler

National Centre for Physics, Quaid-I-Azam University, Islamabad, Pakistan
A. Ahmad, M.I. Asghar, A. Awais, M.I.M. Awan, H.R. Hoorani, W.A. Khan, M.A. Shah, M. Shoaib, M. Waqas

AGH University of Science and Technology Faculty of Computer Science, Electronics and Telecommunications, Krakow, Poland
V. Avati, L. Grzanka, M. Malawski

National Centre for Nuclear Research, Swierk, Poland
H. Bialkowska, M. Bluj, B. Boimska, M. Górski, M. Kazana, M. Szleper, P. Zalewski

Institute of Experimental Physics, Faculty of Physics, University of Warsaw, Warsaw, Poland
K. Bunkowski, K. Doroba, A. Kalinowski, M. Konecki, J. Krolikowski, M. Walczak

Laboratório de Instrumentação e Física Experimental de Partículas, Lisboa, Portugal
M. Araujo, P. Bargassa, D. Bastos, A. Boletti, P. Faccioli, M. Gallinaro, J. Hollar, N. Leonardo, T. Niknejad, M. Pisano, J. Seixas, O. Toldaiev, J. Varela

Joint Institute for Nuclear Research, Dubna, Russia
S. Afanasiev, D. Budkouski, I. Golutvin, I. Gorbunov, V. Karjavine, V. Korenkov, A. Lanev, A. Malakhov, V. Matveev[48,49], V. Palichik, V. Perelygin, M. Savina, D. Seitova, V. Shalaev, S. Shmatov, S. Shulha, V. Smirnov, O. Teryaev, N. Voytishin, B.S. Yuldashev[50], A. Zarubin, I. Zhizhin

Petersburg Nuclear Physics Institute, Gatchina (St. Petersburg), Russia
G. Gavrilov, V. Golovtcov, Y. Ivanov, V. Kim[51], E. Kuznetsova[52], V. Murzin, V. Oreshkin, I. Smirnov, D. Sosnov, V. Sulimov, L. Uvarov, S. Volkov, A. Vorobyev

Institute for Nuclear Research, Moscow, Russia
Yu. Andreev, A. Dermenev, S. Gninenko, N. Golubev, A. Karneyeu, D. Kirpichnikov, M. Kirsanov, N. Krasnikov, A. Pashenkov, G. Pivovarov, D. Tlisov†, A. Toropin

Institute for Theoretical and Experimental Physics named by A.I. Alikhanov of NRC 'Kurchatov Institute', Moscow, Russia
V. Epshteyn, V. Gavrilov, N. Lychkovskaya, A. Nikitenko[53], V. Popov, A. Spiridonov, A. Stepennov, M. Toms, E. Vlasov, A. Zhokin

Moscow Institute of Physics and Technology, Moscow, Russia
T. Aushev

National Research Nuclear University 'Moscow Engineering Physics Institute' (MEPhI), Moscow, Russia
O. Bychkova, R. Chistov[54], M. Danilov[55], P. Parygin, S. Polikarpov[55]

P.N. Lebedev Physical Institute, Moscow, Russia
V. Andreev, M. Azarkin, I. Dremin, M. Kirakosyan, A. Terkulov

Skobeltsyn Institute of Nuclear Physics, Lomonosov Moscow State University, Moscow, Russia
A. Belyaev, E. Boos, V. Bunichev, M. Dubinin[56], L. Dudko, A. Ershov, V. Klyukhin, O. Kodolova, I. Lokhtin, S. Obraztsov, M. Perfilov, S. Petrushanko, V. Savrin

Novosibirsk State University (NSU), Novosibirsk, Russia
V. Blinov[57], T. Dimova[57], L. Kardapoltsev[57], A. Kozyrev[57], I. Ovtin[57], Y. Skovpen[57]

Institute for High Energy Physics of National Research Centre 'Kurchatov Institute', Protvino, Russia
I. Azhgirey, I. Bayshev, D. Elumakhov, V. Kachanov, D. Konstantinov, P. Mandrik, V. Petrov, R. Ryutin, S. Slabospitskii, A. Sobol, S. Troshin, N. Tyurin, A. Uzunian, A. Volkov

National Research Tomsk Polytechnic University, Tomsk, Russia
A. Babaev, V. Okhotnikov

Tomsk State University, Tomsk, Russia
V. Borchsh, V. Ivanchenko, E. Tcherniaev

University of Belgrade: Faculty of Physics and VINCA Institute of Nuclear Sciences, Belgrade, Serbia
P. Adzic[58], M. Dordevic, P. Milenovic, J. Milosevic

Centro de Investigaciones Energéticas Medioambientales y Tecnológicas (CIEMAT), Madrid, Spain
M. Aguilar-Benitez, J. Alcaraz Maestre, A. Álvarez Fernández, I. Bachiller, M. Barrio Luna, Cristina F. Bedoya, C.A. Carrillo Montoya, M. Cepeda, M. Cerrada, N. Colino, B. De La Cruz, A. Delgado Peris, J.P. Fernández Ramos, J. Flix, M.C. Fouz, O. Gonzalez Lopez, S. Goy Lopez, J.M. Hernandez, M.I. Josa, J. León Holgado, D. Moran, Á. Navarro Tobar, A. Pérez-Calero Yzquierdo, J. Puerta Pelayo, I. Redondo, L. Romero, S. Sánchez Navas, L. Urda Gómez, C. Willmott

Universidad Autónoma de Madrid, Madrid, Spain
J.F. de Trocóniz, R. Reyes-Almanza

Universidad de Oviedo, Instituto Universitario de Ciencias y Tecnologías Espaciales de Asturias (ICTEA), Oviedo, Spain
B. Alvarez Gonzalez, J. Cuevas, C. Erice, J. Fernandez Menendez, S. Folgueras, I. Gonzalez Caballero, E. Palencia Cortezon, C. Ramón Álvarez, J. Ripoll Sau, V. Rodríguez Bouza, A. Trapote, N. Trevisani

Instituto de Física de Cantabria (IFCA), CSIC-Universidad de Cantabria, Santander, Spain
J.A. Brochero Cifuentes, I.J. Cabrillo, A. Calderon, J. Duarte Campderros, M. Fernandez, C. Fernandez Madrazo, P.J. Fernández Manteca, A. García Alonso, G. Gomez, C. Martinez Rivero, P. Martinez Ruiz del Arbol, F. Matorras, P. Matorras Cuevas, J. Piedra Gomez, C. Prieels, T. Rodrigo, A. Ruiz-Jimeno, L. Scodellaro, I. Vila, J.M. Vizan Garcia

University of Colombo, Colombo, Sri Lanka
MK Jayananda, B. Kailasapathy[59], D.U.J. Sonnadara, DDC Wickramarathna

University of Ruhuna, Department of Physics, Matara, Sri Lanka
W.G.D. Dharmaratna, K. Liyanage, N. Perera, N. Wickramage

CERN, European Organization for Nuclear Research, Geneva, Switzerland
T.K. Aarrestad, D. Abbaneo, J. Alimena, E. Auffray, G. Auzinger, J. Baechler, P. Baillon[†], D. Barney, J. Bendavid, M. Bianco, A. Bocci, T. Camporesi, M. Capeans Garrido, G. Cerminara, S.S. Chhibra, L. Cristella, D. d'Enterria, A. Dabrowski, N. Daci, A. David, A. De Roeck, M.M. Defranchis, M. Deile, M. Dobson, M. Dünser, N. Dupont, A. Elliott-Peisert, N. Emriskova, F. Fallavollita[60], D. Fasanella, S. Fiorendi, A. Florent, G. Franzoni, W. Funk, S. Giani, D. Gigi, K. Gill, F. Glege, L. Gouskos, M. Haranko, J. Hegeman, Y. Iiyama, V. Innocente, T. James, P. Janot, J. Kaspar, J. Kieseler, M. Komm, N. Kratochwil, C. Lange, S. Laurila, P. Lecoq, K. Long, C. Lourenço, L. Malgeri, S. Mallios, M. Mannelli, A.C. Marini, F. Meijers, S. Mersi, E. Meschi, F. Moortgat, M. Mulders, S. Orfanelli, L. Orsini, F. Pantaleo, L. Pape, E. Perez, M. Peruzzi, A. Petrilli, G. Petrucciani, A. Pfeiffer, M. Pierini, D. Piparo, M. Pitt, H. Qu, T. Quast, D. Rabady, A. Racz, G. Reales Gutiérrez, M. Rieger, M. Rovere, H. Sakulin, J. Salfeld-Nebgen, S. Scarfi, C. Schäfer, C. Schwick, M. Selvaggi, A. Sharma, P. Silva, W. Snoeys, P. Sphicas[61], S. Summers, V.R. Tavolaro, D. Treille, A. Tsirou, G.P. Van Onsem, M. Verzetti, J. Wanczyk[62], K.A. Wozniak, W.D. Zeuner

Paul Scherrer Institut, Villigen, Switzerland
L. Caminada[63], A. Ebrahimi, W. Erdmann, R. Horisberger, Q. Ingram, H.C. Kaestli, D. Kotlinski, U. Langenegger, M. Missiroli, T. Rohe

ETH Zurich - Institute for Particle Physics and Astrophysics (IPA), Zurich, Switzerland
K. Androsov[62], M. Backhaus, P. Berger, A. Calandri, N. Chernyavskaya, A. De Cosa, G. Dissertori, M. Dittmar, M. Donegà, C. Dorfer, F. Eble, T.A. Gómez Espinosa, C. Grab, D. Hits, W. Lustermann, A.-M. Lyon, R.A. Manzoni, C. Martin Perez, M.T. Meinhard, F. Micheli, F. Nessi-Tedaldi, J. Niedziela, F. Pauss, V. Perovic, G. Perrin, S. Pigazzini, M.G. Ratti, M. Reichmann, C. Reissel, T. Reitenspiess, B. Ristic, D. Ruini, D.A. Sanz Becerra, M. Schönenberger, V. Stampf, J. Steggemann[62], R. Wallny, D.H. Zhu

Universität Zürich, Zurich, Switzerland
C. Amsler[64], P. Bärtschi, C. Botta, D. Brzhechko, M.F. Canelli, K. Cormier, A. De Wit, R. Del Burgo, J.K. Heikkilä, M. Huwiler, A. Jofrehei, B. Kilminster, S. Leontsinis, A. Macchiolo, P. Meiring, V.M. Mikuni, U. Molinatti, I. Neutelings, A. Reimers, P. Robmann, S. Sanchez Cruz, K. Schweiger, Y. Takahashi

National Central University, Chung-Li, Taiwan
C. Adloff[65], C.M. Kuo, W. Lin, A. Roy, T. Sarkar[36], S.S. Yu

National Taiwan University (NTU), Taipei, Taiwan
L. Ceard, Y. Chao, K.F. Chen, P.H. Chen, W.-S. Hou, Y.y. Li, R.-S. Lu, E. Paganis, A. Psallidas, A. Steen, H.y. Wu, E. Yazgan, P.r. Yu

Chulalongkorn University, Faculty of Science, Department of Physics, Bangkok, Thailand
B. Asavapibhop, C. Asawatangtrakuldee, N. Srimanobhas

Çukurova University, Physics Department, Science and Art Faculty, Adana, Turkey
F. Boran, S. Damarseckin[66], Z.S. Demiroglu, F. Dolek, I. Dumanoglu[67], E. Eskut, Y. Guler, E. Gurpinar Guler[68], I. Hos[69], C. Isik, O. Kara, A. Kayis Topaksu, U. Kiminsu, G. Onengut, K. Ozdemir[70], A. Polatoz, A.E. Simsek, B. Tali[71], U.G. Tok, S. Turkcapar, I.S. Zorbakir, C. Zorbilmez

Middle East Technical University, Physics Department, Ankara, Turkey
B. Isildak[72], G. Karapinar[73], K. Ocalan[74], M. Yalvac[75]

Bogazici University, Istanbul, Turkey
B. Akgun, I.O. Atakisi, E. Gülmez, M. Kaya[76], O. Kaya[77], Ö. Özçelik, S. Tekten[78], E.A. Yetkin[79]

Istanbul Technical University, Istanbul, Turkey
A. Cakir, K. Cankocak[67], Y. Komurcu, S. Sen[80]

Istanbul University, Istanbul, Turkey
S. Cerci[71], B. Kaynak, S. Ozkorucuklu, D. Sunar Cerci[71]

Institute for Scintillation Materials of National Academy of Science of Ukraine, Kharkov, Ukraine
B. Grynyov

National Scientific Center, Kharkov Institute of Physics and Technology, Kharkov, Ukraine
L. Levchuk

University of Bristol, Bristol, United Kingdom
D. Anthony, E. Bhal, S. Bologna, J.J. Brooke, A. Bundock, E. Clement, D. Cussans, H. Flacher,

J. Goldstein, G.P. Heath, H.F. Heath, L. Kreczko, B. Krikler, S. Paramesvaran, S. Seif El Nasr-Storey, V.J. Smith, N. Stylianou[81], R. White

Rutherford Appleton Laboratory, Didcot, United Kingdom
K.W. Bell, A. Belyaev[82], C. Brew, R.M. Brown, D.J.A. Cockerill, K.V. Ellis, K. Harder, S. Harper, J. Linacre, K. Manolopoulos, D.M. Newbold, E. Olaiya, D. Petyt, T. Reis, T. Schuh, C.H. Shepherd-Themistocleous, I.R. Tomalin, T. Williams

Imperial College, London, United Kingdom
R. Bainbridge, P. Bloch, S. Bonomally, J. Borg, S. Breeze, O. Buchmuller, V. Cepaitis, G.S. Chahal[83], D. Colling, P. Dauncey, G. Davies, M. Della Negra, S. Fayer, G. Fedi, G. Hall, M.H. Hassanshahi, G. Iles, J. Langford, L. Lyons, A.-M. Magnan, S. Malik, A. Martelli, J. Nash[84], M. Pesaresi, D.M. Raymond, A. Richards, A. Rose, E. Scott, C. Seez, A. Shtipliyski, A. Tapper, K. Uchida, T. Virdee[19], N. Wardle, S.N. Webb, D. Winterbottom, A.G. Zecchinelli

Brunel University, Uxbridge, United Kingdom
K. Coldham, J.E. Cole, A. Khan, P. Kyberd, I.D. Reid, L. Teodorescu, S. Zahid

Baylor University, Waco, USA
S. Abdullin, A. Brinkerhoff, B. Caraway, J. Dittmann, K. Hatakeyama, A.R. Kanuganti, B. McMaster, N. Pastika, S. Sawant, C. Sutantawibul, J. Wilson

Catholic University of America, Washington, DC, USA
R. Bartek, A. Dominguez, R. Uniyal, A.M. Vargas Hernandez

The University of Alabama, Tuscaloosa, USA
A. Buccilli, S.I. Cooper, D. Di Croce, S.V. Gleyzer, C. Henderson, C.U. Perez, P. Rumerio[85], C. West

Boston University, Boston, USA
A. Akpinar, A. Albert, D. Arcaro, C. Cosby, Z. Demiragli, E. Fontanesi, D. Gastler, J. Rohlf, K. Salyer, D. Sperka, D. Spitzbart, I. Suarez, A. Tsatsos, S. Yuan, D. Zou

Brown University, Providence, USA
G. Benelli, B. Burkle, X. Coubez[20], D. Cutts, M. Hadley, U. Heintz, J.M. Hogan[86], G. Landsberg, K.T. Lau, M. Lukasik, J. Luo, M. Narain, S. Sagir[87], E. Usai, W.Y. Wong, X. Yan, D. Yu, W. Zhang

University of California, Davis, Davis, USA
J. Bonilla, C. Brainerd, R. Breedon, M. Calderon De La Barca Sanchez, M. Chertok, J. Conway, P.T. Cox, R. Erbacher, G. Haza, F. Jensen, O. Kukral, R. Lander, M. Mulhearn, D. Pellett, B. Regnery, D. Taylor, Y. Yao, F. Zhang

University of California, Los Angeles, USA
M. Bachtis, R. Cousins, A. Datta, D. Hamilton, J. Hauser, M. Ignatenko, M.A. Iqbal, T. Lam, N. Mccoll, W.A. Nash, S. Regnard, D. Saltzberg, B. Stone, V. Valuev

University of California, Riverside, Riverside, USA
K. Burt, Y. Chen, R. Clare, J.W. Gary, M. Gordon, G. Hanson, G. Karapostoli, O.R. Long, N. Manganelli, M. Olmedo Negrete, W. Si, S. Wimpenny, Y. Zhang

University of California, San Diego, La Jolla, USA
J.G. Branson, P. Chang, S. Cittolin, S. Cooperstein, N. Deelen, J. Duarte, R. Gerosa, L. Giannini, D. Gilbert, J. Guiang, R. Kansal, V. Krutelyov, R. Lee, J. Letts, M. Masciovecchio, S. May, M. Pieri, B.V. Sathia Narayanan, V. Sharma, M. Tadel, A. Vartak, F. Würthwein, Y. Xiang, A. Yagil

University of California, Santa Barbara - Department of Physics, Santa Barbara, USA
N. Amin, C. Campagnari, M. Citron, A. Dorsett, V. Dutta, J. Incandela, M. Kilpatrick, J. Kim, B. Marsh, H. Mei, M. Oshiro, M. Quinnan, J. Richman, U. Sarica, D. Stuart, S. Wang

California Institute of Technology, Pasadena, USA
A. Bornheim, O. Cerri, I. Dutta, J.M. Lawhorn, N. Lu, J. Mao, H.B. Newman, J. Ngadiuba, T.Q. Nguyen, M. Spiropulu, J.R. Vlimant, C. Wang, S. Xie, Z. Zhang, R.Y. Zhu

Carnegie Mellon University, Pittsburgh, USA
J. Alison, S. An, M.B. Andrews, P. Bryant, T. Ferguson, A. Harilal, C. Liu, T. Mudholkar, M. Paulini, A. Sanchez

University of Colorado Boulder, Boulder, USA
J.P. Cumalat, W.T. Ford, A. Hassani, E. MacDonald, R. Patel, A. Perloff, C. Savard, K. Stenson, K.A. Ulmer, S.R. Wagner

Cornell University, Ithaca, USA
J. Alexander, Y. Cheng, D.J. Cranshaw, S. Hogan, J. Monroy, J.R. Patterson, D. Quach, J. Reichert, A. Ryd, W. Sun, J. Thom, P. Wittich, R. Zou

Fermi National Accelerator Laboratory, Batavia, USA
M. Albrow, M. Alyari, G. Apollinari, A. Apresyan, A. Apyan, S. Banerjee, L.A.T. Bauerdick, D. Berry, J. Berryhill, P.C. Bhat, K. Burkett, J.N. Butler, A. Canepa, G.B. Cerati, H.W.K. Cheung, F. Chlebana, M. Cremonesi, K.F. Di Petrillo, V.D. Elvira, Y. Feng, J. Freeman, Z. Gecse, L. Gray, D. Green, S. Grünendahl, O. Gutsche, R.M. Harris, R. Heller, T.C. Herwig, J. Hirschauer, B. Jayatilaka, S. Jindariani, M. Johnson, U. Joshi, T. Klijnsma, B. Klima, K.H.M. Kwok, S. Lammel, D. Lincoln, R. Lipton, T. Liu, C. Madrid, K. Maeshima, C. Mantilla, D. Mason, P. McBride, P. Merkel, S. Mrenna, S. Nahn, V. O'Dell, V. Papadimitriou, K. Pedro, C. Pena[56], O. Prokofyev, F. Ravera, A. Reinsvold Hall, L. Ristori, B. Schneider, E. Sexton-Kennedy, N. Smith, A. Soha, W.J. Spalding, L. Spiegel, S. Stoynev, J. Strait, L. Taylor, S. Tkaczyk, N.V. Tran, L. Uplegger, E.W. Vaandering, H.A. Weber

University of Florida, Gainesville, USA
D. Acosta, P. Avery, D. Bourilkov, L. Cadamuro, V. Cherepanov, F. Errico, R.D. Field, D. Guerrero, B.M. Joshi, M. Kim, E. Koenig, J. Konigsberg, A. Korytov, K.H. Lo, K. Matchev, N. Menendez, G. Mitselmakher, A. Muthirakalayil Madhu, N. Rawal, D. Rosenzweig, S. Rosenzweig, K. Shi, J. Sturdy, J. Wang, E. Yigitbasi, X. Zuo

Florida State University, Tallahassee, USA
T. Adams, A. Askew, D. Diaz, R. Habibullah, V. Hagopian, K.F. Johnson, R. Khurana, T. Kolberg, G. Martinez, H. Prosper, C. Schiber, R. Yohay, J. Zhang

Florida Institute of Technology, Melbourne, USA
M.M. Baarmand, S. Butalla, T. Elkafrawy[88], M. Hohlmann, R. Kumar Verma, D. Noonan, M. Rahmani, M. Saunders, F. Yumiceva

University of Illinois at Chicago (UIC), Chicago, USA
M.R. Adams, H. Becerril Gonzalez, R. Cavanaugh, X. Chen, S. Dittmer, O. Evdokimov, C.E. Gerber, D.A. Hangal, D.J. Hofman, A.H. Merrit, C. Mills, G. Oh, T. Roy, S. Rudrabhatla, M.B. Tonjes, N. Varelas, J. Viinikainen, X. Wang, Z. Wu, Z. Ye

The University of Iowa, Iowa City, USA
M. Alhusseini, K. Dilsiz[89], R.P. Gandrajula, O.K. Köseyan, J.-P. Merlo, A. Mestvirishvili[90], J. Nachtman, H. Ogul[91], Y. Onel, A. Penzo, C. Snyder, E. Tiras[92]

Johns Hopkins University, Baltimore, USA
O. Amram, B. Blumenfeld, L. Corcodilos, J. Davis, M. Eminizer, A.V. Gritsan, L. Kang, S. Kyriacou, P. Maksimovic, J. Roskes, M. Swartz, T.Á. Vámi

The University of Kansas, Lawrence, USA
J. Anguiano, C. Baldenegro Barrera, P. Baringer, A. Bean, A. Bylinkin, T. Isidori, S. Khalil, J. King, G. Krintiras, A. Kropivnitskaya, C. Lindsey, N. Minafra, M. Murray, C. Rogan, C. Royon, S. Sanders, E. Schmitz, C. Smith, J.D. Tapia Takaki, Q. Wang, J. Williams, G. Wilson

Kansas State University, Manhattan, USA
S. Duric, A. Ivanov, K. Kaadze, D. Kim, Y. Maravin, T. Mitchell, A. Modak, K. Nam

Lawrence Livermore National Laboratory, Livermore, USA
F. Rebassoo, D. Wright

University of Maryland, College Park, USA
E. Adams, A. Baden, O. Baron, A. Belloni, S.C. Eno, N.J. Hadley, S. Jabeen, R.G. Kellogg, T. Koeth, A.C. Mignerey, S. Nabili, M. Seidel, A. Skuja, L. Wang, K. Wong

Massachusetts Institute of Technology, Cambridge, USA
D. Abercrombie, G. Andreassi, R. Bi, S. Brandt, W. Busza, I.A. Cali, Y. Chen, M. D'Alfonso, J. Eysermans, G. Gomez Ceballos, M. Goncharov, P. Harris, M. Hu, M. Klute, D. Kovalskyi, J. Krupa, Y.-J. Lee, B. Maier, C. Mironov, C. Paus, D. Rankin, C. Roland, G. Roland, Z. Shi, G.S.F. Stephans, K. Tatar, J. Wang, Z. Wang, B. Wyslouch

University of Minnesota, Minneapolis, USA
R.M. Chatterjee, A. Evans, P. Hansen, J. Hiltbrand, Sh. Jain, M. Krohn, Y. Kubota, J. Mans, M. Revering, R. Rusack, R. Saradhy, N. Schroeder, N. Strobbe, M.A. Wadud

University of Nebraska-Lincoln, Lincoln, USA
K. Bloom, M. Bryson, S. Chauhan, D.R. Claes, C. Fangmeier, L. Finco, F. Golf, J.R. González Fernández, C. Joo, I. Kravchenko, M. Musich, I. Reed, J.E. Siado, G.R. Snow†, W. Tabb, F. Yan

State University of New York at Buffalo, Buffalo, USA
G. Agarwal, H. Bandyopadhyay, L. Hay, I. Iashvili, A. Kharchilava, C. McLean, D. Nguyen, J. Pekkanen, S. Rappoccio, A. Williams

Northeastern University, Boston, USA
G. Alverson, E. Barberis, C. Freer, Y. Haddad, A. Hortiangtham, J. Li, G. Madigan, B. Marzocchi, D.M. Morse, V. Nguyen, T. Orimoto, A. Parker, L. Skinnari, A. Tishelman-Charny, T. Wamorkar, B. Wang, A. Wisecarver, D. Wood

Northwestern University, Evanston, USA
S. Bhattacharya, J. Bueghly, Z. Chen, A. Gilbert, T. Gunter, K.A. Hahn, N. Odell, M.H. Schmitt, M. Velasco

University of Notre Dame, Notre Dame, USA
R. Band, R. Bucci, A. Das, N. Dev, R. Goldouzian, M. Hildreth, K. Hurtado Anampa, C. Jessop, K. Lannon, N. Loukas, N. Marinelli, I. Mcalister, T. McCauley, F. Meng, K. Mohrman, Y. Musienko[48], R. Ruchti, P. Siddireddy, M. Wayne, A. Wightman, M. Wolf, M. Zarucki, L. Zygala

The Ohio State University, Columbus, USA
B. Bylsma, B. Cardwell, L.S. Durkin, B. Francis, C. Hill, M. Nunez Ornelas, K. Wei, B.L. Winer, B.R. Yates

Princeton University, Princeton, USA
F.M. Addesa, B. Bonham, P. Das, G. Dezoort, P. Elmer, A. Frankenthal, B. Greenberg, N. Haubrich, S. Higginbotham, A. Kalogeropoulos, G. Kopp, S. Kwan, D. Lange, M.T. Lucchini, D. Marlow, K. Mei, I. Ojalvo, J. Olsen, C. Palmer, D. Stickland, C. Tully

University of Puerto Rico, Mayaguez, USA
S. Malik, S. Norberg

Purdue University, West Lafayette, USA
A.S. Bakshi, V.E. Barnes, R. Chawla, S. Das, L. Gutay, M. Jones, A.W. Jung, S. Karmarkar, M. Liu, G. Negro, N. Neumeister, G. Paspalaki, C.C. Peng, S. Piperov, A. Purohit, J.F. Schulte, M. Stojanovic[16], J. Thieman, F. Wang, R. Xiao, W. Xie

Purdue University Northwest, Hammond, USA
J. Dolen, N. Parashar

Rice University, Houston, USA
A. Baty, M. Decaro, S. Dildick, K.M. Ecklund, S. Freed, P. Gardner, F.J.M. Geurts, A. Kumar, W. Li, B.P. Padley, R. Redjimi, W. Shi, A.G. Stahl Leiton, S. Yang, L. Zhang, Y. Zhang

University of Rochester, Rochester, USA
A. Bodek, P. de Barbaro, R. Demina, J.L. Dulemba, C. Fallon, T. Ferbel, M. Galanti, A. Garcia-Bellido, O. Hindrichs, A. Khukhunaishvili, E. Ranken, R. Taus

Rutgers, The State University of New Jersey, Piscataway, USA
B. Chiarito, J.P. Chou, A. Gandrakota, Y. Gershtein, E. Halkiadakis, A. Hart, M. Heindl, E. Hughes, S. Kaplan, O. Karacheban[23], I. Laflotte, A. Lath, R. Montalvo, K. Nash, M. Osherson, S. Salur, S. Schnetzer, S. Somalwar, R. Stone, S.A. Thayil, S. Thomas, H. Wang

University of Tennessee, Knoxville, USA
H. Acharya, A.G. Delannoy, S. Spanier

Texas A&M University, College Station, USA
O. Bouhali[93], M. Dalchenko, A. Delgado, R. Eusebi, J. Gilmore, T. Huang, T. Kamon[94], H. Kim, S. Luo, S. Malhotra, R. Mueller, D. Overton, D. Rathjens, A. Safonov

Texas Tech University, Lubbock, USA
N. Akchurin, J. Damgov, V. Hegde, S. Kunori, K. Lamichhane, S.W. Lee, T. Mengke, S. Muthumuni, T. Peltola, I. Volobouev, Z. Wang, A. Whitbeck

Vanderbilt University, Nashville, USA
E. Appelt, S. Greene, A. Gurrola, W. Johns, A. Melo, H. Ni, K. Padeken, F. Romeo, P. Sheldon, S. Tuo, J. Velkovska

University of Virginia, Charlottesville, USA
M.W. Arenton, B. Cox, G. Cummings, J. Hakala, R. Hirosky, M. Joyce, A. Ledovskoy, A. Li, C. Neu, B. Tannenwald, S. White, E. Wolfe

Wayne State University, Detroit, USA
N. Poudyal

University of Wisconsin - Madison, Madison, WI, USA
K. Black, T. Bose, J. Buchanan, C. Caillol, S. Dasu, I. De Bruyn, P. Everaerts, F. Fienga, C. Galloni, H. He, M. Herndon, A. Hervé, U. Hussain, A. Lanaro, A. Loeliger, R. Loveless, J. Madhusudanan Sreekala, A. Mallampalli, A. Mohammadi, D. Pinna, A. Savin, V. Shang, V. Sharma, W.H. Smith, D. Teague, S. Trembath-reichert, W. Vetens

†: Deceased
1: Also at TU Wien, Wien, Austria
2: Also at Institute of Basic and Applied Sciences, Faculty of Engineering, Arab Academy for Science, Technology and Maritime Transport, Alexandria, Egypt, Alexandria, Egypt
3: Also at Université Libre de Bruxelles, Bruxelles, Belgium
4: Also at Universidade Estadual de Campinas, Campinas, Brazil
5: Also at Federal University of Rio Grande do Sul, Porto Alegre, Brazil
6: Also at University of Chinese Academy of Sciences, Beijing, China
7: Also at Department of Physics, Tsinghua University, Beijing, China, Beijing, China
8: Also at UFMS, Nova Andradina, Brazil
9: Also at Nanjing Normal University Department of Physics, Nanjing, China
10: Now at The University of Iowa, Iowa City, USA
11: Also at Institute for Theoretical and Experimental Physics named by A.I. Alikhanov of NRC 'Kurchatov Institute', Moscow, Russia
12: Also at Joint Institute for Nuclear Research, Dubna, Russia
13: Also at Cairo University, Cairo, Egypt
14: Also at Helwan University, Cairo, Egypt
15: Now at Zewail City of Science and Technology, Zewail, Egypt
16: Also at Purdue University, West Lafayette, USA
17: Also at Université de Haute Alsace, Mulhouse, France
18: Also at Erzincan Binali Yildirim University, Erzincan, Turkey
19: Also at CERN, European Organization for Nuclear Research, Geneva, Switzerland
20: Also at RWTH Aachen University, III. Physikalisches Institut A, Aachen, Germany
21: Also at University of Hamburg, Hamburg, Germany
22: Also at Department of Physics, Isfahan University of Technology, Isfahan, Iran, Isfahan, Iran
23: Also at Brandenburg University of Technology, Cottbus, Germany
24: Also at Skobeltsyn Institute of Nuclear Physics, Lomonosov Moscow State University, Moscow, Russia
25: Also at Physics Department, Faculty of Science, Assiut University, Assiut, Egypt
26: Also at Eszterhazy Karoly University, Karoly Robert Campus, Gyongyos, Hungary
27: Also at Institute of Physics, University of Debrecen, Debrecen, Hungary, Debrecen, Hungary
28: Also at Institute of Nuclear Research ATOMKI, Debrecen, Hungary
29: Also at MTA-ELTE Lendület CMS Particle and Nuclear Physics Group, Eötvös Loránd University, Budapest, Hungary, Budapest, Hungary
30: Also at Wigner Research Centre for Physics, Budapest, Hungary
31: Also at IIT Bhubaneswar, Bhubaneswar, India, Bhubaneswar, India
32: Also at Institute of Physics, Bhubaneswar, India
33: Also at G.H.G. Khalsa College, Punjab, India
34: Also at Shoolini University, Solan, India
35: Also at University of Hyderabad, Hyderabad, India
36: Also at University of Visva-Bharati, Santiniketan, India
37: Also at Indian Institute of Technology (IIT), Mumbai, India

38: Also at Deutsches Elektronen-Synchrotron, Hamburg, Germany
39: Also at Sharif University of Technology, Tehran, Iran
40: Also at Department of Physics, University of Science and Technology of Mazandaran, Behshahr, Iran
41: Now at INFN Sezione di Bari [a], Università di Bari [b], Politecnico di Bari [c], Bari, Italy
42: Also at Italian National Agency for New Technologies, Energy and Sustainable Economic Development, Bologna, Italy
43: Also at Centro Siciliano di Fisica Nucleare e di Struttura Della Materia, Catania, Italy
44: Also at Università di Napoli 'Federico II', NAPOLI, Italy
45: Also at Riga Technical University, Riga, Latvia, Riga, Latvia
46: Also at Consejo Nacional de Ciencia y Tecnología, Mexico City, Mexico
47: Also at IRFU, CEA, Université Paris-Saclay, Gif-sur-Yvette, France
48: Also at Institute for Nuclear Research, Moscow, Russia
49: Now at National Research Nuclear University 'Moscow Engineering Physics Institute' (MEPhI), Moscow, Russia
50: Also at Institute of Nuclear Physics of the Uzbekistan Academy of Sciences, Tashkent, Uzbekistan
51: Also at St. Petersburg State Polytechnical University, St. Petersburg, Russia
52: Also at University of Florida, Gainesville, USA
53: Also at Imperial College, London, United Kingdom
54: Also at Moscow Institute of Physics and Technology, Moscow, Russia, Moscow, Russia
55: Also at P.N. Lebedev Physical Institute, Moscow, Russia
56: Also at California Institute of Technology, Pasadena, USA
57: Also at Budker Institute of Nuclear Physics, Novosibirsk, Russia
58: Also at Faculty of Physics, University of Belgrade, Belgrade, Serbia
59: Also at Trincomalee Campus, Eastern University, Sri Lanka, Nilaveli, Sri Lanka
60: Also at INFN Sezione di Pavia [a], Università di Pavia [b], Pavia, Italy, Pavia, Italy
61: Also at National and Kapodistrian University of Athens, Athens, Greece
62: Also at Ecole Polytechnique Fédérale Lausanne, Lausanne, Switzerland
63: Also at Universität Zürich, Zurich, Switzerland
64: Also at Stefan Meyer Institute for Subatomic Physics, Vienna, Austria, Vienna, Austria
65: Also at Laboratoire d'Annecy-le-Vieux de Physique des Particules, IN2P3-CNRS, Annecy-le-Vieux, France
66: Also at Şırnak University, Sirnak, Turkey
67: Also at Near East University, Research Center of Experimental Health Science, Nicosia, Turkey
68: Also at Konya Technical University, Konya, Turkey
69: Also at Istanbul University - Cerrahpasa, Faculty of Engineering, Istanbul, Turkey
70: Also at Piri Reis University, Istanbul, Turkey
71: Also at Adiyaman University, Adiyaman, Turkey
72: Also at Ozyegin University, Istanbul, Turkey
73: Also at Izmir Institute of Technology, Izmir, Turkey
74: Also at Necmettin Erbakan University, Konya, Turkey
75: Also at Bozok Universitetesi Rektörlügü, Yozgat, Turkey, Yozgat, Turkey
76: Also at Marmara University, Istanbul, Turkey
77: Also at Milli Savunma University, Istanbul, Turkey
78: Also at Kafkas University, Kars, Turkey
79: Also at Istanbul Bilgi University, Istanbul, Turkey
80: Also at Hacettepe University, Ankara, Turkey

81: Also at Vrije Universiteit Brussel, Brussel, Belgium
82: Also at School of Physics and Astronomy, University of Southampton, Southampton, United Kingdom
83: Also at IPPP Durham University, Durham, United Kingdom
84: Also at Monash University, Faculty of Science, Clayton, Australia
85: Also at Università di Torino, TORINO, Italy
86: Also at Bethel University, St. Paul, Minneapolis, USA, St. Paul, USA
87: Also at Karamanoğlu Mehmetbey University, Karaman, Turkey
88: Also at Ain Shams University, Cairo, Egypt
89: Also at Bingol University, Bingol, Turkey
90: Also at Georgian Technical University, Tbilisi, Georgia
91: Also at Sinop University, Sinop, Turkey
92: Also at Erciyes University, KAYSERI, Turkey
93: Also at Texas A&M University at Qatar, Doha, Qatar
94: Also at Kyungpook National University, Daegu, Korea, Daegu, Korea